University of Newcastle upon Tyne

Collision avoidance: a biologically inspired neural network for the detection of approaching objects

A thesis submitted to the Faculty of Medicine
for the degree of Doctor of Philosophy

Jonathan Mark Blanchard

May 1998

Abstract

The frequently studied lobula giant movement detector (LGMD) system of the locust responds most strongly to approaching objects. This thesis describes simulations which were designed with the ultimate aim of constructing a comprehensive model of the neural circuitry showing the effects of individual neurons on the overall responses of the system.

The Rind and Bramwell neural network model of the LGMD was studied using new stimuli which revealed that the responses of the model are dependent on the shape of the stimulus. A modification of the model removes this dependence and allows the model to respond to more complex stimuli.

Two models of a locust photoreceptor were developed with the aim of producing a detailed model of a light-adapting photoreceptor which could be used to study the responses of the LGMD to natural scenes. The first model, an electrical model of the cell membrane which describes the principal ionic conductances, was found to be overly complex for use in large scale simulations. However, the model was used to calculate from the photoreceptor's impulse response the average conductance change produced by individual photons. The second photoreceptor model, which is suitable for large scale simulations, uses two leaky integrators to mimic the effects of light adaptation on the photoreceptor's response.

An electrical model of the lamina region of the optic lobe allowed the proposal that inhibition in the lamina is produced by electrical presynaptic inhibition to be studied, along with the possible effects of this inhibition on the visual input to the LGMD. The responses of the model correspond well with those measured from the LMCs of locusts and other insects, and their implications for the LGMD system are discussed.

Contents

List of Figures

List of Abbreviations

Throughout this thesis, all units are specified in standard S.I. notation. Additional abbreviations are:

DCMD	Descending Contralateral Movement Detector
LGMD	Lobula Giant Movement Detector
LMC	Large Monopolar Cell
LVF	Long Visual Fibre
SVF	Short Visual Fibre

Preface

I began the research described in this thesis almost by accident. While I was an undergraduate in the Department of Electrical and Electronic Engineering here in Newcastle I developed a strong interest in robotics and asked my lecturer, Charles Allen, whether he had any PhD projects. He had none but, as I had written an essay for him focussing on techniques for collision avoidance in mobile robotics, he pointed me in the direction of the Department of Neurobiology where he was collaborating with an insect neurobiologist, Claire Rind, who was keen to develop a collision avoidance sensor based on the neural system she had been studying.

At first this seemed to me to be a strange turn of events but after an informal meeting held in the coffee room of the Zoology Department I accepted the project. Thus began my introduction to the wonderful world of neurobiology, little did I know what I was letting myself in for!

The results of four and a half years of work are presented here. Despite the original intention of developing a collision avoidance sensor for use on a mobile robot, I became fascinated by the insect visual system. As a result the focus of the project shifted to a more detailed study of the biology of the neural system which was to form the basis of the sensor, the lobula giant movement detector (LGMD) system of the locust. Taking as my starting point a neural network model of the LGMD system developed by Dr. Rind and my predecessor, David Bramwell, I have addressed questions about the processing of visual information by the early visual system and the effects of this processing on the detection of approaching objects by the LGMD system with the ultimate aim of developing a comprehensive model of the neurons which comprise the LGMD system and an understanding of their individual effects on the responses of the system as a whole.

Acknowledgements

I am grateful to my supervisor, Claire Rind, for her help and support throughout this project and particularly during the writing of this thesis.

I also wish to thank Peter Simmons and Gerd Leitinger for their constructive criticisms of the drafts of this thesis, and Ed Childs and Peter for helpful scientific discussions.

During this work I attended two courses, the Crete Course in Computational Neuroscience and the Telluride Workshop For Neuromorphic Systems. I would like to thank the staff and students of both these courses, particularly Erik De Schutter, co-director of the Crete Course, whose input shaped the development of the models described in this thesis.

This work was supported by a Wellcome Trust Mathematical Biology studentship.

Finally, I wish to thank Pamela for her kindness, support and encouragement. Without her, this thesis would not have been written.

Declaration

The model described in chapter 3 emulates an earlier program by Rind and Bramwell (1996). The remainder of the work is mine.

Some of the work has been shown on conference posters. Chapter 4 describes work presented as Blanchard and Rind (1997), and Blanchard and Rind (1998) presented the electrical photoreceptor model of chapter 5.1.

Chapter 1

Introduction

Since the beauty of the compound eye was revealed using the earliest microscopes in the 17th century, many scientists have been fascinated by the visual systems of insects. Today an extensive range of work is conducted, stretching from the study of genetics using the visual mutants of *Drosophila* through electrophysiological investigation of the properties of many visual neurons to the modelling and simulation of visual circuits and functions.

The focus of this thesis is the frequently studied lobula giant movement detector (LGMD) system of the locust. The results of various simulations are presented, which were developed with the ultimate aim of constructing a comprehensive model of the neural circuitry showing the effects of individual neurons on the overall responses of the system. In order to set the scene this introduction presents:

- the visual system of the locust, focussing on the photoreceptor cells of the compound eye, processing in the lamina region of the optic lobe and the responses of the lobula giant movement detector (LGMD) neuron.
- the major techniques used to model neural systems, including single cell models, large neural networks and "neuromorphic engineering".
- an overview of this thesis.

1.1 The locust visual system

The visual systems of many insects, including several species of locust (notably *Locusta migratoria* and *Schistocerca gregaria*), have been studied extensively and many similarities in anatomy and neuronal responses have been found. In this introduction, the early visual processing performed by the photoreceptor cells of the compound eyes and the large monopolar cells of the lamina is described along with a review of movement detection systems, which includes the lobula giant movement detector (LGMD) system of the locust.

Where possible, data obtained from the locust is used: however, in some sections, especially those on phototransduction and the responses of large monopolar cells (LMCs), findings from other insects have been included. These findings are used with caution as significant differences may exist between species due to different evolutionary pressures. However, there are sufficient similarities between the visual systems of many arthropods to suggest that this pooling of information is appropriate.

1.1.1 Anatomy

Before discussing particular components of the locust visual system it is helpful to give a brief description of the basic anatomy. The locust visual system comprises two compound eyes, one located on each side of the head, with three neuropiles (the lamina, the medulla and the lobula) behind each eye. Known collectively as the optic lobe, these neuropiles process the visual information as it passes from the eye to the brain (the protocerebrum). Figure 1.1 shows the structure of the optic lobe behind one eye. (The locust also has three simple eyes, the ocelli, which are not considered in this thesis.)

In *Locusta* each compound eye has an estimated 8500 ommatidia (Shaw 1978) packed into a hexagonal array measuring approximately 3mm by 2mm (Wilson, Garrard and McGinness 1978). The eyes use simple apposition optics where each ommatidium samples a discrete point in space (Nilsson 1989). The spatial resolution (acuity) is determined by both the angular separation of the ommatidia and their receptive field (acceptance angle). The angular separation is not uniform:

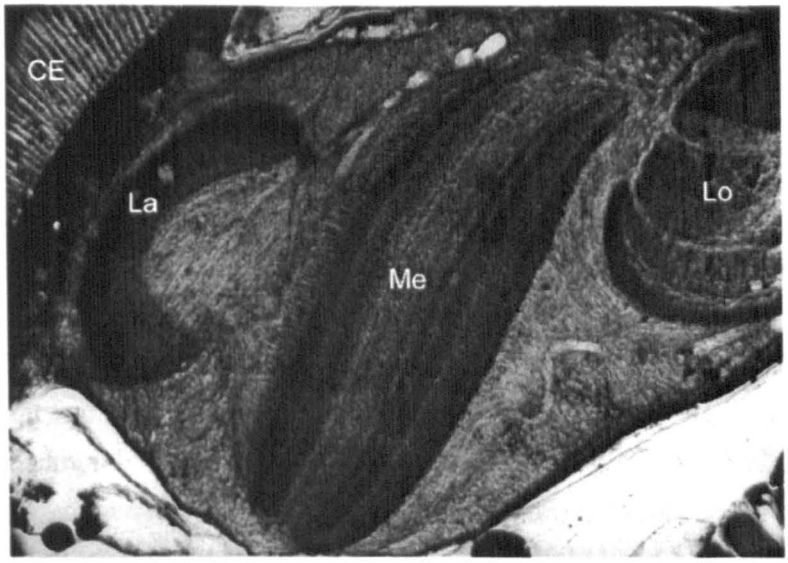

Figure 1.1: Structure of the locust optic lobe, showing the three synaptic regions. Width of figure corresponds to 1.25mm. CE, compound eye; La, lamina; Me, medulla; Lo, lobula. From Burtt and Catton (1964).

there is an acute zone at the front of the eyes looking ahead of the animal (Horridge 1978) while in a region at the dorsal rim of the eyes the ommatidial lenses are smaller and fused (Eggers and Gewecke 1993). Structural changes within the ommatidia (Tunstall and Horridge 1967, Horridge, Duniec and Marčelja 1981) increase the acceptance angle as the ambient light intensity falls (Wilson 1975). The increase in acceptance angle allows light from a wider area to be captured by the ommatidium, improving sensitivity at low light levels (Williams 1983).

Within each ommatidium there are eight photoreceptor (retinula) cells which combine to form a fused rhabdom with their microvilli (Wilson et al. 1978). Six of the photoreceptors (R1-6, also known as short visual fibres (SVFs) because their synaptic terminals are in the lamina) contribute to the rhabdom along the full length of the ommatidium while the remaining two photoreceptors (R7-8, or long visual fibres (LVFs) which have synaptic terminals in the medulla), once thought to be second order cells (Scholes 1965), contribute a small amount in the proximal third of the rhabdom. The rhabdom is the photosensitive structure within the ommatidium, with rhodopsin molecules embedded in the microvillar

membranes of the photoreceptors (Williams 1983)

At the proximal end of an ommatidium the photoreceptor axons form into a bundle which passes through the basement membrane and projects to the first optic neuropile, the lamina (Meinertzhagen 1976). The neurons in the lamina are grouped into cartridges and there is a precise retinotopic mapping from the ommatidia to these cartridges which preserves the spatial information of the visual image.

There are many anatomical similarities between the neurons identified in the locust lamina and those in other insects (Nowel and Shelton 1981, James and Osorio 1996, Strausfeld 1976, Shaw 1984). The terminals of the six SVFs are found in the cartridge: the axons of the LVFs pass through the lamina and project to the medulla. There are six monopolar cells, two of which, M1 and M2, have thickened axons and dendrites confined within the cartridge. These correspond to the large monopolar cells (LMCs) found in flies which receive extensive synaptic input from the six SVF terminals (Nicol and Meinertzhagen 1982). Twelve cell types have been observed in flies (Strausfeld and Campos-Ortega 1977), including the monopolar cells, amacrine cells whose dendrites project across many cartridges and efferent cells from the medulla: it is reasonable to assume that similar cells are present in the locust.

A number of glial cell processes are found around the cartridges which electrically isolate neighbouring cartridges (Shaw 1984). In addition the locust lamina is isolated from the eye and the optic lobe by glial cells and trachea which fill the extracellular space, forming diffusion barriers (Shaw 1977, Shaw 1978).

As with the lamina the second optic neuropile, the medulla, has a retinotopic arrangement of neuronal cartridges. However the visual information is reversed horizontally by the projections from the lamina which cross at the first optic chiasma.

Little is known about the anatomy of the medulla cartridges in the locust. Estimates suggest that each cartridge contains at least 40 distinct cell types (Osorio 1992) and a few of these cell types have been identified (O'Carroll, Osorio, James and Bush 1992, James and Osorio 1996). The anatomy of the fly medulla has been studied in greater detail and many more cell types have been found and identified (Strausfeld 1976, Strausfeld 1989).

The third optic neuropile, the lobula, has a coarse retinotopic arrangement with the positions of the cartridges reverting to their original positions after the second optic chiasma. However, many of the neurons found in the lobula have dendritic trees which cover large areas of the neuropile and hence the visual field. These wide-field neurons can be identified reliably in different individuals from their anatomy. A variety of neurons of this type has been identified in the locust (Rind 1987, Rind 1990) including the lobula giant movement detector (LGMD) (O'Shea and Williams 1974), the neuron at the heart of this thesis.

In addition to the flow of information down the optic lobe from the eye to the brain there are neurons which project in the opposite direction. All of the optic neuropiles receive inputs from the brain and the contralateral eye via efferent neurons with large axonal arborizations which cover large areas of the visual field (Gewecke and Hou 1993, Stern, Thompson, Zhou, Watson, Midgley, Gewecke and Bacon 1995). Other neurons project centrifugally between regions of the optic lobe (Strausfeld 1976, Shaw 1984).

1.1.2 Locust photoreceptors

The photoreceptors of the compound eye are the gateway through which the animal perceives the visual world. As such they play a crucial role in all subsequent processing. A large amount of work has concentrated on the photoreceptors of the locust and, when combined with the knowledge obtained from other insects, a detailed picture of the mechanisms underlying their responses emerges.

Response properties

Locust photoreceptors, and those of all insects, respond to light with predominantly graded depolarisations of their membrane potential. Very low intensity light produces irregularly spaced depolarising bumps at a frequency which is proportional to the intensity (Scholes 1965) and statistical analysis has shown that each bump is produced by a single photon (Lillywhite 1977). The size and shape of the bumps vary due to fluctuations in the phototransduction process (transducer noise) which determines the threshold intensity at which a stimulus is seen (Lillywhite and Laughlin 1979). When two or more bumps are produced together the

total response is nonlinear (French and Kuster 1985).

As the light intensity increases the bumps merge to form a sustained depolarisation, the receptor potential (Scholes 1965) which rises with increasing light intensity. A sudden (step) increase in intensity causes the receptor potential to rise rapidly to an initial peak which decays slowly to a lower steady-state due to light adaptation (Tunstall and Horridge 1967).

A brief, weak flash is often used to characterise the impulse response of photoreceptors. In the locust the duration of the impulse response decreases with increasing background light intensity (Howard 1981, Payne and Howard 1981). Very bright flashes cause a prolonged depolarisation which can take more than an hour to decay (Tsukahara and Horridge 1977, Horridge and Tsukahara 1978). As this afterdepolarisation decays, the sustained receptor potential is replaced by bumps similar to those seen with dim light.

The acceptance angle of the ommatidium determines the angular sensitivity of the photoreceptors. Responses to a point source of light are strongest on the optical axis and reduce gradually as the angle between the axis and the source increases. In the dark the acceptance angle is 2.5°, falling to 1.5° under strong light (Wilson 1975).

Locust photoreceptors are most sensitive to blue-violet light and their response to green light varies between 15% and 100% of the blue-violet sensitivity, with females more sensitive to green than males (Bennett, Tunstall and Horridge 1967). This variation has been attributed to the presence of different proportions of two visual pigments in different cells, with the overall spectral sensitivity determined by the combination of the individual absorption characteristics of the pigments (Shaw 1968).

Membrane mechanisms

The responses of locust photoreceptors begin with the absorption of photons by molecules of rhodopsin embedded in the microvillar membranes (Williams 1983). This triggers the phototransduction cascade (see below) which opens a light-activated sodium conductance in the cell membrane and the inward flow of sodium ions through this conductance depolarises the cell (Fulpius and Baumann 1969).

Removing the sodium from the extracellular fluid decreases the depolarisation (Payne 1982).

The light-induced current is opposed by an outward flow of potassium ions flowing through voltage-dependent conductances (Weckström 1994), which was predicted from the nonlinear summation of bumps seen at low intensities (Pece and French 1992). Two types of potassium conductance have been identified, a fast transient current which activates briefly when the cell depolarises from the resting potential before inactivating, and a sustained conductance whose activation increases with depolarisation, decreasing the membrane time constant (Weckström and Laughlin 1995). The transient conductance will be completely inactivated in a light-adapted photoreceptor but may act to oppose sudden large changes in intensity when the cell is dark-adapted. The characteristics of these conductances have not been studied comprehensively in locusts but similar conductances in blowflies and *Drosophila* have been studied in greater detail (Weckström, Hardie and Laughlin 1991, Hardie 1991a). In particular the sustained potassium conductance is absent in blowfly LVFs which suggests that they form the input to a separate visual process with different frequency requirements (Anderson and Hardie 1996).

An interesting property of the sustained potassium conductance in a locust photoreceptor is the shift of its activation curve to higher (more depolarised) membrane potentials during the night (Cuttle, Hevers, Laughlin and Hardie 1995). This changes the photoreceptor from a fast cell with a high frequency cutoff, common in fast-moving flies, to a slow cell with a low frequency cutoff, characteristic of slow moving nocturnal insects (Laughlin and Weckström 1993). The effect is duplicated by applying serotonin to the eye, a result also observed in *Drosophila* (Cuttle et al. 1995, Hevers and Hardie 1995), suggesting that a serotonergic neuron, similar to the TAN3 cell of the blowfly (Nässel, Hagberg and Seyan 1983), may modulate the conductances of the eye according to the time of day.

There may also be a voltage-dependent conductance within the membrane which produces fast depolarising transients when current is injected into the cell or a sudden increase in light intensity occurs (Weckström 1994). Similar conductances have been found in the photoreceptor terminals of the blowfly (Weckström, Juusola and Laughlin 1992) where they enhance the release of transmitter on the

rising phase of a response (Juusola, Uusitalo and Weckström 1995) and a voltage-dependent sodium conductance which exhibits this behaviour has been found in the photoreceptors of the drone honey bee (Coles and Schneider-Picard 1989) and may help the animal to pursue a mate (Vallet and Coles 1993).

The metabolic state of the cell is probably maintained by a number of ionic pumps. In the blowfly a Na^+-K^+ pump which swaps three intracellular sodium ions for two extracellular potassium ions has been identified (Jansonius 1990). Also in the blowfly a Na^+-Ca^{2+} pump has been identified which removes calcium from the cell in exchange for sodium ions (Hochstrate 1991).

Phototransduction

Although not studied extensively in the locust, much is known about the phototransduction process from *Drosophila*, aided by a number of genetic mutants with various visual deficiencies. The underlying mechanism has been identified as the phosphoinositide cascade (Hardie and Minke 1995) but the final step which activates the light-activated membrane conductance, possibly via the production of an intracellular transmitter (Cone 1973), has not been determined. However, the importance of calcium to the process is beyond doubt, with extracellular calcium needed to maintain the conductance during prolonged illumination (Hardie and Minke 1992) and intracellular calcium playing a role in light adaptation by inactivating light-activated channels (Hardie and Minke 1994).

Several models for the phototransduction cascade have been proposed. Payne and Howard (1981) used a log-normal equation,

$$V(t) = sI.\exp\left[\frac{-(\log\frac{t}{t_p})^2}{2\sigma^2}\right], \tag{1.1}$$

to describe the impulse responses of the cell (figure 1.2). For a flash of I photons/facet/s, both the time-to-peak of the response, t_p, and the sensitivity to each photon in the flash, s, decrease as the light intensity increases while the width of the curve, represented by σ, remains approximately constant. The decreasing values of s and t_p describe the effects of adaptation of the phototransduction cascade.

A more recent model from Contzen and Nagy (1996) describes the light-

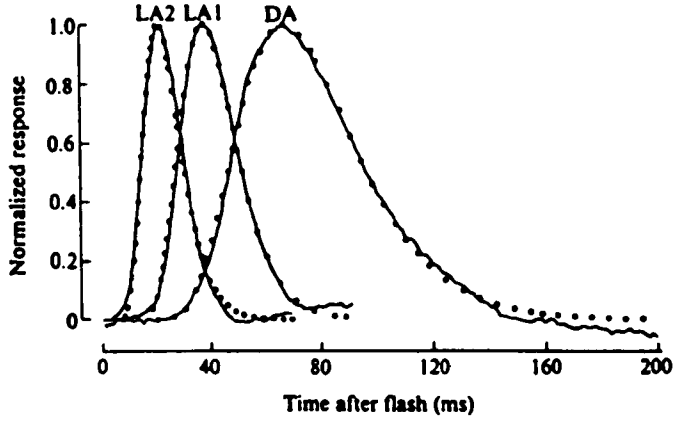

Figure 1.2: Log-normal model of phototransduction fitted to impulse responses at three different background intensities. Parameters: response amplitude, V_{flash}; time-to-peak, t_p; response width, σ; flash intensity, I_{flash}; background intensity, I_{back}. DA (dark-adapted): V_{flash}, 1.5mV; t_p, 74ms; σ, 0.31; I_{flash}, 14 photons/facet; I_{back}, 0 photons/facet/s. LA1: V_{flash}, 1.2mV; t_p, 41ms; σ, 0.27; I_{flash}, 42 photons/facet; I_{back}, $1.3 * 10^4$ photons/facet/s. LA2: V_{flash}, 2.3mV; t_p, 23ms; σ, 0.31; I_{flash}, 420 photons/facet; I_{back}, $1.3 * 10^5$ photons/facet/s. From Payne and Howard (1981).

induced current entering *Limulus* ventral photoreceptors using the equation

$$\frac{dg_L(t)}{dt} = \frac{B}{\sigma}\frac{\exp[-(t-\delta)/\sigma]}{\{1+\exp[-(t-\delta)/\sigma]\}^2} - \frac{1}{\tau}g_L(t), \tag{1.2}$$

which includes a Fermi function for the rise in transmitter concentration and an exponential decay (figure 1.3). The Fermi function describes the enzyme reactions within the cell.

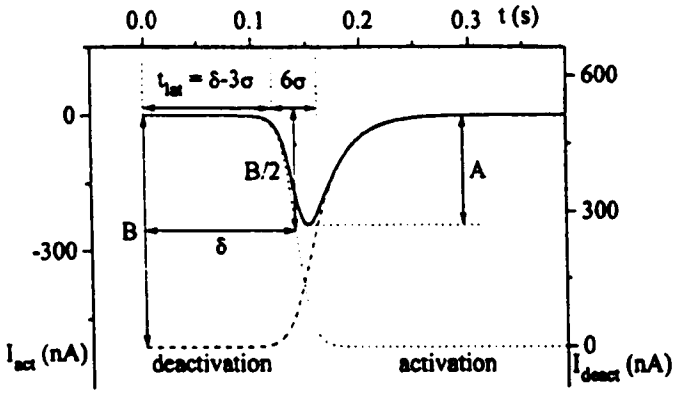

Figure 1.3: Fermi-exponential model of phototransduction. Activation is controlled by the three Fermi function parameters: B, saturating amplitude; δ, activation half-time; σ, activation time constant. The exponential deactivation function has one parameter: τ, deactivation time constant. From Contzen and Nagy (1996).

Light adaptation

The function of light adaptation is to match the working range of a photoreceptor to the mean light intensity allowing the cell to have a high sensitivity to contrast without saturating the response (Laughlin 1989). Thus responses to sudden changes in intensity produce a sharp rise in membrane potential which slowly decays to a steady-state as the cell adapts and plots of the membrane potential versus intensity show a higher gain for the peak than the steady-state (Vishnevskaya, Byzov and Cherkasov 1993). In the locust the contrast gain increases with increasing mean light intensity and is optimal at high light levels (Matić and Laughlin 1981). The frequency response of the cell also changes, with a higher corner frequency

for a light-adapted cell where photon noise is lower (Pinter 1972), and adaptation confers essentially band-pass filter characteristics onto the cell (Juusola and Weckström 1993).

Light adaptation results from a combination of several mechanisms. In addition to the physical changes in the structure of the ommatidia, the size of the response produced by a single photon is reduced and this may be due to a decrease in the number of sodium channels opened or a shortening of the time for which the sodium channels are open (Tsukahara and Horridge 1977). These changes may be due to an increase in calcium concentration within the cell (Walz, Zimmermann and Seidl 1994). The effect of this adaptation can be seen in the light-induced current measured in *Drosophila* (Hardie 1991b) and calculated for *Tipula* (Laughlin 1996). There are also adapting mechanisms within the cell membrane: the sustained potassium conductance activated by the increased membrane potential reduces the membrane resistance and shunts the light-induced current (Weckström et al. 1991), and an increase in the rate of pumping of the Na^+-K^+ exchange pump may act to repolarise the cell by pumping excess sodium out of the cell (Jansonius 1990).

1.1.3 Processing in the lamina

A large amount of anatomical detail on the lamina cartridge is known for flies (Shaw 1984, Strausfeld 1989) but similar data is not available for the locust. Consequently this description is based heavily on the findings from flies but given the similar responses of the LMCs of locusts and flies to white-noise stimuli (James and Osorio 1996, James 1992) it is reasonable to assume that the underlying processes are also similar.

The dominant cells in a cartridge in the lamina are the large monopolar cells (LMCs). In locust these have been identified as M1 and M2 (Nowel and Shelton 1981, James and Osorio 1996) whereas in the flies the names L1 and L2 are used (Shaw 1984). The principle input to these cells comes from six SVFs and there are approximately 200 synapses from each SVF onto each LMC in the housefly (Nicol and Meinertzhagen 1982). In the locust, the SVFs all originate in one ommatidium. However, in flies, which have neural superposition eyes, the cell

bodies of the SVFs are found in the six neighbouring ommatidia and their axons converge in the lamina. Each cell views the same point in space, so the spatial information is preserved in the lamina.

At very low light intensities LMCs respond to each photon received by the photoreceptors with discrete hyperpolarising bumps (Shaw 1968). LMC bumps have a significantly larger amplitude than photoreceptor bumps indicating that the gain of the photoreceptor-LMC synapse is high, which ensures a high signal-to-noise ratio (Laughlin 1973).

As the light intensity rises the bumps fuse and the responses of the LMCs become transient, hyperpolarising in response to an increase in light intensity (ON) and depolarising in response to a decrease in intensity (OFF) (Laughlin and Hardie 1978). The high gain of the synapse restricts the dynamic range of the cell to a smaller range of contrasts than the photoreceptors (Vishnevskaya et al. 1993).

The hyperpolarising ON response is produced by an increase in chloride conductance (Zettler and Straka 1987) produced by the graded release of the neurotransmitter histamine by the photoreceptor synapses (Hardie 1989): as the conductance increases the flow of negative chloride ions into the cell increases. The mechanisms underlying the OFF response are not so clear: a decrease in the chloride conductance is found which produces the initial depolarisation but measurements of the input resistance during the response suggest that other conductances may be activated (Laughlin and Osorio 1989). These may include potassium conductances (Hardie and Weckström 1990) which would act to repolarise the cell and a fast depolarising transient (possibly a sodium conductance) to produce the spike seen on large OFF responses .

The transient nature of these light-adapted responses is produced partly by lateral inhibition, first identified by noting the narrower receptive fields of the LMCs compared to the photoreceptors (Zettler and Järvilehto 1972), which reduces the photoreceptor input presynaptically (Laughlin and Osorio 1989). The inhibition might be due to specific neuronal connections from amacrine cells to the photoreceptor terminals (Strausfeld and Campos-Ortega 1977, Shaw 1984) but the favoured theory involves electrical presynaptic inhibition by an extracellular field potential (Laughlin 1974, Shaw 1975) which depolarises in response to light and may reduce the effective membrane potential of the photoreceptor terminals and

hence the release of transmitter (Laughlin and Osorio 1989).

Two models for the mechanisms underlying the depolarisation of the extracellular field potential have been proposed. In the first model (figure 1.4) (Shaw 1975), derived for the locust, current flowing down an illuminated photoreceptor flows out of the synaptic terminal into the lamina extracellular space and is prevented from flowing back into the eye by a high resistance extracellular barrier (section 1.1.1). Instead, this current flows laterally into the axons of the photoreceptors of neighbouring cartridges which are less strongly illuminated, completing the circuit by flowing out of the photoreceptor somas and back into the original ommatidium.

In the second model (figure 1.5) (Zimmerman 1978), the principal cause of the field potential is the flow of current from the LMC since the membrane resistance of this cell is much lower, and hence the current flow higher, than that of the photoreceptor terminal. Recent work on the blowfly suggests that the contribution of the LMC current is dominant in this species (Kettunen, Laughlin and Weckström, personal communication) but recordings of the responses of the field potential in the locust show no transient components (Shaw 1968) which suggests that the photoreceptor currents play the greater role.

Two aspects of the lamina anatomy are missing from both these models but important for lateral inhibition. The epithelial glial cells which surround the lamina cartridges form a resistance barrier for current flowing laterally between cartridges (Shaw 1984), and the extracellular space in each cartridge (Shaw 1977, Shaw 1978) will act as a capacitance for the accumulation of ions and delay the development of the field potential. Both of these properties are incorporated into the model described in section 6.

Several theories have been proposed to explain the function of the LMCs in the visual system. A theory of predictive coding (Srinivasan, Laughlin and Dubs 1982) suggests that redundant information, which may be constant over long periods of time, over a wide area of the visual field or both, is discarded by LMCs, allowing a higher gain to be used for the remaining information and enhancing the cell's information capacity by matching the response properties of the cell to the characteristics of natural scenes (Laughlin 1981). Another theory proposes that the LMCs are tuned to maximise the flow of information (van Hateren 1992)

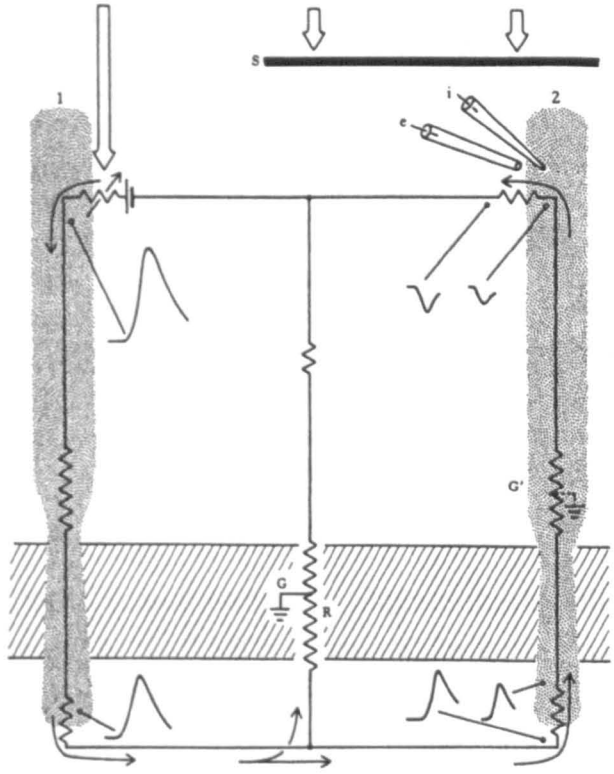

Figure 1.4: Shaw's model of current flow in the lamina. Current flowing down an illuminated photoreceptor enters the lamina through the synaptic terminal membrane and is prevented from flowing back into the eye by the extracellular barrier resistance, R. Instead, the current flows laterally and returns via the axons of neighbouring photoreceptors, which depolarise slightly. G and G' indicate electrical ground. From Shaw (1975).

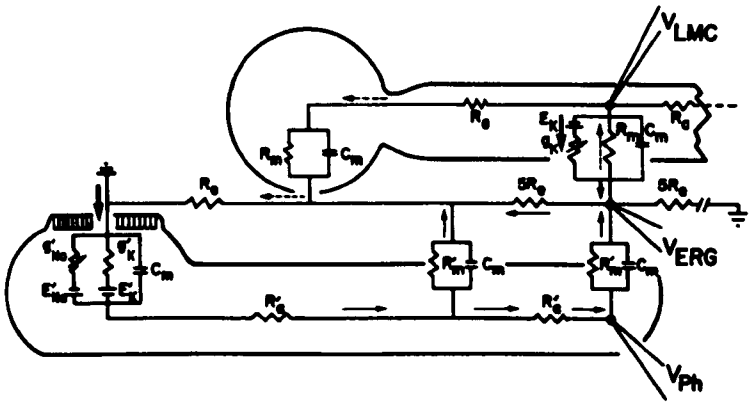

Figure 1.5: Zimmerman's model of current flow in the lamina. The extracellular field potential, V_{ERG}, is produced by current flowing from both the photoreceptor terminal and the LMC. V_{Ph}, photoreceptor terminal membrane potential; V_{LMC}, LMC membrane potential; R_e, extracellular resistance; $5R_e$, resistance of extracellular barriers; R_a, intracellular resistances; R_m, R'_m, membrane resistances; g_{Na}, sodium conductance; E_{Na}, sodium reversal potential; g_K, g'_K, potassium conductances; E_K, E'_K, potassium reversal potentials; C_m, membrane capacitances. The dashed ($'$) parameters are for the photoreceptor. From Zimmerman (1978).

and a recent study using natural time series suggests that the filtering of the visual information performed by the LMCs is optimal for coding natural images (van Hateren 1997). All these theories treat the LMCs as general filters of the visual input. In contrast, a theory from Srinivasan, Pinter and Osorio (1990) proposes that the LMCs are matched filters, optimised for detecting moving edges at high light levels and moving 'blobs' under low light levels.

LMCs, like photoreceptors, are graded potential cells with passive membranes. A model of a blowfly LMC suggests that the design, with a low resistance synaptic zone with long, high resistance axon and terminal is the most expensive metabolically but the most effective at transmitting the graded responses (van Hateren and Laughlin 1990). Thus, LMCs must play a major role in the insect's visual system.

1.1.4 The lobula giant movement detector (LGMD)

The lobula giant movement detector (LGMD) neuron of the locust has been studied for many years and its responses and function have been the subject of controversy several times.

The LGMD is a unique, identified, wide-field neuron and there is one LGMD in the lobula neuropile behind each eye. The anatomy of the LGMD is shown in figure 1.6. It has three dendritic subfields, a large dendritic fan which extends across the full width of the lobula and two smaller subfields protruding from the base of the fan (O'Shea and Williams 1974). Its axon projects to the brain where synapses are made with the descending contralateral movement detector (DCMD) neuron (O'Shea, Rowell and Williams 1974). In turn the axon of the DCMD projects down the contralateral nerve cord to form synapses with interneurons and motoneurons in the thoracic ganglia (Burrows and Rowell 1973, Simmons 1980).

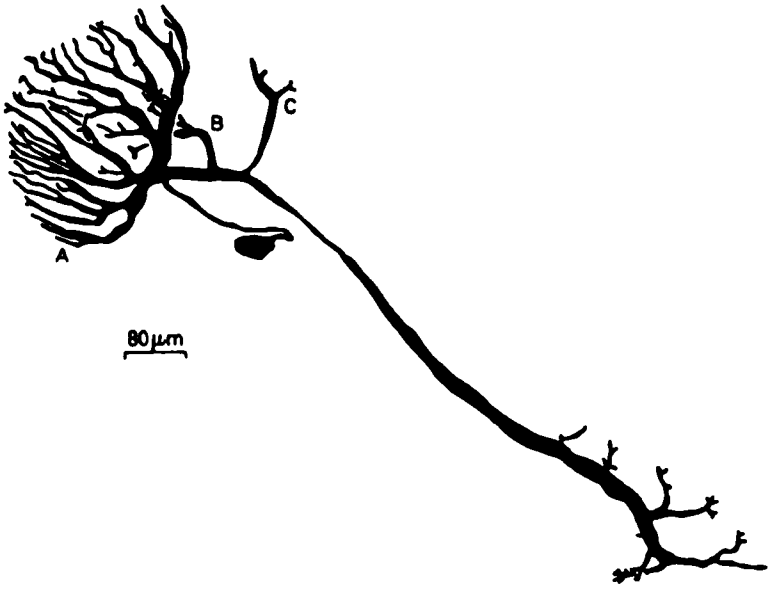

Figure 1.6: Anatomy of the lobula giant movement detector (LGMD) neuron. There are three dendritic subfields, a large dendritic fan (A) and two smaller subfields (B and C). From O'Shea and Williams (1974).

Initially the DCMD was studied owing to the ease with which recordings could be made with extracellular electrodes from the nerve cord, where spikes from

the DCMD are easily identified due to their large amplitude (Rowell 1971). A later study using intracellular recordings established a one-to-one correspondence between spikes in the DCMD and the LGMD (O'Shea et al. 1974), which led to the proposal that the synapse between the two cells was electrical (O'Shea and Rowell 1975b). This was disproved by a detailed examination of the properties of the synapse which revealed a short transmission delay and a slight gain, both of which are characteristics of a chemical synapse (Rind 1984). The one-to-one correspondence between spikes in these neurons, which persists up to frequencies of 400Hz (Rind 1984), allows the responses of the LGMD to be inferred from those of the DCMD.

An early experiment revealed responses in the nerve cord, probably from the DCMD, to increases and decreases of light intensity (ON and OFF) and to movement of illuminated objects (Burtt and Catton 1952). Subsequent experiments using striped stimuli caused a controversy by hinting that the acuity of the visual system was significantly better than expected from the optics of the eye, but these results were later attributed to artifacts in the stimuli (Horridge 1975).

Experiments where small stimuli moved horizontally or vertically produced a short burst of spikes in the LGMD/DCMD. This response habituated if the movement was repeated and showed that the receptive fields of the cells covered the whole field-of-view of the eye. The idea that the neurons were tuned to detect novel movements of small objects was proposed but, despite the suggestion that they may play a role in initiating escape behaviour via the thoracic ganglia, the value to the animal of this non-directional movement detection was questioned (Rowell 1971).

Notwithstanding the lack of a functional reference, a detailed study was undertaken to determine the neuronal circuit underlying this response. The responses to changes in the intensity of a small light source were attributed to the properties of the photoreceptor cells (Rowell and O'Shea 1976b) but a lateral inhibitory network was proposed as the mechanism responsible for the dependence of these responses on the intensity of the surrounding area (Rowell and O'Shea 1976a). Input to the dendritic fan was found to be from transient ON/OFF cells and these cells or their synapses were predicted to be the site of LGMD habituation (Rowell and O'Shea 1976a). Finally, experiments were conducted with stimuli comprising

small objects and large-field moving stripes, and these showed that the response to a small object was reduced by movement of a stripe pattern behind the object and large stimuli produced inhibitory responses (Rowell, O'Shea and Williams 1977).

Taken as a whole, these findings led to the proposal of the model shown in figure 1.7 for the input circuit of the LGMD. In this circuit lateral inhibition between the inputs to the dendritic fan, believed to involve amacrine cells in the medulla region of the optic lobe (Rowell et al. 1977), prevents habituation during movement of the whole visual field (O'Shea and Rowell 1975a, Pinter 1979). Feed-forward inhibition from separate populations of ON- and OFF-sensitive cells projecting onto the smaller dendritic subfields suppresses responses to large stimuli and changes of the whole visual image generated by movements of the animal (Zaretsky and Rowell 1979). Neurons thought to be responsible for the OFF feed-forward connection were identified anatomically in the medulla and the connection was broken by lesioning the dorsal uncrossed bundle of axons which projects from the medulla to the lobula (Rowell et al. 1977). Neurons with properties matching the other proposed cell types have since been found in the medulla (Osorio 1987, Osorio 1991, O'Carroll et al. 1992, James and Osorio 1996), although recent findings using electronmicroscopy have revealed a novel synaptic arrangement around the dendrites of the LGMD which may mediate lateral inhibition directly (Rind, personal communication).

Recordings of the responses of the LGMD to objects moving towards or away from the animal showed an increasing spike rate for an approaching object but only a brief burst of spikes for a receding object, and it was suggested that the neuron is in fact tuned to detect approaching objects, a more relevant stimulus for triggering escape behaviour (Schlotterer 1977). Although this idea was not accepted initially (Pinter, Olberg and Abrams 1982) it has now been verified (Rind and Simmons 1992). In addition, the spike rate has been found to be well correlated with the angular acceleration of the edges of the objects. An increase in the object edge length and an increase in edge velocity are necessary for the cell to distinguish an approaching object from a receding object (Simmons and Rind 1992). The neuron is tightly tuned to objects approaching the animal on a collision course (Judge and Rind 1997): objects moving on a path which deviates from the direct collision trajectory by only a few degrees produce a much weaker

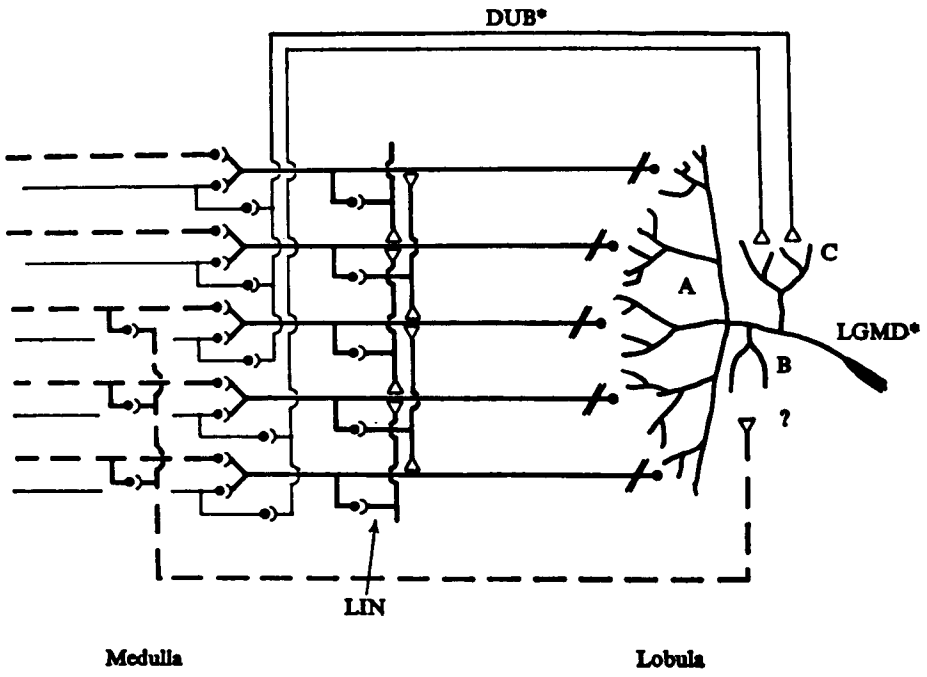

Figure 1.7: Model of the input circuit to the lobula giant movement detector (LGMD) neuron. Refer to text for details. LIN, lateral inhibitory network; DUB, dorsal uncrossed bundle; A, B and C denote the dendritic subfields shown in figure 1.6. Filled circles, excitatory synapses; open triangles, inhibitory synapses; thick solid lines, ON/OFF cells; thick dashed lines, ON units; thin solid lines, OFF units. From Rowell et al. (1977).

response.

The responses to approaching objects occur due to an exponential build-up of excitation in the dendritic fan whereas the responses to receding objects show brief excitation followed by prolonged inhibition, likely to be due to feed-forward inhibition (Rind 1996). A neural network model, described in detail in chapter 3, produces responses which match the spike rate of the LGMD and demonstrates the contributions of excitation and inhibition (Rind and Bramwell 1996).

A recent study suggests that the spike rate peaks before the object reaches the eye (Hatsopoulos, Gabbiani and Laurent 1995) which contradicts earlier findings which show the response continuing to rise until after the collision would have occurred (Rind and Simmons 1992, Rind 1996). Although the difference was

attributed to the stimulus system used (Rind and Simmons 1997), a repeat of the experiments with new equipment has produced similar results to the initial study (Krapp, Gabbiani, Koch and Laurent 1998). The results of the latest study have been fitted with an equation that relates the response to the stimulus and predicts that during responses to objects approaching on a collision course, the LGMD spike rate peaks when the stimulus subtends a fixed angular size on the eye. At the time of writing, the reasons for this contradictory evidence have not been identified.

1.2 Techniques for modelling neural systems

Models are often used to explore the properties of neural systems which are difficult to reveal experimentally. There are many ways of building models of neural systems, ranging from very detailed models of single neurons to large scale networks with simple neurons and the "neuromorphic engineering" approach, and it is helpful to review a few of them here, allowing the models described later in this thesis to be put into context.

One of the most frequently used models in neuroscience is the Hodgkin-Huxley model of active membrane (Hodgkin and Huxley 1952). From a voltage-clamp study of action potentials in the squid giant axon an electrical model of the membrane and a mathematical description of the voltage- and time-dependent properties of the active sodium and potassium conductances was proposed and forms the basis of much of the modelling carried out today. In this thesis, the model in chapter 5.1 owes much to this pioneering work.

An extension of the Hodgkin-Huxley model is the compartmental model often used to describe the electrical structure of neurons with complex dendritic trees (Segev, Fleshman and Burke 1989). The neuron is divided into small sections (compartments) where the membrane potential in each part can be considered uniform and a set of simultaneous differential equations derived, one for the potential in each compartment. In order to simulate the behaviour of the neuron this set of equations must be evaluated numerically, a task which requires considerable computing power and has only recently become feasible. This technique has been applied in studies of pyramidal cells of the cortex and Purkinje cells of the

cerebellum (de Schutter 1994).

Cable theory can also be applied to the study of complex dendritic trees but it is limited to passive systems (Jack 1979, Rall 1989). As with compartmental modelling the neuron is divided, but here the properties of each section are modelled with a passive low-pass filter circuit. These sections can then be combined analytically to find the membrane potential at any point within the tree. Cable theory has been used to study passive models of fly photoreceptors and LMCs (van Hateren 1986a, van Hateren and Laughlin 1990).

A major decision when developing a model of a neural system is the level of complexity to include (Rall 1995), and as the number of neurons in a model increases, their complexity typically decreases. A common approximation is the integrate-and-fire neuron which emulates the behaviour of a spiking cell without the computational burden of the Hodgkin-Huxley equations for the ion channels. A leaky integrator (see section 2.1.3) filters the inputs to the cell passively and if the filtered input exceeds a set threshold a spike is produced. In order to model the refractory period of the cell after the spike, either the integrator is reset or the threshold is increased, decaying slowly back to the previous value.

The use of simple model neurons in large networks reduces the computational complexity of the network but might omit subtle effects created by the actual processing performed by each neuron in the biological system. On the other hand complex models of single cells which describe the properties of ion channels, dendritic trees, etc. may provide an understanding of the processing capabilities of the cell but are often too large and complex to include in simulations involving more than only a very small number of neurons.

Several computer programs have been written to aid the development of complex neural models (Murre 1995) including GENESIS (Bower and Beeman 1995). These provide the mathematical machinery necessary to run the simulations and provide templates for the different types of neuron models. One aim of these systems is to encourage scientists to use a common framework for their models, allowing data and results to be shared more easily (Wilson and Bower 1989).

A radical new approach to modelling began in the late 1980s when the similarity between the processing performed by neurons and the properties of analogue electronic components was realised (Mead 1989). This led to the field of

research which became known as "neuromorphic engineering", a combination of modelling neural systems and developing useful electronic circuits where, instead of using only a few high speed, high precision digital components to process data, as in a modern computer, many low speed, low precision analogue components process the data in parallel, as in a neural system. From the point of view of modelling, these models operate in a similar way to a neural system (analogue voltages, continuous time) and may reveal fundamental issues about the dynamics of real neurons that are obscured in computer simulations (Douglas, Mahowald and Mead 1995).

A number of models of visual processing have been produced. An early success of this approach was the silicon retina (Mahowald and Mead 1991). Using only a single integrated circuit the responses of the vertebrate retina were approximated, including adaptation. A number of developments since this original work include models of an adapting photoreceptor (Delbrück and Mead 1994), the fly retina (photoreceptors and LMCs) (Liu in press) and directionally selective neurons (Harrison and Koch in press). The LGMD model proposed by Hatsopoulos et al. (1995) has also been implemented (Indiveri in press).

Neuromorphic models have also been developed for single neurons (Mahowald and Douglas 1991) which describe the behaviour of voltage-dependent ion channels. These will form the basis of an ambitious project nicknamed the "silicon cortex", an attempt to understand the complex dynamics of cortical information processing (Douglas, personal communication).

1.3 Overview of this thesis

The aim of the research described in this thesis was the development of a biologically inspired neural network for detecting approaching objects based on the lobula giant movement detector (LGMD) system of the locust. Particular emphasis was given to aspects of the biological system not considered previously. This thesis presents the results of the individual areas of research in separate chapters which include the specific methods and discussions. In addition, chapters describing the general methods and overall conclusions are included.

Chapter 2 outlines several of the methods used during this project. The key

simulation and mathematical techniques are described along with the method developed for generating visual stimuli.

Chapter 3 describes the neural network model of the LGMD system published by Rind and Bramwell (1996). The dependence of the model's responses on the shape of the stimulus is revealed and the cause of this dependence is identified. A modification of the model, presented in chapter 4, removes this dependence and allows the model to respond to more complex stimuli.

In chapter 5 two models of a locust photoreceptor are described. These models were developed with the aim of producing a detailed model of a light-adapting photoreceptor which could be used to study the responses of the LGMD to natural scenes. The first model, an electrical model of the cell membrane which describes the principal ionic conductances, was found to be overly complex for use in large scale simulations. However, the model was used to calculate the conductance change produced by an individual photon from the photoreceptor's impulse response. The second photoreceptor model, which is suitable for large scale simulations, uses two leaky integrators to mimic the effects of light adaptation on the photoreceptor's response.

An electrical model of the lamina region of the optic lobe based on those described by Shaw (1975) and Zimmerman (1978) is described in chapter 6. This model was used to study the proposal that inhibition in the lamina is produced by electrical presynaptic inhibition and to assess the possible effects of this inhibition on the visual input to the LGMD. The responses of the model correspond well with those measured from the LMCs of locusts and other insects. Possible mechanisms for generating the ON and OFF cell responses of the LGMD system are proposed.

Finally, chapter 7 draws conclusions from the results of the simulations and outlines future directions of research.

Chapter 2

Methods

The details of the mathematical models developed during this study are presented in later chapters of this thesis. However, the techniques that were common to several models are described here.

This chapter describes:

- the simulation techniques, which comprise the MATLAB environment, numerical integration and a leaky integrator model.
- a method for generating stimuli "offline", giving the rationale for this approach and the mathematics used.

2.1 Simulation

2.1.1 Environment

Simulations were performed using MATLAB (Cambridge Control Systems, Cambridge) running on a Silicon Graphics Indigo^2 Extreme workstation (Silicon Graphics Ltd., Manchester). To obtain maximum processing speed the parameter search described in section 5.1 was written with the C programming language. The operating system of the workstation was IRIX 5.3.

MATLAB was chosen because it simplified program development by providing a straightforward yet versatile scripting language and also predefined modules

for producing graphs, user interfaces, etc. The mathematical engine within MATLAB is designed for computation using matrices. This was exploited for the neural network simulations where calculations for each element of a given type within the network were performed using a single equation instead of one equation for each element. Another useful feature is the ability to write extra modules in the C programming language which can be called from within a MATLAB script. This provides a significant increase in speed with program structures such as loops for which the scripting language is not suited, and several extra modules were written to aid the curve fitting procedure described in section 5.1.

2.1.2 Numerical integration

Many of the simulations required the evaluation of ordinary differential equations. The evaluation method selected was fourth-order Runge-Kutta numerical integration (Cheney and Kincaid 1994) which provides a good compromise between calculation speed and numerical accuracy (Jeffrey 1989).

For a set of differential equations

$$\frac{d\mathbf{X}}{dt} = \mathbf{F}(t, \mathbf{X}), \tag{2.1}$$

where $\mathbf{X}$ is a vector and $\mathbf{F}$ is the set of equations of equal size, the value of $\mathbf{X}$ after the next time step h is given by

$$\mathbf{X}(t+h) = \mathbf{X}(t) + \frac{h}{6}(\mathbf{F}_1 + 2\mathbf{F}_2 + 2\mathbf{F}_3 + \mathbf{F}_4), \tag{2.2}$$

where h is the time step. Four estimates of the gradient, $\mathbf{F}_{1..4}$, are calculated for each iteration using the equations

$$\begin{aligned} \mathbf{F}_1 &= \mathbf{F}(\mathbf{X}(t)), \\ \mathbf{F}_2 &= \mathbf{F}(\mathbf{X}(t) + \tfrac{1}{2}h\mathbf{F}_1), \\ \mathbf{F}_3 &= \mathbf{F}(\mathbf{X}(t) + \tfrac{1}{2}h\mathbf{F}_2), \\ \mathbf{F}_4 &= \mathbf{F}(\mathbf{X}(t) + h\mathbf{F}_3). \end{aligned} \tag{2.3}$$

2.1.3 Leaky integrator

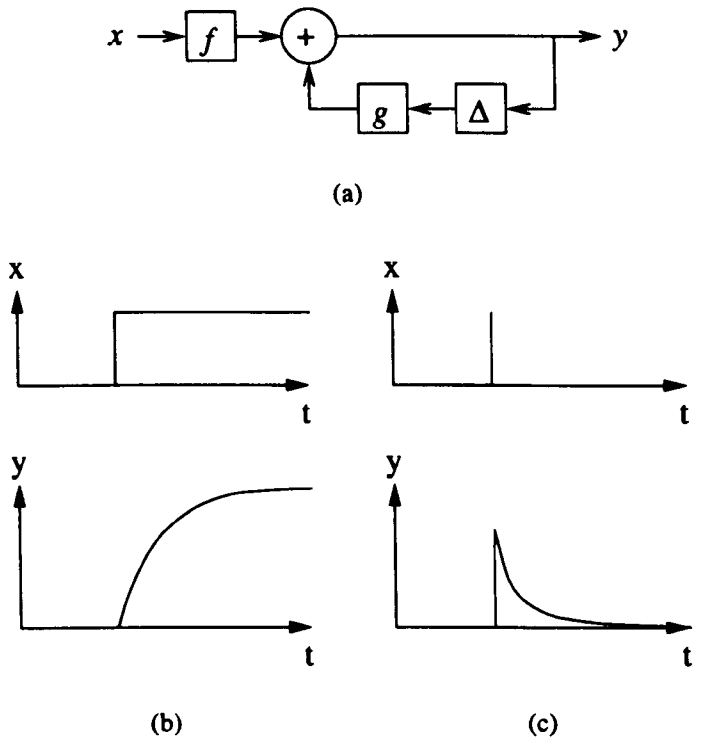

Figure 2.1: (a) Structure of a discrete-time leaky integrator. x, input; y, output; f, feedforward weight; g, feedback weight; Δ, delay of one time step. (b) Response to a step input rises exponentially to a steady-state. (c) Response to an impulse is a sudden peak followed by exponential decay back to the baseline.

Several of the models use a discrete time leaky integrator. In response to a step input this produces an output which rises exponentially to the steady-state value, while an impulse input produces a sudden rise in output which decays exponentially. Figure 2.1 shows the structure of the integrator and illustrates these two responses.

The time constant of the exponential rise of the step response and decay of the impulse response is set by the value of the feedback weight g which is given by

$$g = \left(\frac{1}{e}\right)^{\frac{\delta t}{\tau}}, \tag{2.4}$$

where τ is the time constant and δt is the time step. For the output to be stable g must be less than 1, which is satisfied by all positive integer values of τ and δt. The steady-state gain is specified by the feedforward weight f which is given by

$$f = G*(1-g), \tag{2.5}$$

where G is the required steady-state gain.

It is important to note here that, while this leaky integrator is useful for modelling the responses of many systems to prolonged changes of input, its response to impulse inputs is less general. For a rapid system where the impulse produces an immediate response which decays slowly, such as synaptic transmitter release, the use of this leaky integrator model is appropriate. However, for systems where the peak of the impulse response occurs some time after the impulse, as is the case for most photoreceptors responding to brief flashes of light, this leaky integrator is not a good model. In this study, the use of leaky integrators is confined to situations where the input is prolonged.

2.2 Generation of stimulus files

As mentioned in chapter 1 the photoreceptors in the compound eyes of the locust have wide and overlapping receptive fields. An important part of this study was to examine the effect of these receptive fields on subsequent processing of visual information and the method of "offline" stimulus generation described here was developed.

2.2.1 Rationale for "offline" stimulus generation

For all the simulations described in this thesis, there is no feedback from the model to the visual world (i.e. no motor output) and a given stimulus is identical in every simulation. Therefore, it is more efficient for complex stimuli, or for complex receptive fields, to be processed "offline" and saved to disk, prior to running any simulations. The stimuli can then be used repeatedly without further need to process the visual information.

2.2.2 Method

To facilitate processing both complex stimuli and complex receptive fields the IRIS GL graphics commands of a Silicon Graphics Indigo^2 Extreme workstation are exploited. Conceptually, the stimulus is drawn on the monitor screen in the usual way (Judge and Rind 1997) and the view of each photoreceptor in the "eye", which is located a specified distance from the centre of the screen, is calculated.

The detailed steps of the method are summarised in figure 2.2.

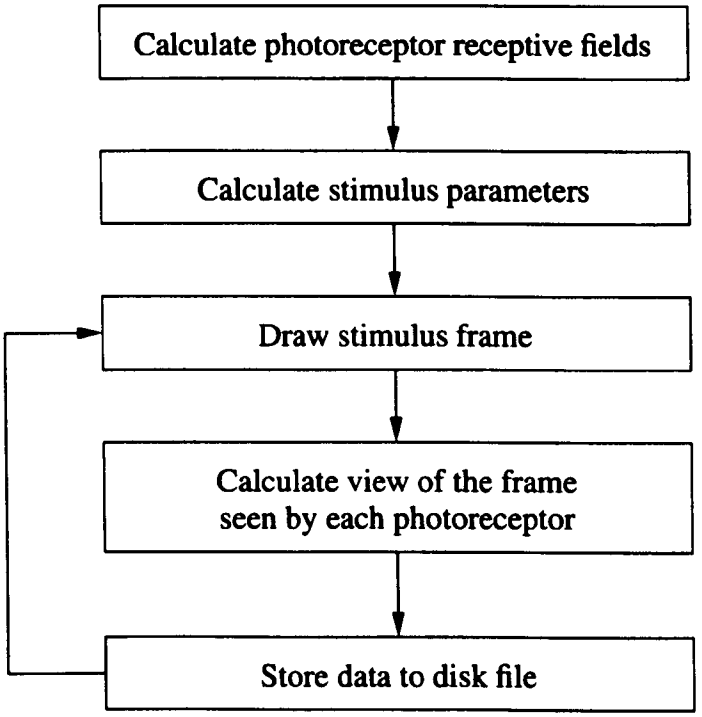

Figure 2.2: Method for "offline" generation of stimulus files. The details for each stage of the method are given in the text.

The receptive fields of the photoreceptors, which are modelled with a symmetrical 2-dimensional Gaussian distribution (figure 2.3), are calculated by finding the position of the optical axes on the screen and a weighted sum of the surrounding pixels.

The geometry of the stimulus system is shown in figure 2.4 where the eye is a distance z away from the screen. The position of the optical axis of a photoreceptor

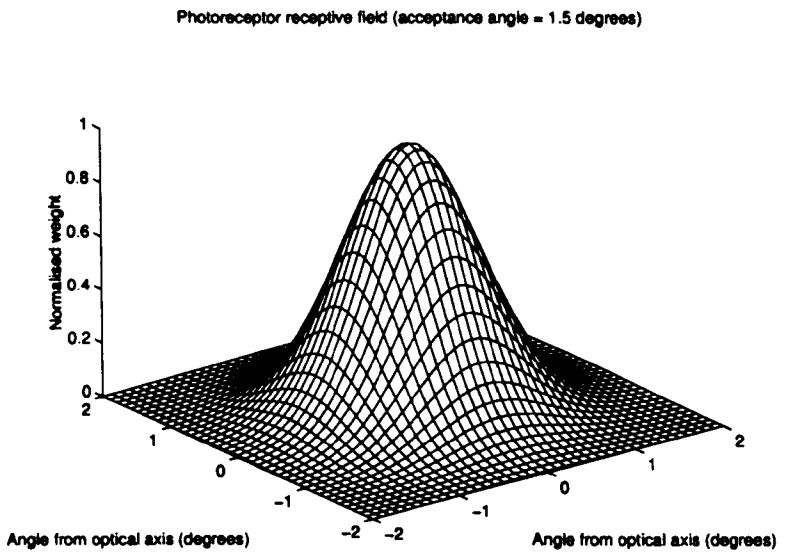

Figure 2.3: Example of the symmetrical Gaussian distribution used to model the receptive field of a locust photoreceptor. The acceptance angle for the graph was 1.5°.

(the centre of the receptive field) on the screen, (x_a, y_a, z), is calculated using

$$x_a = z \tan \alpha_x, \tag{2.6}$$

where x_a is the horizontal distance of the optical axis from the centre of the "eye" and α_x is the angular distance between the optical axis and the centre of the "eye" horizontally, and

$$y_a = z \tan \alpha_y, \tag{2.7}$$

where y_a is the horizontal distance of the optical axis from the centre of the "eye" and α_y is the angular distance between the optical axis and the centre of the "eye" vertically.

For a pixel at point (x_p, y_p, z), the angular distance θ from the optical axis is given by

$$\theta = \arccos \frac{\underline{a}.\underline{p}}{|a||p|}, \tag{2.8}$$

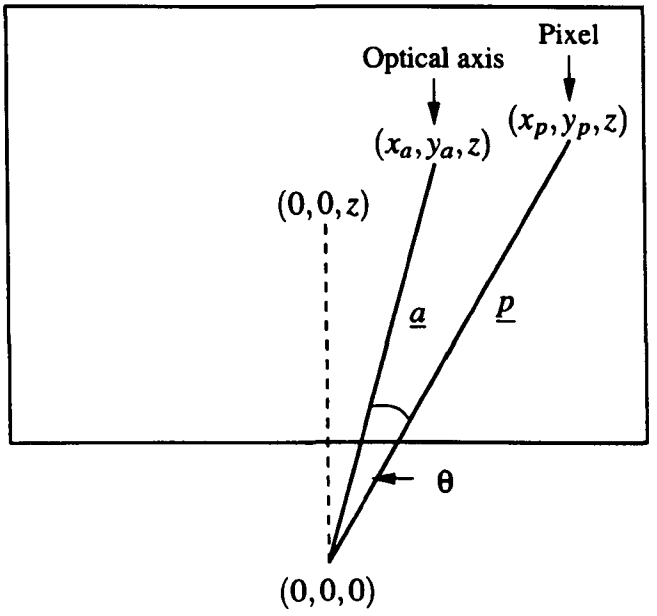

Figure 2.4: Calculation of the receptive field of a photoreceptor. The centre of the "eye", located at (0,0,0), views the centre of the screen (0,0,z), where z is the distance of the "eye" from the screen. The position of the optical axis of the receptive field on the screen is (x_a, y_a, z) and the vector from the "eye" is $\underline{a}$. For a pixel at (x_p, y_p, z), the vector $\underline{p}$ is an angle θ from the vector $\underline{a}$. The calculation of the weight for this pixel is given in the text.

where $\underline{a}$ is the vector from (0,0,0) to (x_a, y_a, z), $\underline{p}$ is the vector from (0,0,0) to (x_p, y_p, z), $|a|$ and $|p|$ are the lengths of the vectors and $\underline{a}.\underline{p}$ is the scalar product.

Knowing θ, the weight of the pixel for a symmetrical Gaussian distribution with a half-width (acceptance angle) of ω is given by

$$weight = \exp \frac{-\theta^2}{2\sigma^2}, \tag{2.9}$$

where

$$\sigma = \sqrt{\frac{-\left(\frac{\omega}{2}\right)^2}{2\ln(0.5)}}. \tag{2.10}$$

The perspective of the graphics system is matched to the distance of the "eye" from the screen to ensure that the stimuli move correctly relative to the "eye". The

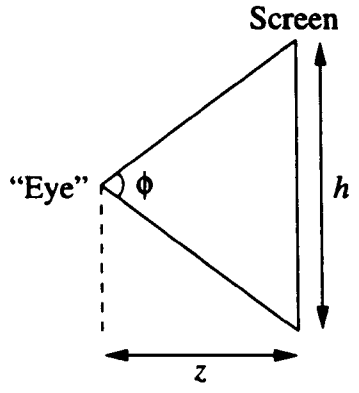

Figure 2.5: Perspective of the stimulus system. The "eye" is a distance z from the screen which has a height h. The angle ϕ is the angular size of the screen at the "eye". See text for calculation of ϕ.

angular size of the screen as seen by the "eye" is given by

$$\phi = 2 \arctan \frac{h}{2d}, \tag{2.11}$$

where ϕ is the angular size of the screen, h is the height of the screen and z is the distance from the "eye" to the screen as before. Figure 2.5 illustrates these parameters. The value of ϕ is used to initialise the graphics calculations performed by the workstation using the `perspective` command.

Stimuli are generated by specifying the initial and final positions and size of an object and the speed of movement. For an initial position of $(x_{init}, y_{init}, z_{init})$ and a final position of $(x_{fin}, y_{fin}, z_{fin})$, the total distance of movement, d, is given by

$$d = \sqrt{(x_{fin} - x_{init})^2 + (y_{fin} - y_{init})^2 + (z_{fin} - z_{init})^2}. \tag{2.12}$$

The time, t, required to move this distance at the required speed, s, is given by

$$t = \frac{d}{s}, \tag{2.13}$$

and the number of time steps, n, needed is given by

$$n = \frac{t}{\delta t}, \tag{2.14}$$

where δt is the size of the time step.

The changes in position of the object between each time step are given by

$$d_x = \frac{x_{fin} - x_{init}}{n}, d_y = \frac{y_{fin} - y_{init}}{n}, d_z = \frac{z_{fin} - z_{init}}{n}, \tag{2.15}$$

where d_x, d_y and d_z are the changes in the x, y and z directions respectively.

For all the neural network simulations described in this thesis, a time step of 1ms was chosen as a compromise between speed and accuracy.

For each frame, the stimulus is advanced by one time step. The view seen by a photoreceptor is calculated by reading the value of each pixel within the receptive field, multiplying by the weights, adding and normalising. This is given by

$$v = \sum_{i=1}^{n} (w_i . p_i) / \sum_{i=1}^{n} w_i, \tag{2.16}$$

where v is the view of a photoreceptor and w_i is the weight of pixel p_i, with a total of n pixels within the receptive field.

This method allows complex stimuli to be viewed by "eyes" with complex receptive fields. However, there are two limitations. The first problem is that when the "eye" is positioned close to the screen, the number of pixels seen by each photoreceptor is small. This adds noise to the stimulus, which appears to move in a series of jumps rather than smoothly, and the amount of noise is greater for slower moving stimuli. The noise could be reduced by using anti-aliasing which blends the pixels around the edges of the object according to the amount of each pixel the object covers. Unfortunately, anti-aliasing was not available on the workstation used.

The other problem is the speed of operation. With large "eyes", and particularly those where the photoreceptor receptive fields overlap, the time required to generate a stimulus is long. For example, an "eye" with 2900 photoreceptors, an acceptance angle of 1.5° and an angular separation of 1.25° required more than

24 hours to generate a 5 second stimulus. The speed can be increased by moving the "eye" closer to the screen but the pixel noise described above increases. A compromise has to be made between pixel noise, speed and the eye parameters (overlapping receptive fields require that many pixels are read multiple times by the program).

Chapter 3

Evaluating the Rind-Bramwell LGMD model

The obvious place to begin to develop a comprehensive model of the circuitry of the LGMD system is with the existing neural network model of Rind and Bramwell (1996). Using the original C program for reference, the model was rewritten in the MATLAB scripting language with the cell's outputs normalised and minor rounding errors corrected. However, the stimulus system, which was an integral part of the earlier program, was replaced with an offline stimulus generation system (section 3.2). This allowed new stimuli to be presented to the model and led to the discovery that the responses of the model are strongly dependent on the shape of the stimulus for certain directions of movement. This dependence is at odds with the responses of the biological system, which produces consistent responses for several stimulus shapes (Rind and Simmons 1992).

This chapter describes:

- the processing performed by the model.
- the method used to generate the new stimuli.
- the responses of the model, highlighting the dependence on the shape of the stimulus and identifying the cause of this dependence.

3.1 Structure

Although the structure of the model was described thoroughly in the original paper it is useful to repeat it here in order to reveal inaccuracies in the original description and to simplify the description of the modified model presented in chapter 4. This description applies to the rewritten MATLAB version, which differs only slightly from the earlier C model.

Figure 3.1 illustrates the structure of the model. The network consists of an array of 289 retinotopic units which comprise four cell types: P (photoreceptive), E (excitatory), I (inhibitory) and S (summing). There is also one F (feed-forward inhibition) cell and the LGMD cell.

The P cells are the input elements of the model and each views a single point in space. These points are arranged in rings with each ring separated from the next by 3.3° (figure 3.2). Any change in the light intensity within its receptive field produces an output from a cell. Formally these properties can be described by

$$S(\theta) = \begin{cases} 1 & \text{for } \theta = 0^{\circ}, \\ 0 & \text{otherwise}, \end{cases} \tag{3.1}$$

where $S(\theta)$ is the sensitivity of the cell at θ° from the centre of the cell's receptive field, and

$$P_{out}(t) = \begin{cases} 1 & \text{for } P_{in}(t) \neq P_{in}(t-1), \\ 0 & \text{otherwise}, \end{cases} \tag{3.2}$$

where $P_{in}(t)$ and $P_{out}(t)$ are the input and output of the cell at time t respectively and $P_{in}(t-1)$ is the input at time $t-1$. These properties combine to produce a pulse when the edge of an object crosses the receptive field (figure 3.1).

The outputs of the P cells pass down the network retinotopically to the E and I cells. When these cells receive a pulse they fire, provided they are not within their refractory period. After firing, when the output is maximal, the output decays exponentially until another pulse is received (figure 3.1). Taking $t = 0$ as the time

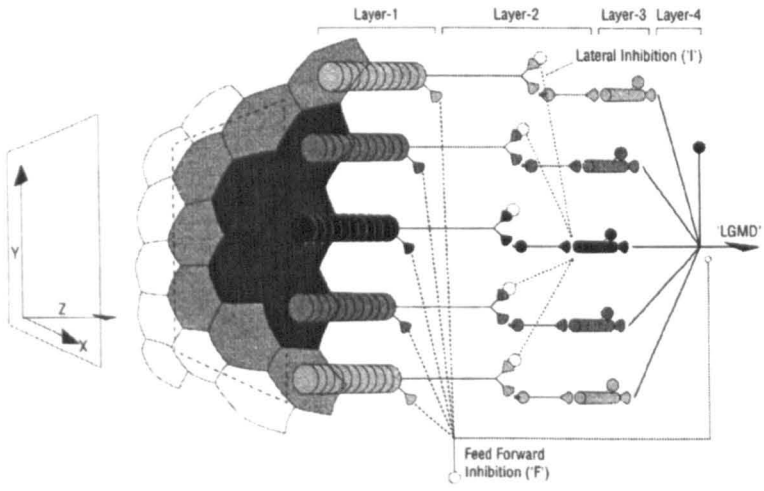

(a)

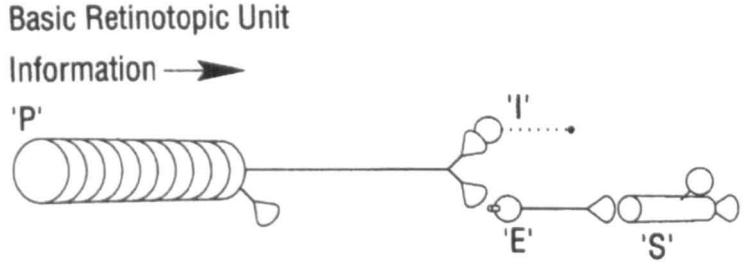

(b)

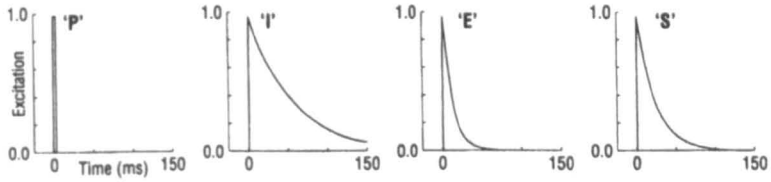

(c)

Figure 3.1: The Rind and Bramwell neural network model of the LGMD. (a) Structure of the network. (b) Structure of the retinotopic units. (c) Responses of the cells. See text for details. P, photoreceptive cell; I, inhibitory cell; E, excitatory cell; S, summing cell. From Rind and Bramwell (1996).

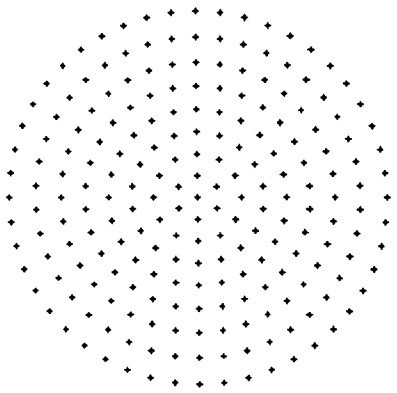

Figure 3.2: Distribution of the receptive fields of the input P cells. The fields are evenly spaced around rings separated by 3.3°.

of the last firing, the output of an E cell can be written as

$$E_{out}(t) = \begin{cases} 1 & \text{for } P_{out}(t) = 1 \text{ and } t > T_{refract_E}, \\ \exp(-\frac{t}{\tau_E}) & \text{otherwise,} \end{cases} \tag{3.3}$$

where $E_{out}(t)$ is the output of the cell at time t, $T_{refract_E}$ is the refractory period and τ_E is the time constant of the cell's decay, and the output of an I cell can be written as

$$I_{out}(t) = \begin{cases} 1 & \text{for } P_{out}(t) = 1 \text{ and } t > T_{refract_I}, \\ \exp(-\frac{t}{\tau_I}) & \text{otherwise,} \end{cases} \tag{3.4}$$

where $I_{out}(t)$ is the output of the cell at time t, $T_{refract_I}$ is the refractory period and τ_I is the decay time constant of the cell.

Whilst the outputs of the E cells project retinotopically onto the S cells, the outputs of the I cells form a lateral inhibitory network by projecting to the nearest and next-nearest neighbouring S cells (figure 3.1). The lateral projections are delayed relative to the E cell responses and are weighted. The input to an S cell can be written as

$$S_{in}(t) = E(t) - \frac{w_n}{6}\sum_{c=1}^{6} I_{n,c}(t-\Delta_n) - \frac{w_{nn}}{12}\sum_{c=1}^{12} I_{nn,c}(t-\Delta_{nn}), \tag{3.5}$$

where $S_{in}(t)$ is the S cell input at time t, $E(t)$ is the E cell output, $I_{n,c}(t-\Delta_n)$ is the output of cth of 6 nearest neighbour I cells at time $t-\Delta_n$ and $I_{nn,c}(t-\Delta_{nn})$ is the output of cth of 12 next-nearest neighbour I cells at time $t-\Delta_{nn}$. w_n and w_{nn} are the weights and Δ_n and Δ_{nn} are the delays for the connections from the nearest and next-nearest neighbours respectively within the lateral inhibitory network.

The outputs for the S cells are calculated in a similar way to the outputs of the E and I cells (figure 3.1), but a firing threshold must be exceeded for the S cells to fire. Assuming that a cell last fired at time $t=0$, this can be written as

$$S_{out}(t) = \begin{cases} 1 & \text{for } S_{in}(t) > S_{Thresh} \text{ and } t > T_{refract_S}, \\ \exp(-\frac{t}{\tau_S}) & \text{otherwise,} \end{cases} \tag{3.6}$$

where $S_{in}(t)$ and $S_{out}(t)$ are the input and output from the cell at time t respectively, S_{Thresh} is the firing threshold, $T_{refract_S}$ is the refractory period of the cell and τ_S is the time constant of the decay of the cell's output.

Inspection of the original program revealed that the calculations performed by the LGMD and F cells differed from that described in the paper. Instead of the linear summation of S and F cell inputs by the LGMD, representing subtraction by the feed-forward inhibition, the F cell output effectively divides the sum of the S cell outputs, modelling more closely shunting inhibition.

Feed-forward inhibition, carried by the F cell, is generated when the number of P cells active at one time exceeds a threshold. The input to the F cell is given by

$$F_{in}(t) = \begin{cases} LGMD_{out}(t).\frac{1}{N}\sum_{i=1}^{N} P_{out_i}.\delta_F & \text{for } \frac{100}{N}\sum_{i=1}^{N} P_{out_i} > F_{Thresh}, \\ 0 & \text{otherwise,} \end{cases} \tag{3.7}$$

where $F_{in}(t)$ is the input to the F cell at time t, $LGMD_{out}(t)$ is the output of the LGMD, P_{out_i} is the output of the ith P cell, δ_F is the gradient of the F cell's activation and F_{Thresh} is the threshold for activation, expressed as a percentage of the

total number of P cells, N. The strength of the subsequent inhibition is given by

$$F_{out}(t) = F_{out}(t-1).F_{in}(t).\left(\frac{100 - decay_F}{100}\right), \tag{3.8}$$

where $decay_F$ represents the rate of decay of the output.

The output of the LGMD is given by the linear sum of the S cell activity minus the F cell output and can be written as

$$LGMD_{out}(t) = \frac{1}{N}\sum_{i=1}^{N} S_{out_i}(t) - F_{out}(t - \Delta_F), \tag{3.9}$$

where $LGMD_{out}(t)$ is the output of the LGMD at time t, N is the total number of S cells in the model, $S_{out_i}(t)$ is the output of the ith S cell at time t and $F_{out}(t-\Delta_F)$ is the output of the F cell at time $t-\Delta_F$. Δ_F represents the delay in the feed-forward inhibition projection. The feedback of the LGMD output into the calculation of the feed-forward inhibition results in a shunting-type inhibition.

The values of the parameters used during the simulations are shown in table 3.1.

LGMD model parameter values							
E cell		I cell		S cell		F cell	
τ_E	11.11ms	τ_I	50ms	τ_S	20ms	$decay_F$	5
$T_{refract_E}$	0ms	$T_{refract_I}$	0ms	$T_{refract_S}$	2ms	δ_F	25
		w_n	170%	S_{thresh}	10%	F_{thresh}	5%
		Δ_n	2ms			Δ_F	4ms
		w_{nn}	70%				
		Δ_{nn}	4ms				

Table 3.1: LGMD model parameter values

3.2 Stimuli

Stimuli for the model were generated using the offline scheme shown in figure 2.2. However, the method for calculating the view of each photoreceptor (the P cells

in this model) described in section 2.2.2 was unsuitable due to the small receptive fields used in this model, as the point viewed by a P cell often fell between pixels on the screen. Instead, a method was adopted which calculated the view of each cell rather than rendering the stimulus on the computer monitor screen and "viewing" it. This method produces the exact view of the stimulus.

The positions of the view points of the P cells were calculated along with the positions of the edges of the stimulus object. These positions were compared to find which P cells were viewing the object and which were viewing the background. These views were stored in disk files for later use.

This method is best suited for use with simple stimuli comprising only a few objects with uniform intensity against a uniform background. For more complex stimuli, such as those with textured surfaces, or larger P cell receptive fields, the method described in section 2.2.2 is more suitable.

3.3 Responses

The responses of the model to stimuli comprising squares, rectangles or edges were described in the original study. For this study, extra stimuli were tested. This section compares the responses to squares and circles, highlighting the marked difference between the responses and identifying the cause of this difference.

Figure 3.3 shows the responses to approaching and receding squares. For approaching squares, the responses rise at an increasing rate throughout the movement, and the rate of increase is higher for higher approach speeds. At the end of the movement, the response is highest and may be cut back by the activation of the F cell producing feed-forward inhibition (6m/s and 12m/s). The responses to receding squares reaches a peak after a short time (between 5 and 10ms) and are then strongly inhibited by the F cell.

The responses to circles are shown in figure 3.4. For receding circles, the responses are similar to those for receding squares with a brief peak followed by strong feed-forward inhibition. However, the responses to approaching circles bear no resemblance to the responses to approaching squares. The response to circles approaching at all the speeds simulated shows a series of peaks of approximately the same height for all speeds. After each peak the response either decays

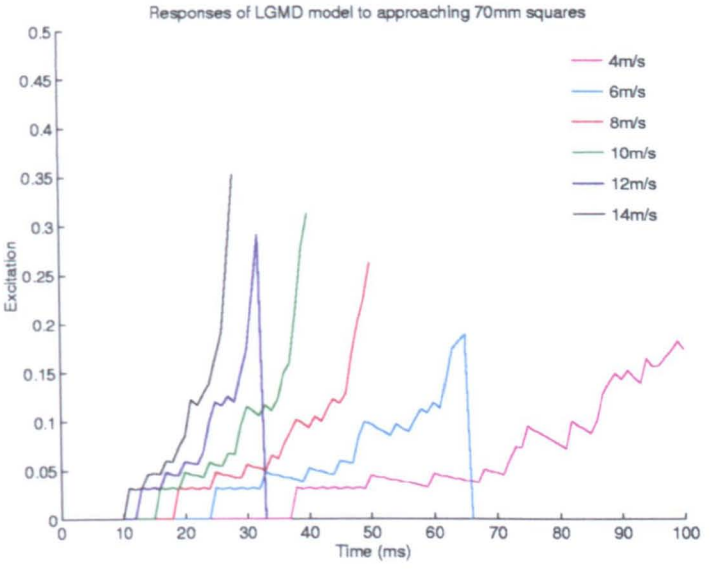

(a)

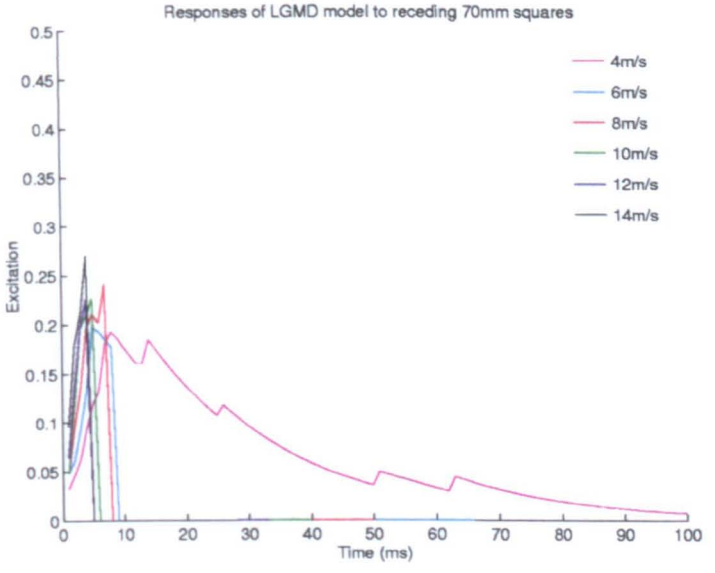

(b)

Figure 3.3: Responses of the model to approaching and receding 70mm squares. The stimuli moved directly towards or away from the model between points 100mm and 500mm distant. The speeds of movement are shown in the graphs. (a) Approaching. (b) Receding.

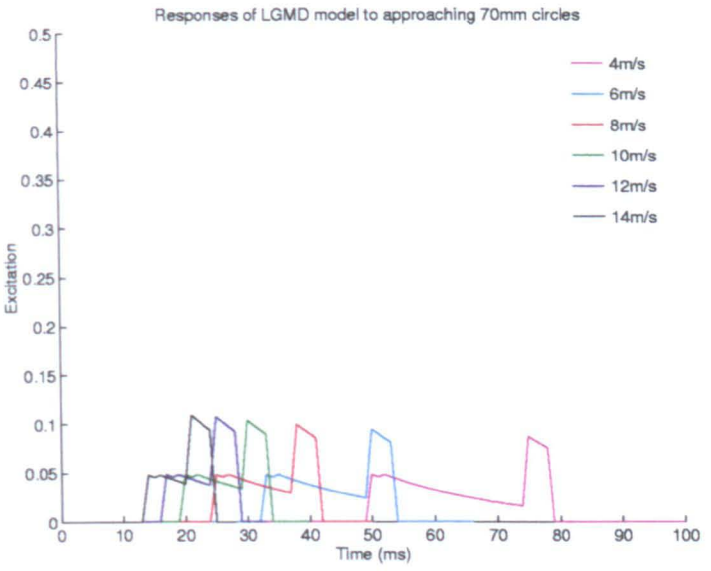

(a)

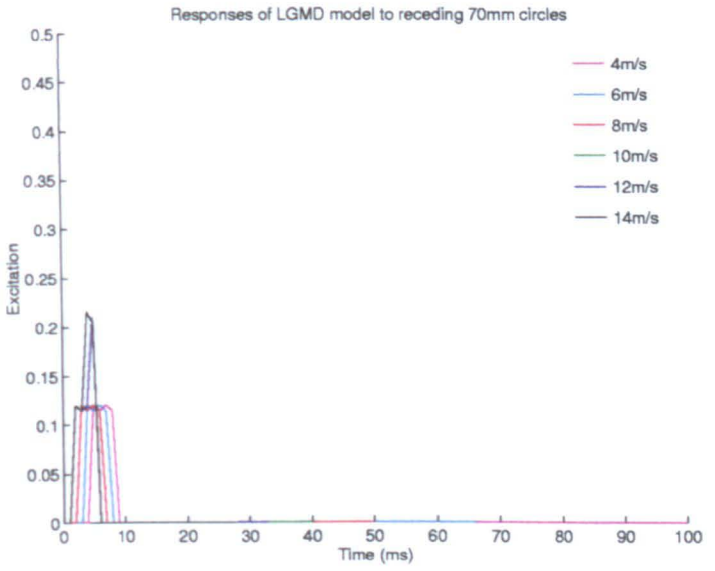

(b)

Figure 3.4: Responses of the model to approaching and receding 70mm circles. The objects moved directly towards or away from the model between points 100mm and 500mm distant. The speeds of movement are shown in the graphs. (a) Approaching. (b) Receding.

exponentially (during the early part of the stimulus) or is inhibited strongly by the F cell.

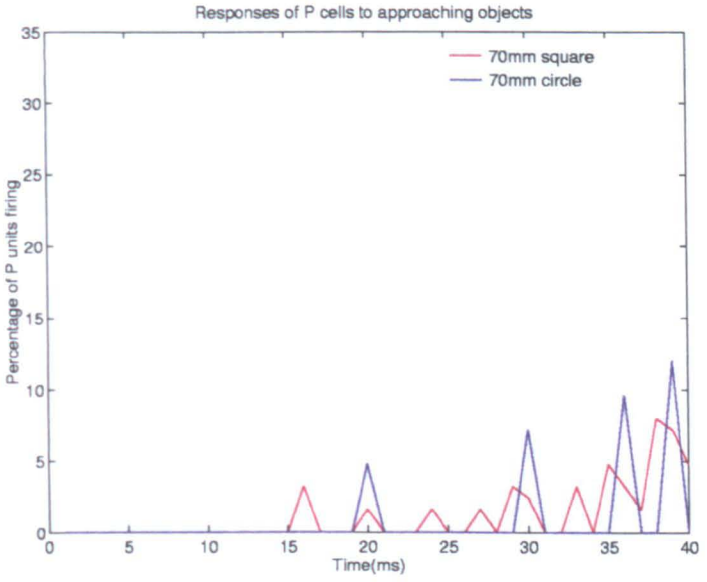

Figure 3.5: Percentage activity in the P cells during the approach of a 70mm square (red line) and a 70mm circle (blue line). The object moved at 10m/s from a distance of 500mm to a distance of 100mm from the model.

The differences in the responses are due to the activity in the P cells during the approach of a square and a circle (figure 3.5). For the square, the activity in the P cells is spread throughout the approach with only a few cells responding at any time until the late stages of the stimulus. This spread of activity results from the P cells usually being able to see at least part of the edge which crosses any given ring of receptive fields in a staggered fashion (figure 3.6 a,c,e).

However, the P cell activity during approach of the circle shows four distinct large peaks in activity separated by periods of no activity. The later peaks are large enough to exceed the threshold for activity in the F cell and produce feed-forward inhibition. The peaks are due to the precise matching of the circle's edge with the circular receptive field distribution when the centres of the model and the circle are aligned: the whole of the edge is seen at one time by one ring of P cells, producing a peak, and is not seen again until the edge crosses the next ring of receptive fields (figure 3.6 b,d,f). This effect is not seen if the centres of the

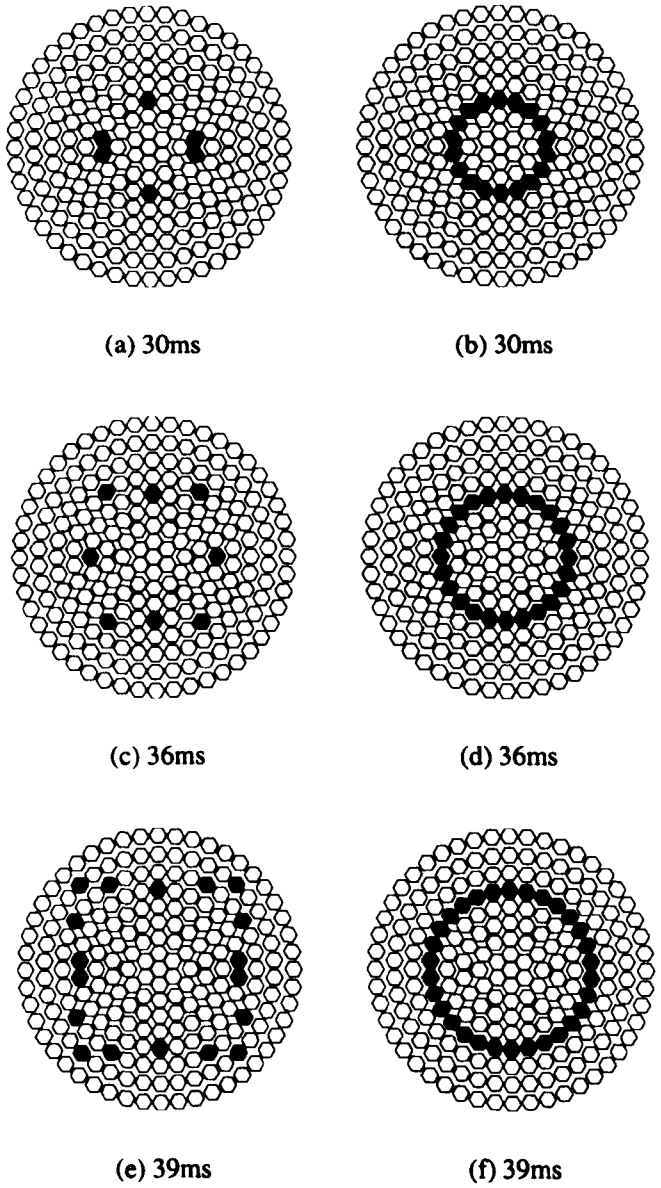

Figure 3.6: The activity in the P cells during the approach of (a,c,e) a 70mm square and (b,d,f) a 70mm circle at 10m/s. The objects moved from 500mm from the model to 100mm from the model.

model and the circle are not aligned: in this case, the response to the edge of the circle is staggered as for the square.

3.4 Reason for shape dependence

The reason for these marked differences in the responses to approaching squares and circles is the size of the P cell receptive fields. Because the receptive fields are single points in space there are large areas of the visual field not seen (see figure 3.2) and when the edge of an object is in these areas there is no response from the P cells. Only when the edge crosses the receptive field of a cell is there a response and if the edge matches the receptive field distribution, there will be a large response which will activate the F cell and inhibit the LGMD cell. For a different distribution of receptive fields the shapes involved would differ but the outcome would be the same.

Receding objects do not show shape dependence because their response is dominated by F cell activity. When any shape moves close to the model a large number of P cells are activated due to the length of the edge and the high speed at which the edges move. This produces an initial peak in the LGMD response and activates the F cell. The subsequent feed-forward inhibition persists for the remainder of the stimulus and suppresses further responses.

3.5 Discussion

The responses of the model are strongly dependent on the shape of the stimulus when the stimulus is aligned with the centre of the model. In contrast, recordings from the locust show that the LGMD responds equally well to several stimulus shapes (Rind and Simmons 1992). Although it is possible that the locust has a similar shape dependence, and that this has never been recorded because the stimuli have never been sufficiently well aligned with the eye, this seems unlikely and suggests that the model must be modified before it can accurately reproduce LGMD responses.

The dependence of the model's responses is due to the small receptive field

size of the P cells which leaves large areas of the visual field uncovered. When the edges of the stimulus are moving in these uncovered areas they are effectively invisible. In the animal each photoreceptor has an acceptance angle of approximately 1.5° (Wilson 1975) and the angular separation of the photoreceptors is 1.25° over much of the eye (Horridge 1978). Consequently the whole of the visual field is covered by greater than 50% photoreceptor sensitivity and the edges of the stimulus are always visible. The next chapter describes the effect of expanding the P cell receptive fields on the model's responses.

Chapter 4

A modified LGMD model

The existing LGMD model of Rind and Bramwell (described in chapter 3) was modified in order to remove the dependence of its responses on the stimulus shape. Both the receptive field and the internal processing of the P cells were changed and the parameters of the other cell types adjusted to produce a model which responds equally well to a variety of stimuli. The model also responds well to textured stimuli.

This chapter describes:

- the modified receptive fields and internal processing of the P cells.
- the responses of this model to a variety of stimulus shapes and to textured stimuli.

4.1 Modifications

In order to cover the whole visual field, the receptive fields of the P cells were expanded using the 2-dimensional Gaussian function described in section 2.2.2. The receptive field distribution was also changed into a hexagonal array (of 17*17 elements) which resembles the distribution (although not the size) of the locust compound eye. The angular separation between receptive fields remained at 3.3° and the acceptance angle was set to 2.0°. Figure 4.1 shows the field-of-view for the model with these parameters, showing almost complete, although not uniform,

coverage of the visual field. The high value for the angular separation was used to extend the field-of-view of the model without the need for extra elements. The acceptance angle was made smaller than the angular separation in order to reduce the overlap between neighbouring P cell receptive fields. This reduced significantly the time needed to generate stimuli.

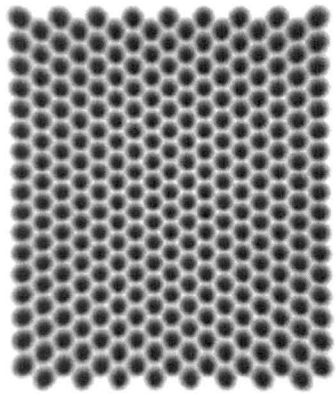

Figure 4.1: Expanded receptive field of the modified LGMD model. The angular separation between neighbouring P cell receptive fields was 3.3° and the acceptance angle of each was 2.0°. Darker areas are more strongly weighted.

The processing in the P cells was modified to take advantage of the larger receptive fields. The change in intensity is compared with a threshold and if the change is greater the P cell is activated. This can be written as

$$P_{out}(t) = \begin{cases} 1 & \text{for } P_{in}(t) - P_{in}(t-1) > P_{thresh}, \\ 0 & \text{otherwise,} \end{cases} \tag{4.1}$$

where $P_{out}(t)$ is the output of the cell at time t, $P_{in}(t)$ and $P_{in}(t-1)$ are the inputs to the cell at times t and $t-1$ respectively and P_{thresh} is the threshold for activity. The addition of the threshold ensures that the cell only responds to significant changes, for example, the passage of an edge across the receptive field.

The remaining processing steps in the model were unchanged but the parameters were adjusted. The refractory periods of the E and I units ($T_{refract_E}$ and $T_{refract_I}$) were set because the expanded receptive fields allow the P cells to re-

spond with a prolonged pulse of activity as an edge moves through their receptive fields. The threshold of the F cell (F_{thresh}) was increased to take account of the greater activity in the model. Table 4.1 shows the parameter values used in the simulations.

Modified LGMD model parameter values							
E cell		I cell		S cell		F cell	
τ_E	5ms	τ_I	25ms	τ_S	5ms	$decay_F$	5
$Trefract_E$	2ms	$Trefract_I$	2ms	$Trefract_S$	2ms	δ_F	25
P_{thresh}	8%	w_n	170%	S_{thresh}	10%	F_{thresh}	16.25%
		Δ_n	2ms			Δ_F	5ms
		w_{nn}	70%				
		Δ_{nn}	4ms				

Table 4.1: Modified LGMD model parameter values

4.2 Stimuli

Stimuli for the model were generated using the offline method shown in figure 2.2. The P cell receptive fields had an acceptance angle of 2.0° and were arranged in a hexagonal array separated by 3.3° from their nearest neighbours. These parameters minimised the overlap between receptive fields while still covering the visual field (figure 4.1). The distance of the "eye" from the screen was set to 100mm, a compromise between the speed of calculation and the noise due to the screen pixels.

Textured stimuli were produced by using texture mapping. The texture was a pattern of squares of random intensity applied to both the stimulus and a background object. The average intensities of the stimulus and background were set to 0.25 and 0.75 relative to the maximum intensity of the graphics system respectively: the maximum and minimum relative intensities in the texture were 0.5 and 0 respectively. A textured square stimulus is shown in figure 4.2.

Before stimuli were presented, the model was adapted to the first frame. This ensured that the model responded only to the edges of the object during a stimulus and not to its appearance.

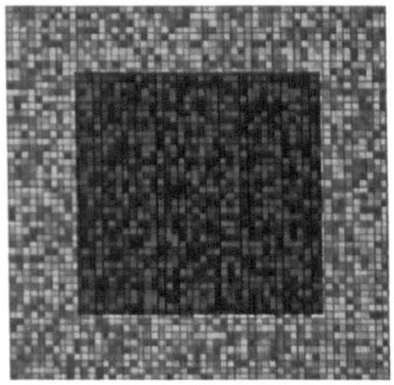

Figure 4.2: A textured square stimulus. The average relative intensity of the square was 0.25 with a maximum of 0.5 and a minimum of 0. For the background, the average was 0.75 with a maximum of 1 and a minimum of 0.5.

4.3 Responses

Figures 4.3, 4.4 and 4.5 show the responses of the modified model to objects approaching and receding at different velocities. The sizes of the shapes were selected so that the perimeters of the objects had an equal length. For all shapes of stimulus the response during approach rises at an increasing rate and the final values are approximately equal. The responses to receding objects all have an initial peak which is inhibited rapidly.

The selectivity of the model for approaching objects is not affected by the size of the stimulus. Figures 4.6, 4.7 and 4.8 show the responses to different sizes of stimulus approaching and receding at 10m/s, with lines of one colour indicating objects with perimeters of equal length. For larger approaching objects the responses are larger and begin earlier than the responses to smaller objects but all the responses rise at an increasing rate. All sizes produce a brief initial peak as the stimulus recedes, followed by rapid inhibition.

Examining the activity in the P cells (figure 4.9) shows that their larger receptive fields produce smoother responses for all stimulus shapes. This removes the dependence of the model on stimulus shape seen with the smaller receptive fields of the original model. The total activity in the P cells is higher than in the old model (figure 3.5) because more of the edge of the object is seen at any time due

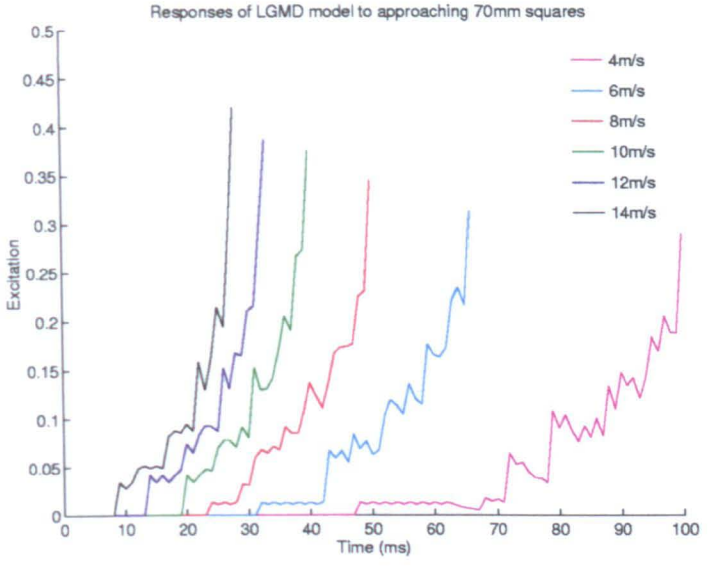

(a)

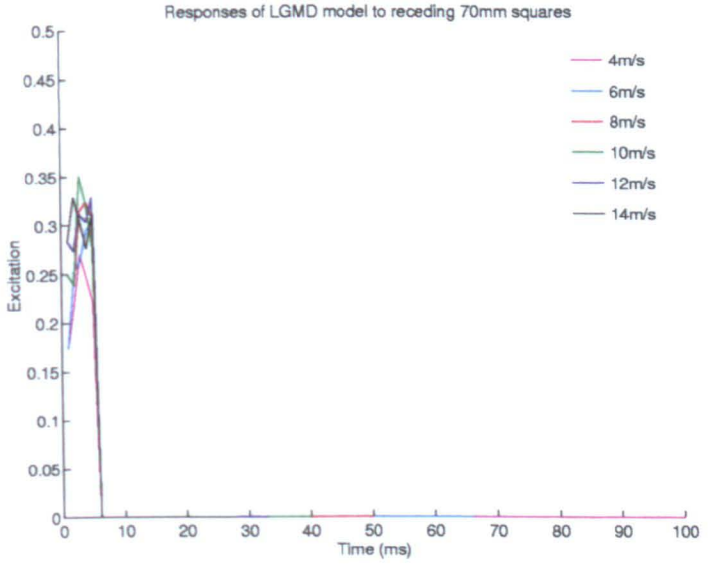

(b)

Figure 4.3: Responses of the model to 70mm squares moving at different velocities. The objects moved between points 500mm and 100mm away from the model. (a) Approaching. (b) Receding.

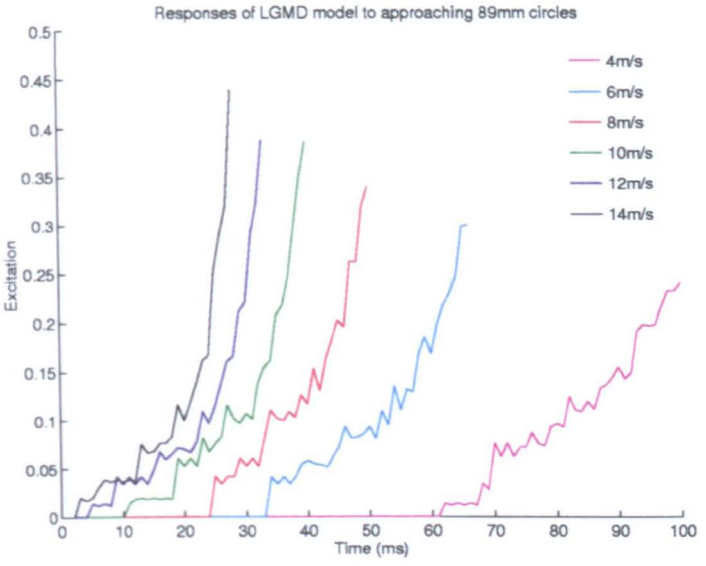

(a)

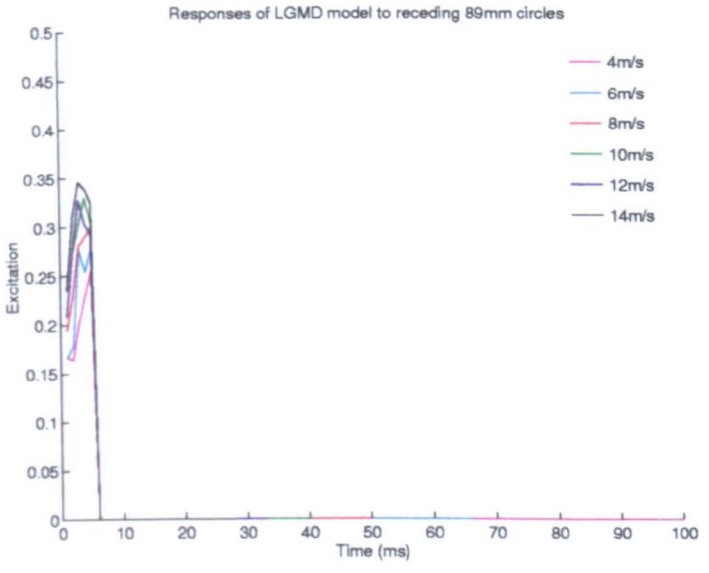

(b)

Figure 4.4: Responses of the model to 89mm circles moving at different velocities. The objects moved between points 500mm and 100mm away from the model. (a) Approaching. (b) Receding.

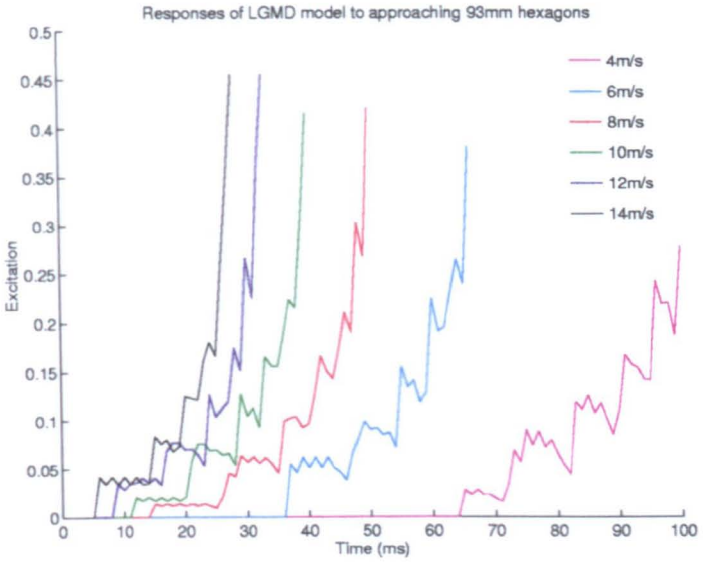

(a)

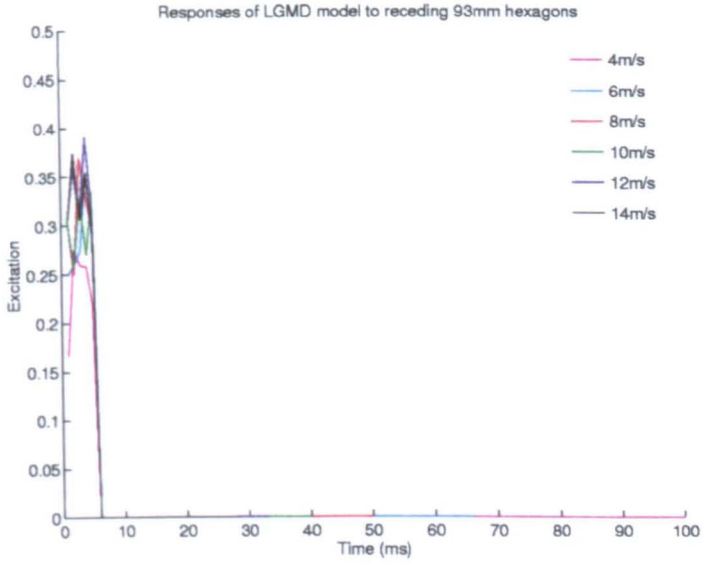

(b)

Figure 4.5: Responses of the model to 93mm hexagons moving at different velocities. The objects moved between points 500mm and 100mm away from the model. (a) Approaching. (b) Receding.

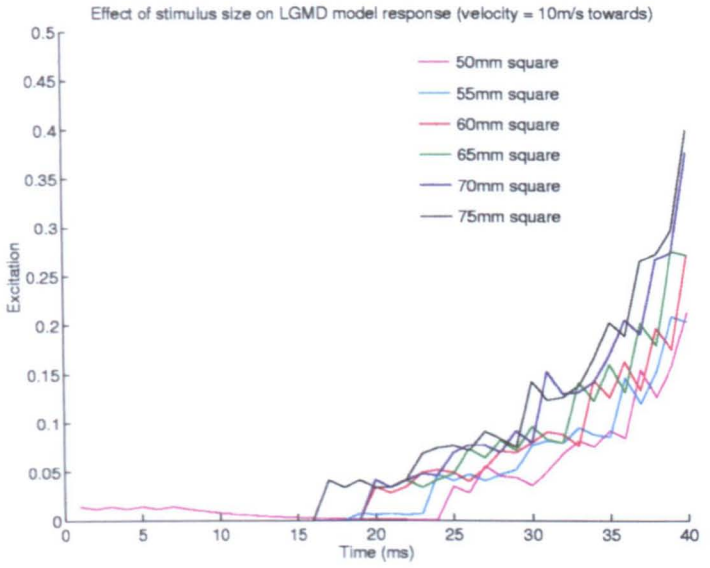

(a)

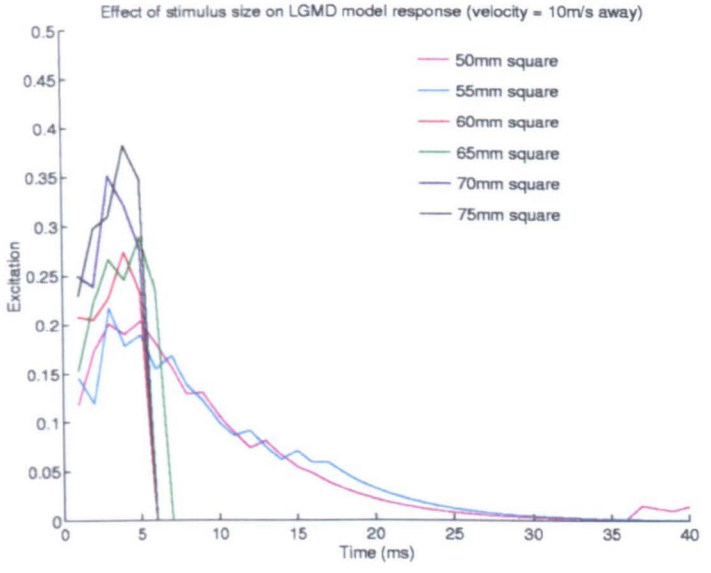

(b)

Figure 4.6: Responses of the model to different sized squares. The objects moved between points 500mm and 100mm away from the model at 10m/s. (a) Approaching. (b) Receding.

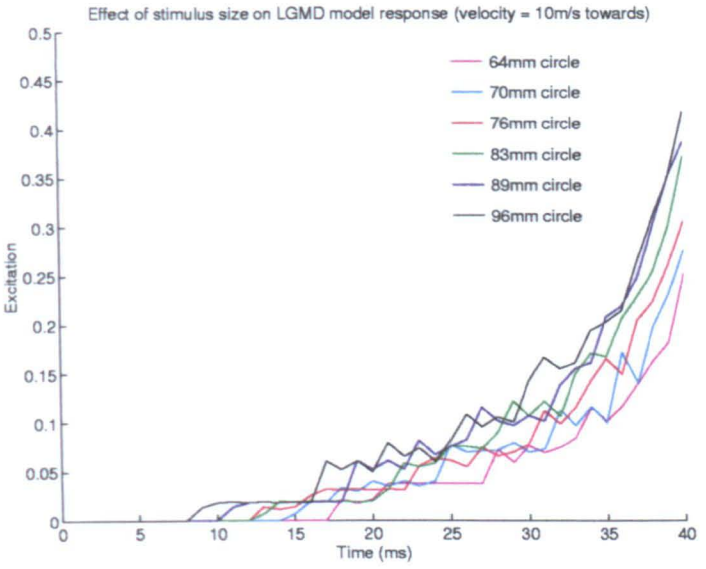

(a)

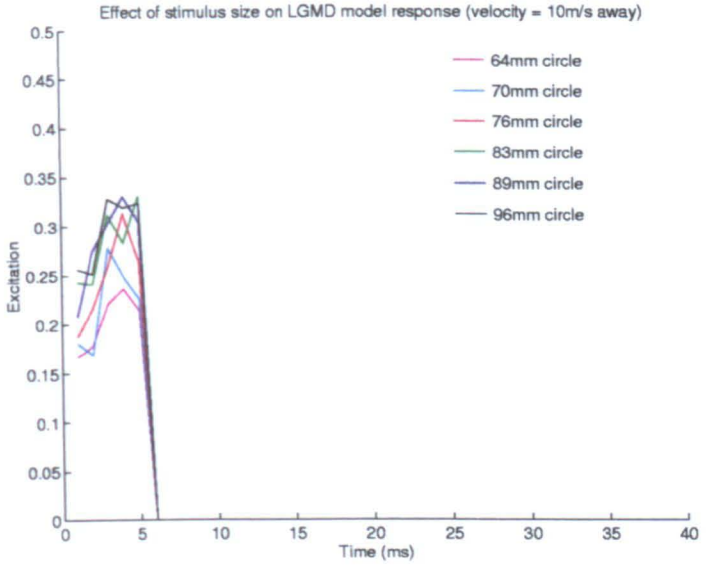

(b)

Figure 4.7: Responses of the model to different sized circles. The line colours indicate objects with perimeter lengths equal to the squares in figure 4.6. The objects moved between points 500mm and 100mm away from the model at 10m/s. (a) Approaching. (b) Receding.

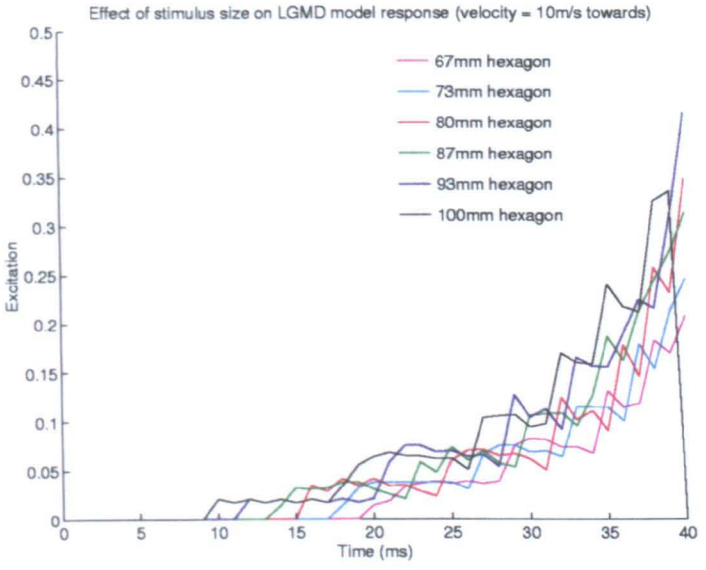

(a)

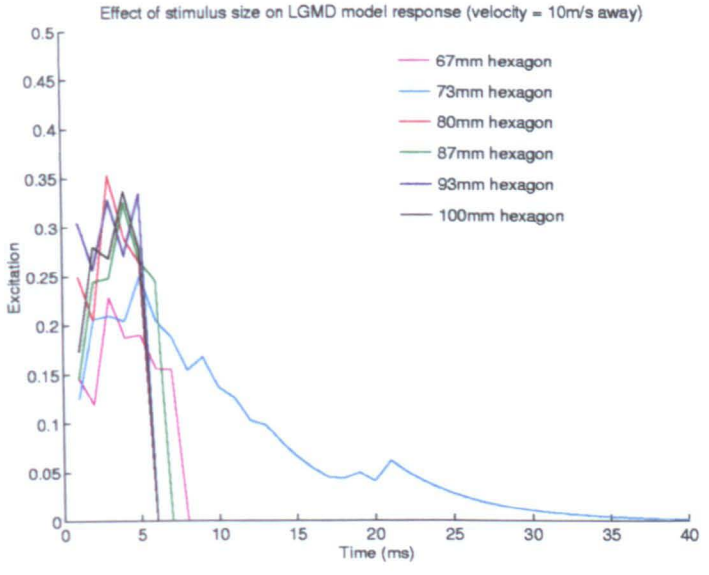

(b)

Figure 4.8: Responses of the model to different sized hexagons. The line colours indicate objects with perimeter lengths equal to the squares in figure 4.6. The objects moved between points 500mm and 100mm away from the model at 10m/s. (a) Approaching. (b) Receding.

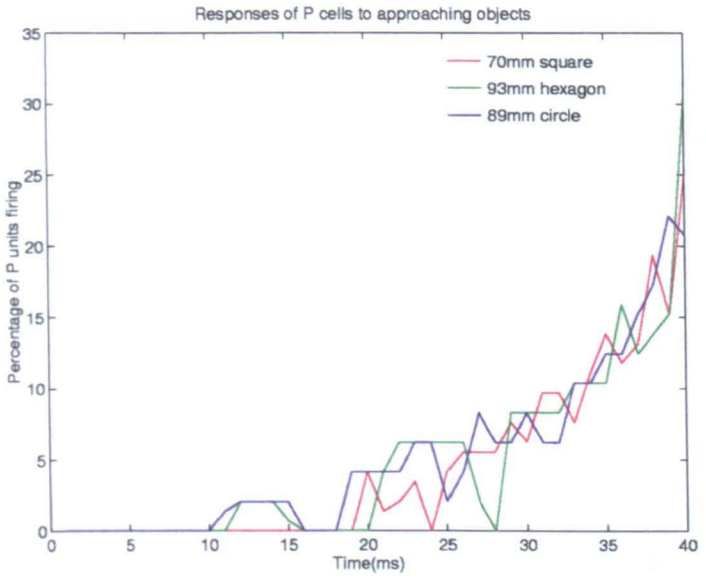

Figure 4.9: Activity in the P cells during object approach. The sizes of the objects were chosen to match the lengths of the perimeters. The objects approached from 500mm to 100mm from the model at 10m/s.

to the wider coverage of the visual field. Figure 4.10 shows the responses of the P cells to the three stimulus shapes at various times during approach. The number of cells active at a given time is approximately equal for all shapes.

The model was challenged with textured stimuli and the responses, shown in figures 4.11 and 4.12, are similar to those seen for simple stimuli. Figure 4.13 shows the activity of the P cells at three times during approach and illustrates the similarity between the response to a plain square and the response to a textured square. The texture fails to mask the edges of the objects due to the threshold of the P cells: the change in intensity produced by the texture is insufficient to exceed this threshold.

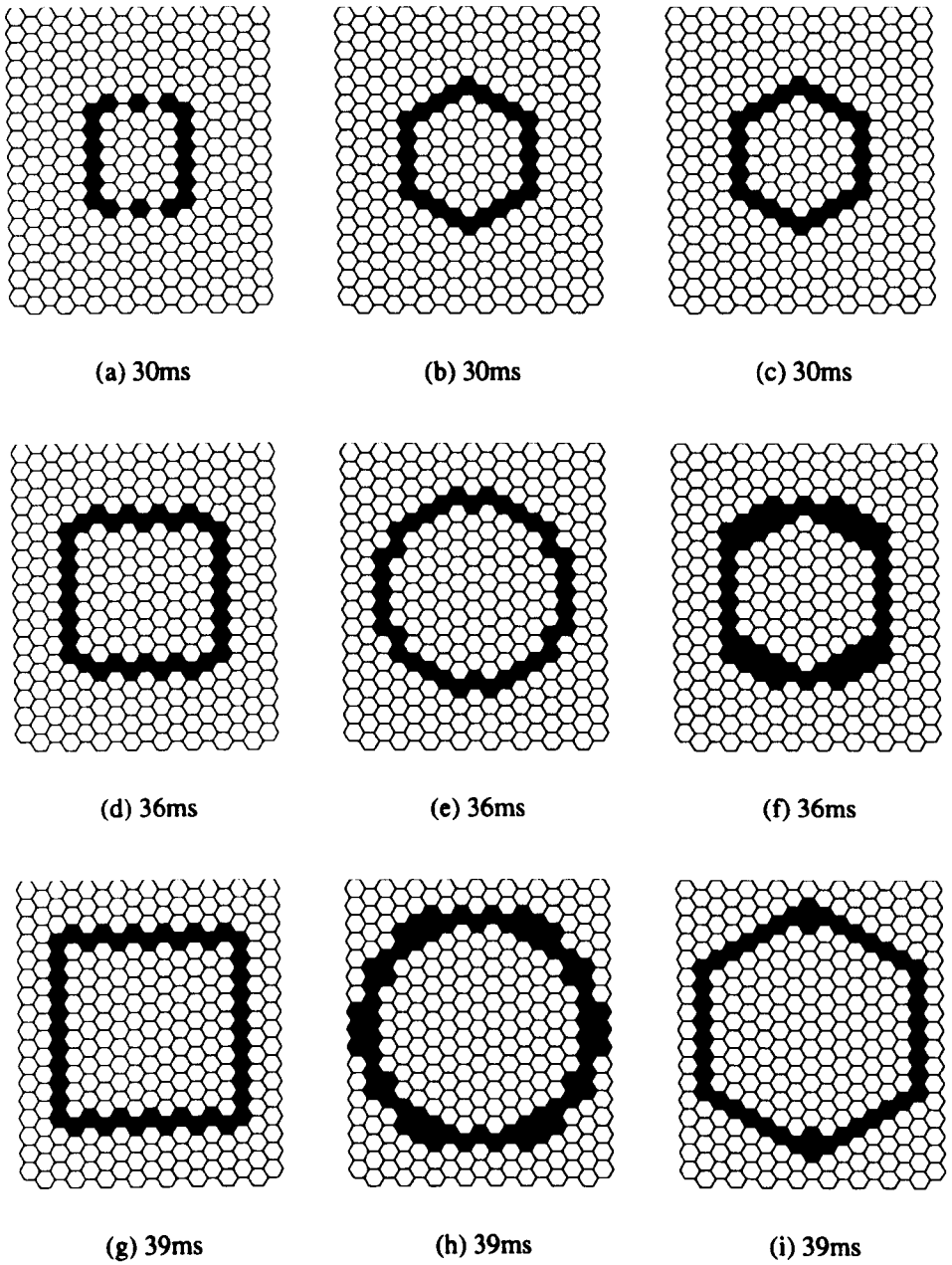

Figure 4.10: The activity in the P cells during the approach of (a,d,g) a 70mm square, (b,e,h) an 89mm circle and (c,f,i) a 93mm hexagon at 10m/s. The objects moved from 500mm from the model to 100mm from the model, and their sizes were selected in order to match the lengths of their perimeters. Black represents active units, white represents inactive units.

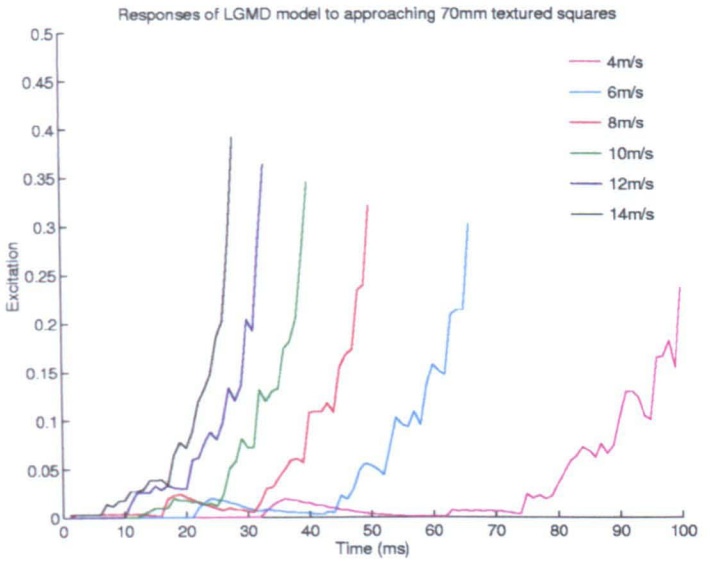

(a)

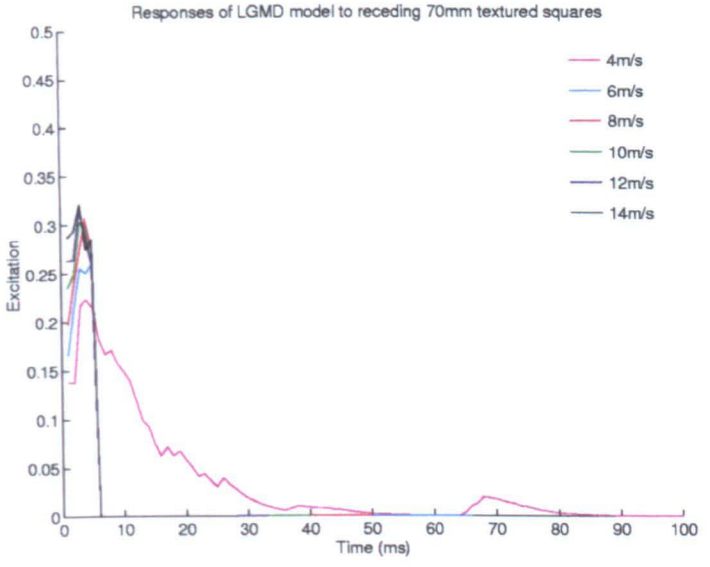

(b)

Figure 4.11: Responses to a textured 70mm square. The stimulus moved between points 500mm and 100mm from the model at the speeds indicated in the graph. (a) Approaching. (b) Receding.

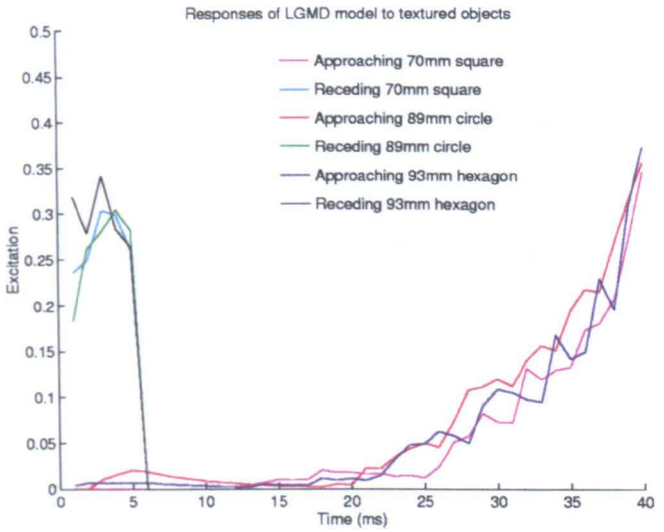

Figure 4.12: Comparison of different textured stimuli. The objects moved at 10m/s between points 500mm and 100mm and the sizes were chosen to match the perimeter lengths.

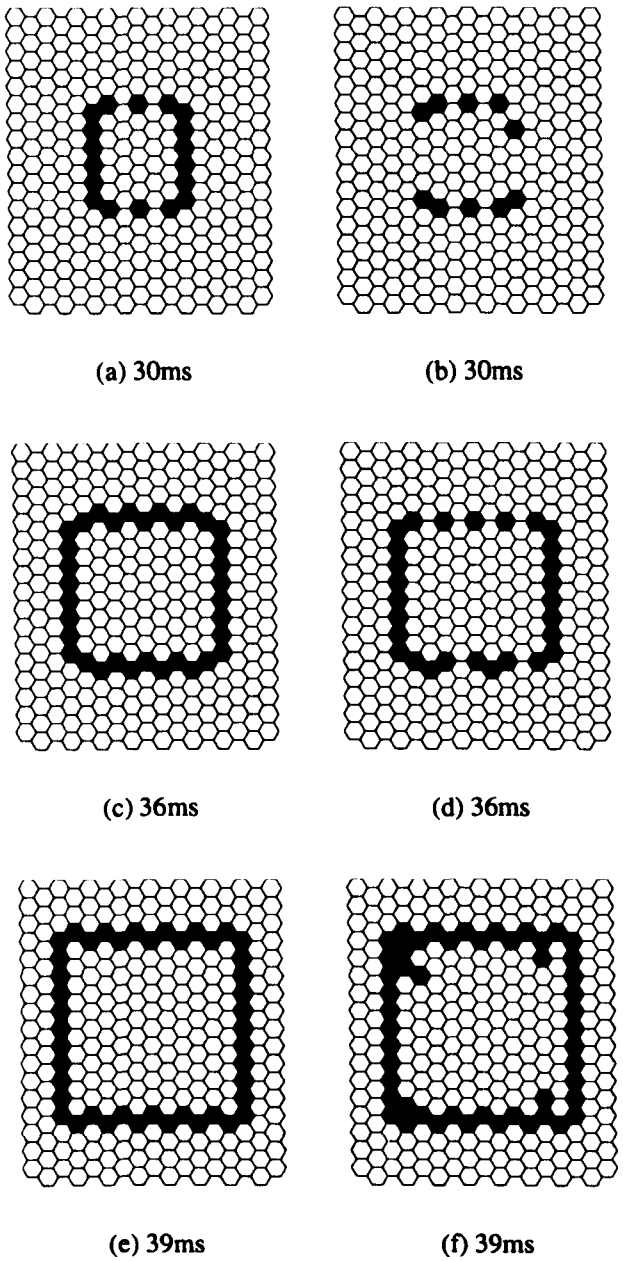

Figure 4.13: The activity in the P cells during the approach of (a,c,e) a plain 70mm square and (b,d,f) a textured 70mm square. The objects moved from 500mm from the model to 100mm from the model at 10m/s. The irregular response to the textured square is due to the texture masking the edges of the object (b,d) or falsely triggering the P cells (f). Black represents active units, white represents inactive units.

4.4 Discussion

The model presented in this chapter is a modified version of the Rind and Bramwell model of the LGMD. By using enlarged receptive fields for the P cells, the responses of the modified model are independent of the shape of the stimulus. This independence is due to the ability of the model to see the edges of the stimulus at all times. Also, the strength of the response is equal for objects with the same perimeter length approaching at equal speeds.

The inclusion of a threshold in the P cells enables the model to discriminate between the edges of a stimulus and its internal texture, and the responses to such a stimulus are approximately equal to those for a plain stimulus of equal size moving at the same speed. These texture independent responses allow the LGMD to time the triggering of behaviours robustly, such as preparation for landing and escape from an advancing predator.

Another property of the P cells is the suppression of responses to edges moving at low angular velocities since the slow changes of input which they produce are insufficient to exceed the threshold. For approaching objects this implies that the model only begins to respond when the object is sufficiently close for its edges to excite the P cells. This property corresponds well with the preference for fast moving edges shown by the model of the lamina described later in this thesis (see chapter 6).

The identity of the biological equivalents of the P cells is uncertain. The LMCs can be discounted because while these cells produce a graded response to changes in the visual image their responses are not rectified (an increase in intensity produces a transient hyperpolarisation whereas a decrease produces a transient depolarisation). A possible candidate is the input to the ON/OFF transient cells thought to provide the input to the LGMD dendritic fan (Rowell and O'Shea 1976a). In this role the P cell outputs may represent the net concentration of neurotransmitter released from presynaptic ON and OFF cells.

The outputs of the E and I cells may also represent transmitter concentrations. Recent anatomical work has revealed a novel synaptic arrangement around the dendrites of the LGMD fan where the release of transmitter from a synaptic terminal may excite the LGMD and inhibit both the terminal itself and its neighbours

(Rind and Simmons 1998). Within this framework the output of the E and I cells may represent the excitatory effect of the transmitter on the LGMD dendrite and the inhibitory effect on the neighbouring synaptic terminals respectively, although self-inhibition onto the originating synaptic terminal is not captured in the current model. In this interpretation the S cells represent discrete areas of the LGMD dendritic fan which perform the local computation.

Comparision with other motion detecting systems

The LGMD is an example of a neuron that is selective for motion towards the animal (Rind and Simmons 1992). Its responses to motion in a plane parallel to the eye are non-directionally selective with an equal response to movement in any direction (Rowell, O'Shea and Williams 1977). In contrast, cells which respond selectively to movement in one direction in this plane have been found in many insects including the locust (Rind 1990) and notably the flies (Egelhaaf and Borst 1993a).

The basis of directionally selective responses is the elementary movement detector (EMD) which responds strongly to movement in its preferred direction but produces little or no response to movement in other directions. The computation of the direction of motion is performed locally and the outputs of arrays of EMDs are integrated spatially by wide-field neurons to detect specific patterns of motion (Egelhaaf and Borst 1993b, Krapp and Hengstenberg 1996).

Recent work to discover the processes which form the EMDs has focussed on connections between the medulla and lobula plate in flies where small retinotopic neurons with directionally selective responses have been found (Douglass and Strausfeld 1996), and on the function of the dendrites of the wide-field neurons (Single, Haag and Borst 1997). This latter work addressed the question of whether the input to the wide-field neurons shows a strong directional selectivity, or whether the processing in the dendrite combines weakly tuned inputs to enhance the selectivity. Dendritic processing of this form is similar to that proposed by Rind and Simmons (1998) for the LGMD dendrites with the exception that the interaction between inputs occurs presynaptically for the LGMD.

The LGMD model presented here does not use EMDs because their use would

necessitate a fixed centre of expansion from which the preferred directions of the EMDs would radiate. Instead the processing, which is performed by the E, I and S cells, detects motion in any direction in the plane parallel to the eye. The selectivity for approaching objects is performed by the LGMD which uses increasing edge length and edge velocity to distinguish approach from motion in other directions (Simmons and Rind 1992).

Behavioural experiments on bees suggest that insects may possess more than one motion detection mechanism. When bees fly between two vertically striped walls they centre their flight path along the midline irrespective of the pattern of stripes on the two walls (Srinivasan, Lehrer, Kirchner and Zhang 1991). Srinivasan, Zhang and Chandrashekara (1993) argue that to achieve this the bee must be able to measure the speed of motion relative to the two walls independently of their structure, and show that this is inconsistent with the spatial summation of the responses of an array of EMDs.

Chapter 5

Models of a locust photoreceptor

The photoreceptors of the compound eye are the source of the visual information processed by the LGMD and their response properties, both spatial and temporal, will influence the responses of the LGMD. In this chapter the temporal response properties of locust photoreceptors are examined. The aim of this work was the development of a light-adapting photoreceptor model, which would allow the responses of the LGMD to natural stimuli to be studied. Two different approaches were adopted.

The first photoreceptor model developed was an electrical model of the photoreceptor membrane, describing the principal ionic conductances. This model was found to be overly complex for use in large scale simulations. However, this model was used to calculate from the photoreceptor's light-adapted impulse responses the average conductance changes produced by single photons.

A second photoreceptor model was developed for use in large simulations. The model uses two leaky integrators, one to mimic the effects of membrane filtering and the other to represent light adaptation. This model requires fewer parameters than the electrical model and the amount of computation needed during simulations is reduced.

This chapter describes:

- the electrical model of the photoreceptor membrane.
- the method for calculating the average conductance change produced by a single photon.

- the average conductance changes estimated from the results of a parameter search.
- the design and responses of the leaky integrator photoreceptor model.

5.1 An electrical model

The first photoreceptor model developed was an electrical model of the membrane which resembled the basic structure proposed by Hodgkin and Huxley (1952) for the voltage-dependent conductances in the membrane of the squid giant axon. A similar model was used by Weckström and Laughlin (1995) to study the functional properties of voltage-dependent potassium channels in blowfly photoreceptors. Although this model was found to be overly complex for use in large simulations, it was used to calculate the average conductance change produced by a single photon. This conductance change represents the output of the phototransduction cascade and is a useful quantity for studying the effects of light adaptation on the cascade. The work presented here should be considered as a suggestion, more thorough experimental work is needed before any firm conclusions can be drawn.

5.1.1 Structure

The model, shown in figure 5.1, describes the principle conductances of the photoreceptor soma membrane: the light-activated conductance, g_L; the sustained voltage-dependent potassium conductance, g_K (Weckström 1994, Cuttle, Hevers, Laughlin and Hardie 1995); and the membrane leakage conductance, g_m. C represents the membrane capacitance. The axon is not included in the model because, with its high membrane resistance and low capacitance relative to the soma, the current flow from the soma into the axon is negligible (Weckström and Laughlin 1995).

The behaviour of the model is described by

$$C\frac{dV}{dt}(t) + g_L(t)(V(t) - E_L) + g_K(t)(V(t) - E_K) + g_m(V(t) - E_m) = 0, \quad (5.1)$$

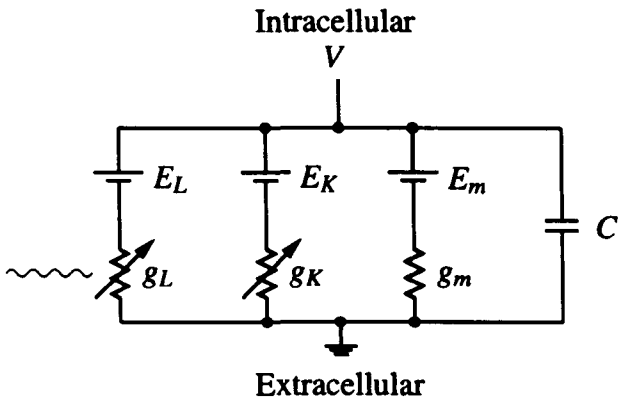

Figure 5.1: An electrical model of the photoreceptor soma membrane. g_L, light-activated conductance; E_L, light-activated conductance reversal potential; g_K, sustained voltage-dependent potassium conductance; E_K, potassium reversal potential; g_m, membrane leakage conductance; E_m, membrane leakage reversal potential; C, membrane capacitance; V, membrane potential.

where C is the membrane capacitance, $V(t)$ and $\frac{dV}{dt}(t)$ are the membane potential and the rate of change of the membrane potential at time t respectively, $g_L(t)$ is the light-activated conductance at time t, $g_K(t)$ is the potassium conductance at time t, g_m is the membrane leakage conductance and E_L, E_K and E_m are the reversal potentials of the three conductances respectively. The values of the reversal potentials and the passive membrane properties are assumed to be constants, while all other terms are variables.

For the voltage-dependent potassium conductance, the activation characteristics are approximated with a linear function of membrane potential as shown in figure 5.2 with the steady-state activation given by

$$g_K = \delta g_K (V - V_{0_{g_K}}), \tag{5.2}$$

where δg_K is the gradient of the activation curve and $V_{0_{g_K}}$ is the membrane potential at which the linear approximation gives a conductance of zero. Below $V_{0_{g_K}}$ the value of g_K is set to zero.

The temporal characteristics of the conductance activation are modelled using a leaky integrator with time constant τ_{g_K} to delay any changes of the membrane potential V. Figure 5.3 illustrates the complete model of the voltage-dependent

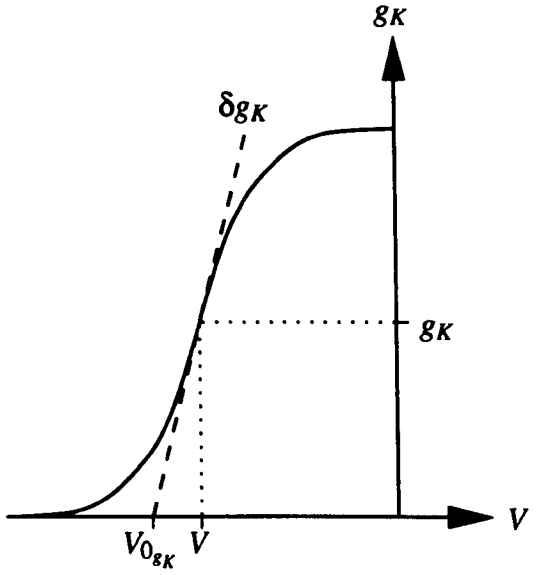

Figure 5.2: The potassium conductance activation curve (solid line) is approximated with a linear function of membrane potential (dashed line). g_K, potassium conductance; V, membrane potential; δg_K, gradient of activation curve; $V_{0_{g_K}}$, membrane potential giving zero conductance.

conductance.

This approximation reduces the number of parameters required to describe the conductance from the four used by Weckström, Hardie and Laughlin (1991), who used a Hodgkin-Huxley model (Hodgkin and Huxley 1952), to three (δg_K, $V_{0_{g_K}}$ and τ_{g_K}). There are two motives for this simplification:

1. The potassium conductances in the locust have not been studied as thoroughly as those of the blowfly and the Hodgkin-Huxley parameters have not been published.

2. The simplified parameters are more intuitive.

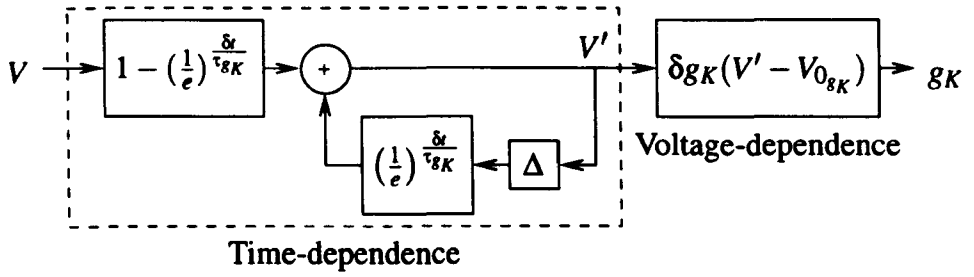

Figure 5.3: The voltage dependent potassium conductance model. V, photoreceptor membrane potential; τ_{g_K}, activation time constant; δt, simulation time step; Δ, delay of one time step; δg_K, gradient of activation curve; $V_{0_{g_K}}$, membrane potential giving zero conductance; g_K, potassium conductance.

5.1.2 Calculating the light-activated conductance

The light-activated conductance, g_L, can be calculated using the model above by rearranging equation (5.1) to give

$$g_L(t) = \frac{1}{E_L - V(t)} \left[C\frac{dV(t)}{dt} + g_K(t)(V(t) - E_K) + g_m(V(t) - E_m) \right]. \quad (5.3)$$

In this equation, g_L is dependent on both the membrane potential, V, and the time, t. Since the potassium conductance, g_K, is also dependent on the membrane potential the model can not be treated as a passive RC filter because the frequency response is not constant. Hence, for the locust and other insects which have voltage-dependent potassium conductances in their photoreceptors, the light-activated conductance must be calculated in the time domain.

For the impulse response produced by a brief flash, the conductance change produced by the flash, $g_{L_{flash}}$, is calculated by assuming that each of the I_{flash} photons in the flash produces the same average conductance change as the I_{back} photons/s in the background. This assumption requires that no significant adaptation of the phototransduction cascade occurs during the response, and that these conductances sum linearly. An early test for this assumption is whether the calculated values of g_L(t) are greater than or equal to the steady-state conductance at all values of t. If g_L drops below the steady-state level this shows that the average

conductance change produced by each photon has reduced due to light adaptation. Using the assumption, $g_{L_{flash}}$ is given by

$$g_{L_{flash}}(t) = g_L(t) - g_{L_{back}}, \tag{5.4}$$

where $g_{L_{flash}}(t)$ and $g_L(t)$ are the conductance produced by the flash and the total light-activated conductance at time t respectively and $g_{L_{back}}$, the steady-state conductance produced by the background intensity, is given by

$$g_{L_{back}} = \frac{1}{E_L - V_{back}} \left[\delta g_K (V_{back} - V_{0_{g_K}})(V_{back} - E_K) + g_m (V_{back} - E_m) \right]. \tag{5.5}$$

The average conductance due to a single photon, $g_{L_{photon}}$, is calculated using

$$g_{L_{photon}}(t) = \frac{g_{L_{flash}}(t)}{I_{flash}}, \tag{5.6}$$

where $g_{L_{photon}}(t)$ is the conductance produced by the photon at time t. $g_{L_{photon}}$ can be compared against $g_{L_{back}}$ to assess the assumptions made during the calculation of $g_{L_{flash}}$. The equation

$$g^*_{L_{back}} = I_{back} \int_0^1 g_{L_{photon}} dt, \tag{5.7}$$

where $\int_0^1 g_{L_{photon}} dt$ is the average conductance produced by a photon per second, yields a prediction of the steady-state conductance, $g^*_{L_{back}}$, based on $g_{L_{photon}}$, which can be compared with $g_{L_{back}}$. If the assumptions made earlier are correct, these values will be equal, but if $g^*_{L_{back}}$ is less than $g_{L_{back}}$ then significant adaptation occurred during the response.

This model was used to calculate the conductance changes underlying the light-adapted impulse responses (LA1 and LA2) published by Payne and Howard (1981), which were described in section 1.1.2. The values of the membrane potential, V, were calculated using the log-normal equation (equation (1.1)) which

was rewritten to give

$$V(t) = V_{flash}.\exp\left[\frac{-(\log\frac{t}{t_p})^2}{2\sigma^2}\right] + V_{back}, \tag{5.8}$$

where $V(t)$ is the membrane potential at time t, V_{back} is the steady-state depolarisation produced by the background intensity, V_{flash} is the height of the peak of the response above V_{back}, t_p is the time of the peak and σ describes the width of the response. Values for the rate of change of the membrane potential, $\frac{dV(t)}{dt}$, were obtained from the differential of the log-normal equation,

$$\frac{dV(t)}{dt} = -\frac{\log(\frac{t}{t_p}).(V(t) - V_{back})}{\sigma^2 t}. \tag{5.9}$$

A parameter search program was written in the C programming language. The program calculates the light-activated conductance for specified sets of parameter by combining equations 5.3, 5.8 and 5.9. If $g_{L_{flash}}$, calculated using equations 5.4 and 5.5, is all positive, $g_{L_{photon}}$ is calculated using equation 5.6. The prediction of the steady-state conductance is made using equation 5.7.

Parameter sets for the program comprised values for the reversal potentials (E_L, E_K and E_m), the passive membrane parameters (g_m and C), the potassium conductance parameters (δg_K, $V_{0_{g_K}}$ and τ_{g_K}) and the steady-state membrane potential (V_{back}), which was not specified by Payne and Howard. All parameters could be treated as free parameters and their values varied within specified ranges during a search. These ranges were divided into specified numbers of steps and all combinations of the resulting parameter values were tested. Parameter sets were written to a disk file if they satisfied the criterion

$$g_{L_{error}} = \frac{|g_{L_{back}} - g^*_{L_{back}}|}{g_{L_{back}}} * 100\% < tolerance, \tag{5.10}$$

where $g_{L_{error}}$ is the percentage error between the steady-state conductances calculated using equation 5.5 and predicted using equation 5.7, $|g_{L_{back}} - g^*_{L_{back}}|$ is the absolute difference and *tolerance* is the maximum percentage error for a parameter set to be valid.

Each parameter set which satisfied also equation 5.10 was fitted with two equations proposed for the phototransduction cascade, the Fermi-exponential equation of Contzen and Nagy (1996) and the log-normal equation of Payne and Howard (1981). These equations were described in section 1.1.2. The `nlinfit` function in the Statistics Toolbox of MATLAB, which implements the Gauss-Newton algorithm for curve fitting, was used, and the parameters of the fitted equations were written in a second disk file.

5.1.3 Results

For both LA1 and LA2, the ranges of parameters shown in table 5.1 were searched to find solutions with a *tolerance* of 1%. Each range was divided into the specified number of values, giving a total of 54,000 possible parameter sets. The ranges for each parameter were based on estimates made from the literature. Values for g_m, E_m, E_K, C have been measured in the locust (Weckström 1994, Cuttle et al. 1995). The range for E_L was taken as the range between the measured values for *Drosophila* (Hardie 1991b) and tipulids (Laughlin 1996). The potassium conductance parameter ranges were estimated from the data for the locust (Weckström 1994, Cuttle et al. 1995) and the blowfly (Weckström et al. 1991). The range for the steady-state membrane potential, V_{back}, was set to suitable physiological values.

The parameter search revealed 1,165 valid parameter sets for LA1 (2.16% of the parameter sets searched) and 1,334 valid parameter sets for LA2 (2.47%). The best parameter set for LA1 gives an error of only 0.0004% while an error of -0.0006% results from the best parameter set for LA2.

The conductance changes produced by the best solutions are shown in figure 5.4. At the higher level of light adaptation (LA2) the conductance is both smaller and faster than that at the lower light intensity. Both conductances have prolonged tails when compared with the impulse responses (figure 1.2).

Table 5.2 shows the dependence of the best solutions on individual parameters. There is little dependence on the majority of parameters, with only variations of $V_{0_{g_K}}$ and V_{back} producing large changes. The effects of g_m, C and τ_{g_K} are negligible.

	Minimum	Maximum	Divisions	Notes
g_m(nS)	28.57	28.57	1	$R_m = 35\text{M}\Omega$
E_m(mV)	-65	-65	1	
E_K(mV)	-85	-85	1	
E_L(mV)	-10	10	5	
C(nF)	0.43	0.43	1	$\tau_m = 15\text{ms}$
δg_K(nS/mV)	0.5	15	30	
$V_{0_{g_K}}$(mV)	-90	-50	9	
τ_{g_K}(ms)	30	100	8	
V_{back}(mV)	-60	-40	5	

Table 5.1: Parameter values searched. The range for each parameter was divided into the specified number of divisions, and all 54,000 possible combinations of values were tested. Rm, membrane leakage resistance; τ_m, membrane time constant. The ranges were based on Weckström (1994), Cuttle et al. (1995), Hardie (1991b), Laughlin (1996) and Weckström et al. (1991).

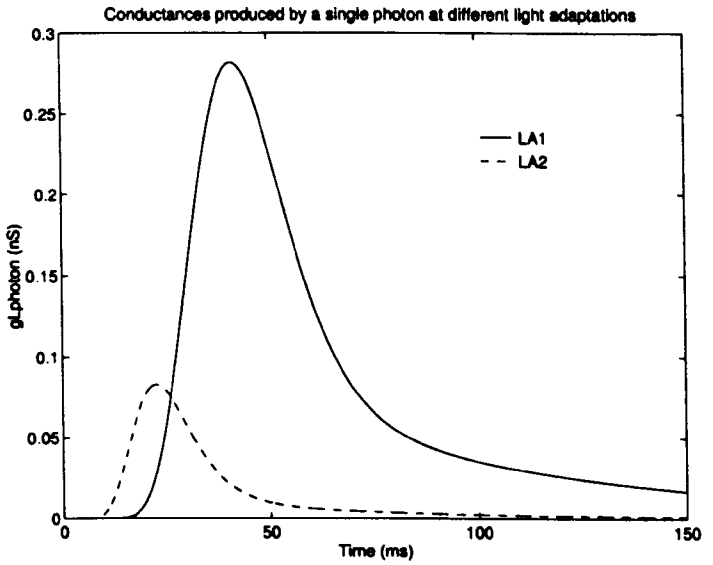

Figure 5.4: Conductance changes produced by single photons at two levels of light adaptation, calculated from the best parameter sets. Solid line, LA1: E_L, 0mV; δg_K, 11.5nS/mV; $V_{0_{g_K}}$, -80mV; τ_{g_K}, 70ms; V_{back}, -55mV. Dashed line, LA2: E_L, -5mV; δg_K, 5.5nS/mV; $V_{0_{g_K}}$, -90mV; τ_{g_K}, 50ms; V_{back}, -45mV. Values of g_m, E_m, E_K and C were as listed in table 5.1.

		LA1($g_{L_{error}}$)	LA2($g_{L_{error}}$)
g_m(nS)	min, 25	-0.11	-0.030
	max, 33.3	0.15	0.038
E_m(mV)	min, -75	-2.49	-1.73
	max, -55	2.66	1.83
E_K(mV)	min, -95	-9.13	-6.75
	max, -75	17.82	10.92
E_L(mV)	min, -10	4.64	5.47
	max, 10	-3.19	-10.26
C(nF)	min, 0.29	0.0004	-0.0006
	max, 0.57	0.0004	-0.0006
δg_K(nS/mV)	min, 0.5	11.70	1.51
	max, 15	-0.21	-0.15
$V_{0_{g_K}}$(mV)	min, -90	-12.30	-0.0006
	max, -50	-317.02*	160.43
τ_{g_K}(ms)	min, 30	0.46	0.27
	max, 100	-0.50	-0.49
V_{back}(mV)	min, -60	18.32	31.30
	max, -40	-21.75	-1.86

Table 5.2: Dependence of the best solutions on the values of individual parameters. Marked (*) value of $g_{L_{error}}$ for LA1 was calculated with $V_{0_{g_K}}$ set to -55mV.

The time-to-peak of the conductances in figure 5.4 is equal to the time-to-peak of the impulse response and examining all valid parameter sets reveals that most share this coincident peak (figure 5.5). The majority of the remaining parameter sets have a shorter time-to-peak than the impulse response but a small number, those with large gains and short time constants for the potassium conductance, have a longer time-to-peak.

Figure 5.6 shows the fits of the phototransduction model equations of Payne and Howard (1981) and Contzen and Nagy (1996) to the conductances produced by the best parameter sets. For both LA1 and LA2, the fit between the equations and the conductance is close for the majority of the conductance but both models fail to fit the prolonged tail. For the log-normal model, the values of the peak conductance, $g_{L_{pk}}$, and the time-to-peak, t_p, are lower for the more light-adapted response, but the width of the response, σ, is approximately constant. The values of the Fermi-exponential parameters are all lower for LA2, indicating lower amplitude and increased speed in all phases of the response.

5.2 A leaky integrator model

The electrical model of a photoreceptor described above is not suitable for use in large neural network simulations owing to its complexity and the current shortage of experimental data from which to estimate the parameter values. Also, extra parameters are required to model light-adaptation, increasing the complexity still further. Therefore, a second model of a locust photoreceptor was developed which mimics the effects of light-adaptation but requires only five parameters.

5.2.1 Structure

The model, shown in figure 5.7, centres around a pair of leaky integrators (section 2.1.3). The first (the input integrator), in conjunction with the time delay Δ, filters the input light intensity I to produce I_f while the second (the adaptation

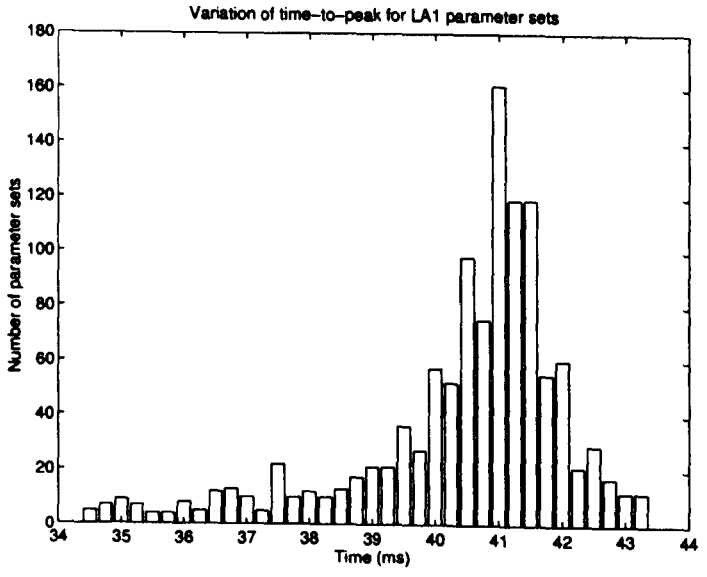

(a)

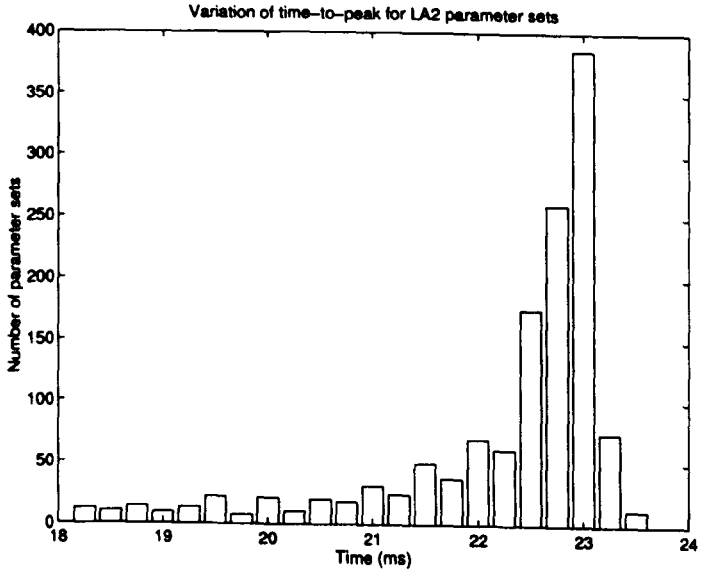

(b)

Figure 5.5: Times-to-peak for all valid parameter sets. Bin size, 0.25ms. (a) LA1. (b) LA2.

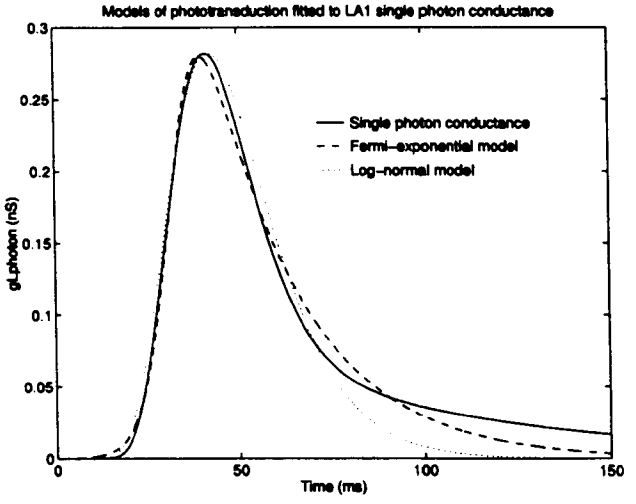

(a)

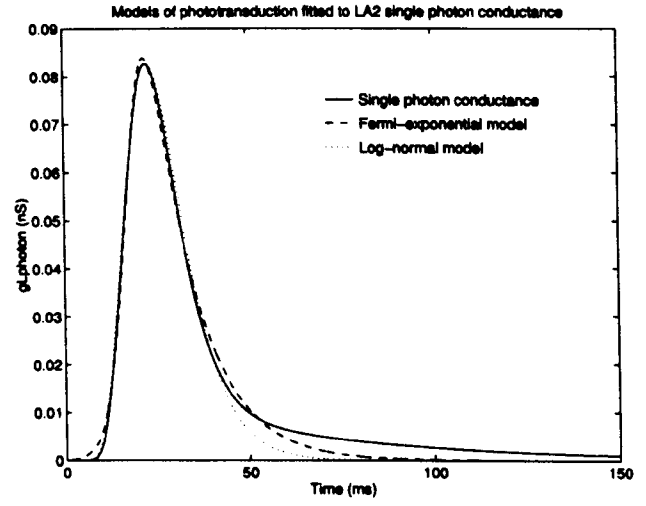

(b)

Figure 5.6: Fits of the phototransduction model equations of Payne and Howard (1981) and Contzen and Nagy (1996) to the conductances produced by the best parameter sets. Solid line, conductance; dashed line, Fermi-exponential model; dotted line, log-normal model. (a) LA1. Log-normal: $g_{L_{pk}}$, 0.28nS; t_p, 42.18ms; σ, 0.32. Fermi-exponential: B, 0.45nS; δ, 31.67ms; σ, 3.74ms; τ, 24.54ms. (b) LA2. Log-normal: $g_{L_{pk}}$, 0.08nS; t_p, 22.82ms; σ, 0.34. Fermi-exponential: B, 0.15nS; δ, 17.35ms; σ, 2.51ms; τ, 11.87ms.

integrator) generates an estimate of the background intensity I_b. Formally,

$$I_f(t) = I(t)\left[1 - \left(\frac{1}{e}\right)^{\frac{\delta t}{\tau_f}}\right] + I_f(t-1)\left(\frac{1}{e}\right)^{\frac{\delta t}{\tau_f}} \tag{5.11}$$

and

$$I_b(t) = I_f(t)\left[1 - \left(\frac{1}{e}\right)^{\frac{\delta t}{\tau_b}}\right] + I_b(t-1)\left(\frac{1}{e}\right)^{\frac{\delta t}{\tau_b}}, \tag{5.12}$$

where $I(t)$, $I_f(t)$ and $I_b(t)$ are the input, filtered and estimated background light intensities at time t respectively, $I_f(t-1)$ and $I_b(t-1)$ are the filtered and estimated background intensities at time $t-1$ respectively, δt is the simulation timestep and τ_f and τ_b are the time constant of the input and adaptation integrators respectively.

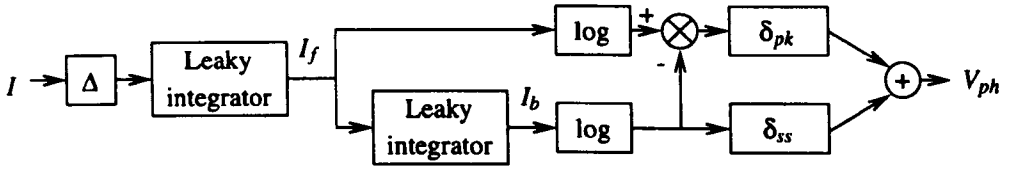

Figure 5.7: Leaky integrator model of a locust photoreceptor. I, incoming light intensity; Δ, time delay; I_f, filtered light intensity; I_b, estimate of background light intensity; δ_{pk}, gain producing peak response; δ_{ss}, gain producing steady-state response; V_{ph}, photoreceptor membrane potential.

The output of the model is given by

$$V_{ph} = \delta_{pk}(\log I_f - \log I_b) + \delta_{ss} \log I_b, \tag{5.13}$$

where δ_{pk} is the gain for changes in intensity (transient gain) and δ_{ss} is the gain for the background intensity (steady-state gain). These gains are constants: justification for this comes from the photoreceptor voltage-log intensity characteristics which are approximately linear for moderate contrasts (Matić and Laughlin 1981, Vishnevskaya, Byzov and Cherkasov 1993).

5.2.2 Responses

Figure 5.8 shows the normalised responses of the leaky integrator photoreceptor model. After the initial delay due to the element Δ, the step response rises gradually to a peak and then decays slowly to a steady-state. This response matches qualitatively the response of a locust photoreceptor to an increase in light intensity. By contrast, the impulse response rises to a peak immediately after the delay and then decays rapidly to a weakly hyperpolarised state from which it recovers slowly. This impulse response is very different from the impulse response of a locust photoreceptor (section 1.1.2).

The operation of the model is also illustrated in figure 5.8. During the step response the filtered input intensity, I_f, rises rapidly due to the short time constant of the input integrator, τ_f. This results in a large difference between I_f and the estimated background intensity, I_b, which rises much more slowly because of the longer time constant of the adaptation integrator, τ_b. This large difference is multiplied by the high transient gain, δ_{pk}, to give a large output, V_{ph}. Gradually I_b rises towards I_f, reducing the transient response. I_b is multiplied by the lower steady-state gain, δ_{ss}, and the sum of the transient and steady-state responses is less than the initial transient response. Ultimately, I_b equals I_f and the response reaches a steady-state.

The responses of the model can be tuned by altering the values of the five parameters. Figure 5.9 shows the influence of the gains δ_{pk} and δ_{ss} on the step response, while the effects of the time constants τ_f and τ_b are shown in figure 5.10. Adjusting the initial delay element, Δ, shifts the start of the response but has no other effects.

The amplitude of the transient response is proportional to the transient gain, δ_{pk}: increasing the transient gain increases the transient response for a given stimulus, with the steady-state response unchanged. If $\delta_{pk} = 0$, the transient response is zero and the output, V_{ph}, is proportional to the steady-state response. The steady-state response is controlled by the steady-state gain, δ_{ss}. Larger gains produce higher steady-state outputs, reducing the effects of light adaptation. If $\delta_{ss} = 0$, the steady-state output is zero.

Increasing the input time constant, τ_f, delays the output and reduces the am-

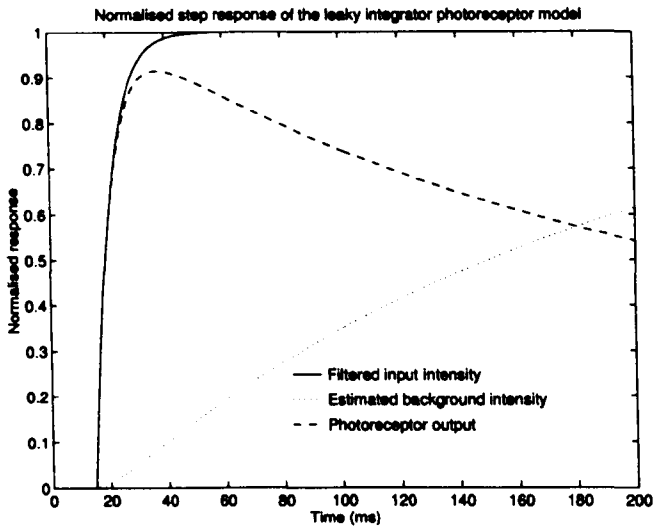

(a)

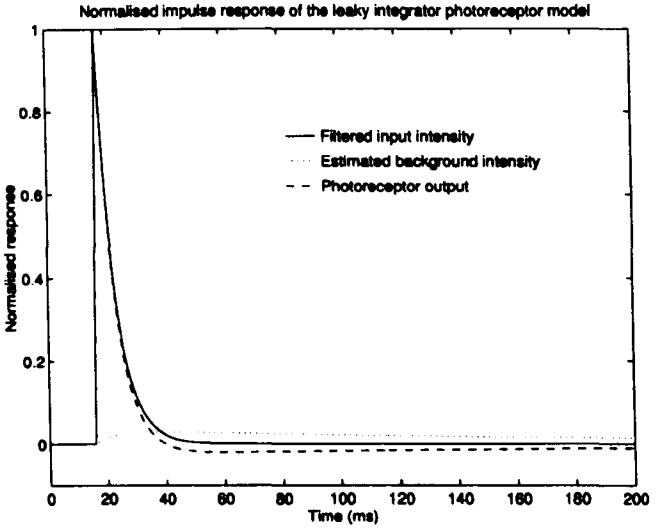

(b)

Figure 5.8: Normalised responses of the leaky integrator photoreceptor model. (a) Step response. (b) Impulse response. Δ, 15ms; δ_{pk}, 40mV/decade; δ_{ss}, 10mV/decade; τ_f, 6ms; τ_b, 200ms.

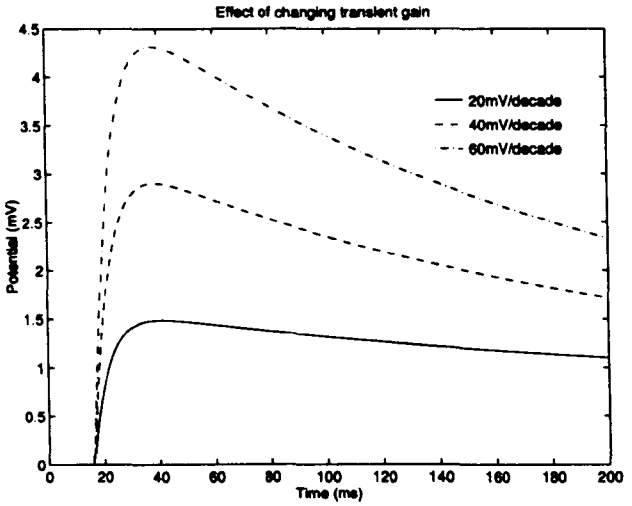

(a)

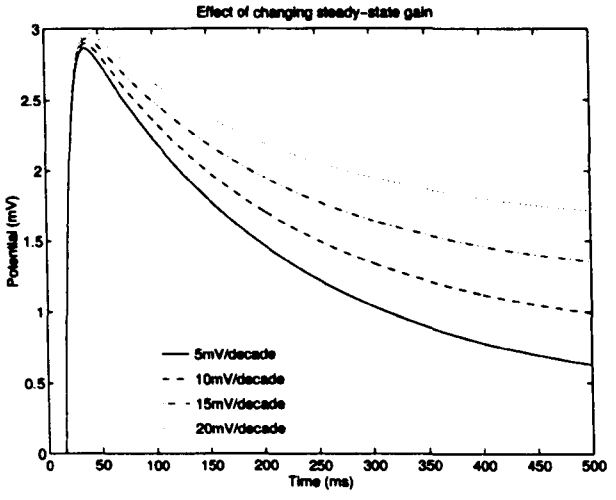

(b)

Figure 5.9: Effect of altering the gains of the leaky integrator photoreceptor model. For all responses: Δ, 15ms; τ_f, 6ms; τ_b, 200ms. (a) Transient gain, δ_{pk}: solid line, 20mV/decade; dashed line, 40mV/decade; dash-dot line, 60mV/decade. δ_{ss}, 10mV/decade. (b) Steady-state gain, δ_{ss}: solid line, 5mV/decade; dashed line, 10mV/decade; dash-dot line, 15mV/decade; dotted line, 20mV/decade. δ_{pk}, 40mV/decade.

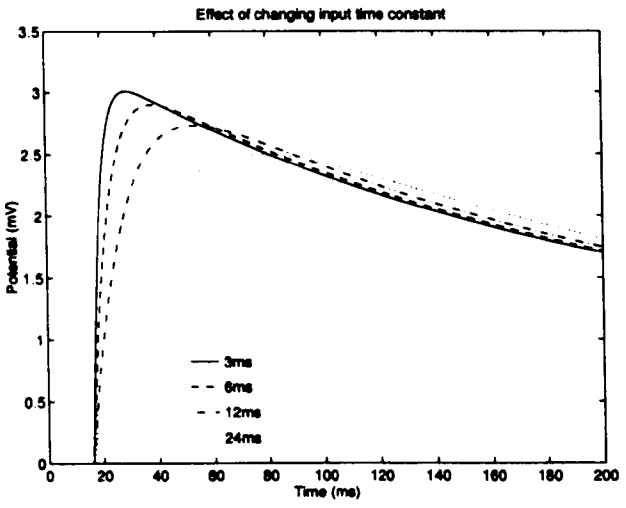

(a)

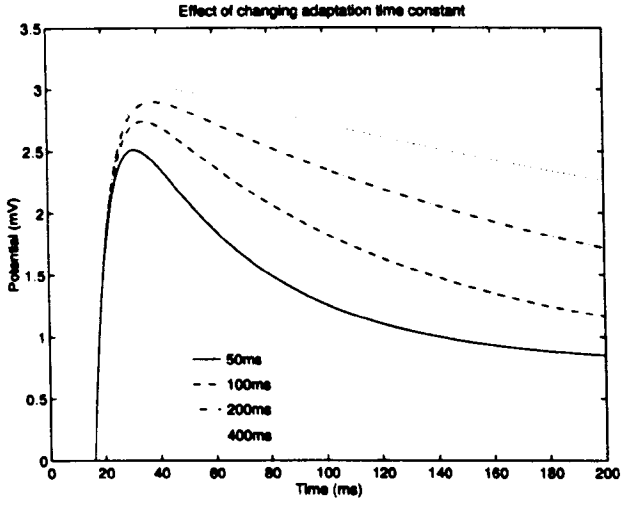

(b)

Figure 5.10: Effect of altering the time constants of the leaky integrator photoreceptor model. For all responses: Δ, 15ms; δ_{pk}, 40mV/decade; δ_{ss}, 10mV/decade. (a) Input time constant, τ_f: solid line, 20mV/decade; dashed line, 40mV/decade; dash-dot line, 60mV/decade. δ_{ss}, 10mV/decade. (b) Steady-state gain, δ_{ss}: solid line, 5mV/decade; dashed line, 10mV/decade; dash-dot line, 15mV/decade; dotted line, 20mV/decade. δ_{pk}, 40mV/decade.

plitude of the peak response. This is caused by the filtered intensity, I_f, rising more slowly due to the longer time constant, and the difference between I_f and I_b being smaller. Increasing the adaptation time constant, τ_b, has the opposite effect on the peak, with longer time constants producing larger responses. The speed of adaptation is also reduced, but the steady-state response amplitude is unaffected.

5.3 Discussion

Electrical model

A model similar to the one described here was used successfully by Weckström and Laughlin (1995) to study the effect of voltage-dependent potassium conductances on the responses of blowfly photoreceptors. However, with the data available for the locust, this approach was found to be unsuitable for developing a light-adapting photoreceptor model.

Two approximations limit the accuracy of this model, the simplification of the voltage-dependent conductance and the omission of the membrane's ionic pumps.

1. In the measured activation curves for the potassium conductances in locust photoreceptors (Weckström 1994), the gradient δg_K varies sigmoidally as the membrane potential increases. The linear approximation used in this model is only accurate around specific membrane potentials, but for studying responses where the membrane potential varies by only a few millivolts the gradient can be assumed to be constant and this approximation is appropriate.

   Also, the model only describes the sustained conductance found in a locust photoreceptor. There is also an inactivating conductance present which is active near the cell's resting potential but becomes inactive only a few millivolts above this potential (Weckström 1994, Cuttle et al. 1995). The omission of this inactivating conductance restricts the use of the model to light-adapted cells where this conductance is inactivated.

2. The omission of the membrane's ionic pumps may also restrict the model to a specific membrane potential. Although not studied extensively in the locust, work on fly photoreceptors indicates the presence of electrogenic Na^+-K^+ and Na^+-Ca^{2+} pumps in the membrane. The Na^+-K^+ pump exchanges 3 intracellular Na^+ ions for 2 extracellular K^+ ions, hyperpolarising the membrane (Jansonius 1990), while Na^+-Ca^{2+} exchange is believed to depolarise the cell and produce the sustained depolarisation observed after very strong stimulation (Hochstrate 1991), a response which is also present

in the locust (Tsukahara and Horridge 1977). The effects of these pumps may cancel at all membrane potentials, but if this is not the case they will combine to shift the resting potential of the membrane, changing the reversal potential of the membrane leakage reversal potential, E_m.

A more detailed model is required to describe the responses of a photoreceptor accurately. For example, a recent model of the honeybee worker photoreceptor from Becker and Backhaus (1998) simulates the effects of light activation well. However, for the analysis of brief, weak responses such as the impulse response, the model presented here is suitable and has the advantage of a more restricted, and easily obtained, set of parameters (9 compared with 23 used by Becker and Backhaus).

The model is useful for calculating the average conductance change produced by individual photons. Earlier studies have measured (Hardie 1991b) or calculated (Laughlin 1996) the current underlying the responses of insect photoreceptors to light in order to study the effects of light adaptation. However, this current, which is produced by the flow of ions through a conductance activated by the absorption of photons via the phototransduction cascade, is determined by the membrane potential which may mask the true effects of adaptation. The light-activated conductance calculated here is a better measure as it is independent of the filtering effects of the membrane.

This study illustrates a method which can be used to isolate this conductance. By obtaining values for the nine parameters used by the model and recording the impulse response, the light-activated conductance change can be calculated directly, and by making the assumption that negligible adaptation occurs during the response, the average conductance produced by a single photon can also be found. This conductance represents the average conductance underlying the quantum bumps produced by individual photons (Lillywhite 1977). At low light intensities, individual quantum bumps show substantial variations in amplitude, latency and width (Howard 1983), and although single photon responses have not been recorded at higher light levels, it is reasonable to assume that this variability persists.

The calculation of the conductance change produced by a single photon relies

on this conductance change being constant throughout the response, ie. that negligible adaptation occurs. This seems likely due to the short duration and small amplitude of the impulse response, but the calculation method offers two opportunities to test this assumption. The first test requires examination of the total light-activated conductance. If, during the response, the conductance falls below the level of the steady-state conductance, the size of the average conductance change produced by each photon has decreased due to light-adaptation. However, passing the first test does not guarantee that light adaptation has not occurred. The second test is to compare the predicted steady-state light-activated conductance with the actual conductance. If these are equal then no adaptation has occured, but if the predicted value is lower, the average conductance change per photon has reduced during the response. If the first test is passed, this scenario requires the phototransduction cascade to adapt more quickly than the cell membrane can respond which seems implausible, especially when calcium, thought to be responsible for light adaptation, enters the cell through the light-activated conductances (Hardie 1991b). However, recent work by Oberwinkler and Stavenga (1998) shows that the increase in intracellular calcium concentration is very rapid in blowfly photoreceptors.

Calculation of the light-activated conductance in the time domain contrasts with the study of Laughlin (1996) who used the frequency domain to calculate the light-induced current in tipulids. In these slow-flying, nocturnal insects the voltage-dependent potassium conductances are inactivated in light-adapted photoreceptors, allowing the cells to be modelled accurately with passive RC filters.

The accuracy of the fits between the single photon conductance change and the equations of Payne and Howard (1981) and Contzen and Nagy (1996) is encouraging. In a large scale study of phototransduction at a wide range of light adaptation levels, it may be possible to relate the variation in these parameters between the different adaptation levels to a single value representing intracellular calcium concentration, which will help to quantify the effects of light adaptation. Also, from the point of view of developing a more detailed model of a photoreceptor, the ability to describe all the aspects of the light response in terms of a single variable simplifies the task of modelling light adaptation.

The conductance changes presented in this chapter are unlikely to represent

the actual responses, since the parameter search used was fairly course and many combinations of physiological parameters were not examined. However, the results of the search reveal two interesting features, the coincidence between the conductance change and impulse response peaks, and the prolonged tail of the single photon conductance changes.

Laughlin (1996), working with tipulid photoreceptors, found that the peak of the light-induced current occurred before the peak of the impulse response. This is due to the frequency response of the essentially passive membrane being slower than the response to light in the photoreceptors of this nocturnal insect. This study has shown that, in the photoreceptors of the diurnal locust, the conductance change is the slower component. This is not surprising given the presence of the sustained voltage-dependent potassium conductance in these cells (Weckström 1994, Cuttle et al. 1995), which lowers the membrane resistance and hence the time constant of the cell, increasing the frequency response. It would be interesting to see whether, in a night state locust photoreceptor which has a deactivated the sustained voltage-dependent potassium conductance (Cuttle et al. 1995) and thus a higher membrane time constant, the relationship between the peaks resembles that seen in tipulids.

The presence of the prolonged tails in the calculated conductance changes may be an artefact caused by the use of the log-normal model data instead of actual experimental results. Examination of the log-normal fits for LA1 and LA2 in figure 1.2 shows that the fit is poor at the end of the impulse response. Repeating this analysis with experimental results would eliminate this possibility. An alternative explanation is that the tails are caused by the activity of the potassium conductance, which decays to its steady-state value more slowly than the membrane potential. This would be expected if the values for the activation time constant used in the parameter search were excessively high, but the range of time constants used was based on data from the blowfly (Weckström et al. 1991) according to the ideas expressed in Howard, Dubs and Payne (1984) Laughlin and Weckström (1993). For the locust, which has a slower photoreceptor response than a blowfly, it is likely that the time constant for the activation of the potassium conductance will be longer, although this remains to be confirmed experimentally.

Leaky integrator model

The leaky integrator photoreceptor model is useful for large simulations. In contrast with the electrical model, this model has only five parameters, consumes very little memory (only the current input and previous output are needed) and requires few calculations. The principal features of locust photoreceptors which are captured by this model are the latency and low-pass filtering of responses to transient signals and the gain control of light adaptation. Although comprehensive data with which to compare the model's responses is not available for the locust, this model allows the effects of photoreceptor filtering and light adaptation on higher level processing to be studied qualitatively.

As it is presented in this chapter, the model is suitable only for small contrast changes around which the responses of locust photoreceptors are approximately linear. However, the model can be enhanced in several ways:

- The sigmoidal relationship between the steady-state potential and the background intensity (Vishnevskaya et al. 1993) can be added by replacing the constant steady-state gain δ_{ss} with a bell shaped curve corresponding to the rate of change of the potential with background intensity.

- The sigmoidal shape of the relationship between the transient potential and intensity is not constant in locust photoreceptors, with a lower slope at lower intensities (Matić and Laughlin 1981). This can be added to the model by using an estimate of the background intensity to calculate the slope, and a nonlinear gain function.

- The time constants of the leaky integrators can also be adapted by using estimates of the background intensity and feedback from the output potential of the model.

These enhancements would allow the model to reproduce more accurately the responses to a wider range of stimuli including natural images, which contain many high contrast components (van Hateren 1997).

One property of locust photoreceptors which is difficult to model is the adaptation of the acceptance angle produced by structural changes in the ommatidium

(Williams 1983). However, the time course of these changes is long (for example, a change of 0.7^{o} can take 20 minutes) and the amount of disk space which would be needed to store a stimulus of sufficient length to produce this adaptation is prohibitive.

For the reasons outlined in section 2.1.3, this model needs to be used with caution because while it produces a good approximation of a photoreceptor step response, its impulse response is very inaccurate. This problem could be overcome by replacing the input integrator with a low-pass filter with an impulse response matched to that of a locust's photoreceptor, perhaps by using a finite impulse response filter with weights calculated using the log-normal model. Using the log-normal model would allow light adaptation to be modelled by adapting the values of the time-to-peak and the sensitivity.

Chapter 6

Electrical inhibition in the locust lamina

The axons of the six main photoreceptors (SVFs) within each ommatidium project retinotopically into the lamina cartridges where they make many synapses with the large monopolar cells (LMCs). While it is not known that the LMCs are on the input pathway to the LGMD, both their prominence in the optic lobe (Nowel and Shelton 1981, Shaw 1984) and the fast transient nature of their responses (Laughlin and Osorio 1989) suggest that this is the case. With this in mind it is important to consider how LMC responses might affect the visual input to the LGMD.

LMC responses show the effects of strong inhibition, thought to be mediated presynaptically by an extracellular field potential (Laughlin 1974, Shaw 1975). When the eye is illuminated, a local field potential builds up within each lamina cartridge (Shaw 1968): this may suppress the release of transmitter from the photoreceptor terminals by reducing their effective membrane potential. Two previous models for the production of the field potential were presented in section 1.1.3. However, neither of these models is sufficient to explain the inhibitory effects seen in the responses of the LMCs: the model of Shaw fails to explain the generation of the field potential, while Zimmerman's model omits the lateral flow of current.

A new model of electrical presynaptic inhibition in the lamina was developed for this thesis in order to study the possible effects of this inhibition on the visual

input to the LGMD. The model is based on the idea of Shaw (1975) and Laughlin (1974) that the field potential is due to the current from the photoreceptors. Owing to the lack of experimental data for the field potential and the mechanism of inhibition in the locust, the model is generic and could apply equally to other insect species.

This chapter describes:

- the new model of electrical presynaptic inhibition in the lamina.
- the responses of the model to a variety of visual stimuli.
- the implications of these responses for the LGMD..

6.1 Structure

The model comprises a $17 * 17$ hexagonal array of retinotopic units, each of which describes a photoreceptor and the extracellular space in a single lamina cartridge. Figure 6.1 shows the structure of a unit.

The photoreceptor element represents all six short visual fibres in one ommatidium which, in the locust, view the same point in space. For most types of stimulus the leaky integrator model of section 5.2 was used, with the following parameters: Δ, 15ms; δ_{pk}, 40mV/decade; δ_{ss}, 10mV/decade; τ_f, 6ms; τ_b, 200ms. However, when the impulse response was important the log-normal model of (Payne and Howard 1981) was used, with the responses of the photoreceptor assumed to be linear. The following parameters were used: t_p, 23ms; σ, 0.31.

The extracellular space in the lamina is modelled with the capacitance C_c while g_c represents the leakage conductance of the resistance barriers which isolate the lamina from the eye and the remainder of the optic lobe. g_s models the connections from a cartridge to its six neighbours through the glial cells which surround the cartridge. The value of g_s is the total conductance which is six times larger than the conductance to a single cartridge. g_{ph} represents the total conductance of the photoreceptor terminals, and is six times greater than the terminal conductance of a single photoreceptor, which was set to 10nS (equivalent to 100MΩ) .

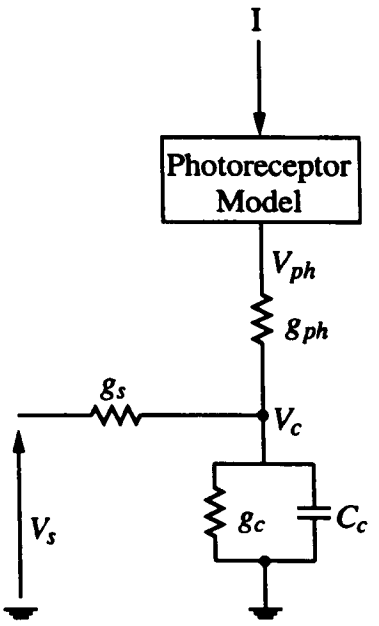

Figure 6.1: Electrical model of a single cartridge in the locust lamina. Current from the photoreceptor accumulates in the extracellular space, represented by C_c, resulting in a field potential, V_c, within the cartridge. I, light intensity; V_{ph}, photoreceptor membrane potential; g_{ph}, photoreceptor terminal conductance; V_c, field potential in cartridge; g_c, cartridge leakage conductance; C_c, cartridge capacitance; g_s, conductance to surrounding cartridges; V_s, average potential in surrounding cartridges.

The field potential, V_c, is calculated by considering the flow of currents within the cartridge. It is given by

$$\frac{dV_c}{dt} = \frac{1}{C_c}\left[g_{ph}V_{ph} + g_sV_s - (g_c + g_s + g_{ph})V_c\right], \tag{6.1}$$

where $\frac{dV_c}{dt}$ is the rate of change of the cartridge field potential, V_c, and V_s is the mean of the field potentials in the six surrounding cartridges. This equation was evaluated using the 4th-order Runge Kutta numerical integration technique described in section 2.1.2.

The response of the LMCs within the cartridge is assumed to be linearly dependent on the difference between the photoreceptor membrane potential and the cartridge field potential, such that

$$V_{LMC} = \delta_{LMC}(V_{ph} - V_c), \tag{6.2}$$

where δ_{LMC} is the gain of the photoreceptor-LMC synapse.

The model is biased so that at a background intensity of $I = 1$, all the responses are zero. Changes of intensity produce positive and negative responses around this bias point, with the responses of the model's elements coding the contrast change rather than the absolute intensity.

6.2 Stimuli

Stimuli were generated using the method of section 2.2.2. For most simulations the acceptance angle and angular separation of the photoreceptor elements was the same as for the LGMD models of chapters 3 and 4 (2.0° and 3.3° respectively). However, for several simulations these values were matched to those of the locust eye (1.5° and 1.25° respectively) in order to compare the two cases. For convenience these two "eyes" are refered to as "wide" and "narrow" in the remainder of this chapter.

A range of static and moving stimuli were used. The static stimuli were: a "centre" stimulus comprising a 1° diameter circle centred on a cell's optical axis; a "surround" stimulus comprising an annulus centred on a cell's optical axis with

an inner diameter of 3° and an outer diameter of 6°; and a wide field intensity change. The moving stimuli included the moving shapes previously used with the LGMD models and also edges moving at constant angular velocities. The contrast of the moving stimuli was 0.2.

6.3 Responses

6.3.1 Static stimuli

The data presented below were taken from the central unit in the model (figure 6.2).

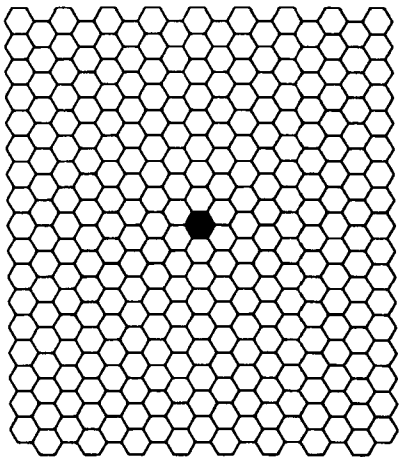

Figure 6.2: Recording site in the model for static stimuli

Impulses

The model was tuned by matching the LMC impulse responses with the first order kernels calculated by James and Osorio (1996) as closely as possible (see discussion). Figure 6.3 shows these responses for the wide eye while figure 6.4 shows the responses for the narrow eye. Brief (1ms) flashes of the centre stimulus produce a transient hyperpolarisation followed by a short weak depolarisation. In contrast, flashes of the surround stimulus produce a slow depolarisation of lower amplitude. The responses to wide field impulses are similar to the centre responses,

but the following depolarisation is more prominent, especially for the narrow eye (figure 6.4(b)).

Table 6.1 shows the parameters used for the two eye sizes. Only the size of the lateral conductance, g_s, changes to compensate for the closer proximity and greater overlap between the receptive fields of neighbouring photoreceptor elements in the narrow eye. The value of δ_{LMC} was chosen to produce a synaptic gain of 6, matching (arbitrarily) the value calculated for the blowfly (Laughlin, Howard and Blakeslee 1987).

	Wide eye	Narrow eye
g_s (nS)	5	75
g_c (nS)	1	1
C_c (nF)	1	1
δ_{LMC}	-10	-10

Table 6.1: Lamina model parameter values

The potential changes within a cartridge which underly the impulse responses in the wide eye are shown in figure 6.5. For the centre stimulus the photoreceptor depolarises before the extracellular field, producing the initial hyperpolarisation of the LMC. After the photoreceptor potential peak the difference between the photoreceptor potential and the extracellular field potential decreases, reducing the LMC hyperpolarisation, then reverses, depolarising the LMC. Gradually both the photoreceptor and field potentials decay, reducing and ultimately eliminating the LMC response. In contrast, the surround stimulus produces no depolarisation in the photoreceptor (the stimulus is outside its receptive field) but the extracellular field depolarises due to lateral currents flowing from the surrounding stimulated cartridges, depolarising the LMC.

The potential changes underlying the impulse responses in the narrow eye are similar (figure 6.6). However, the extracellular field potential never exceeds the photoreceptor potential for the centre stimulus which results in a purely hyperpolarising impulse response.

As a result of the broadly similar responses of the models to stimuli "seen" through both the wide and narrow eyes, the remaining responses are shown for the wide eye, for which stimuli are more easily generated, unless stated otherwise.

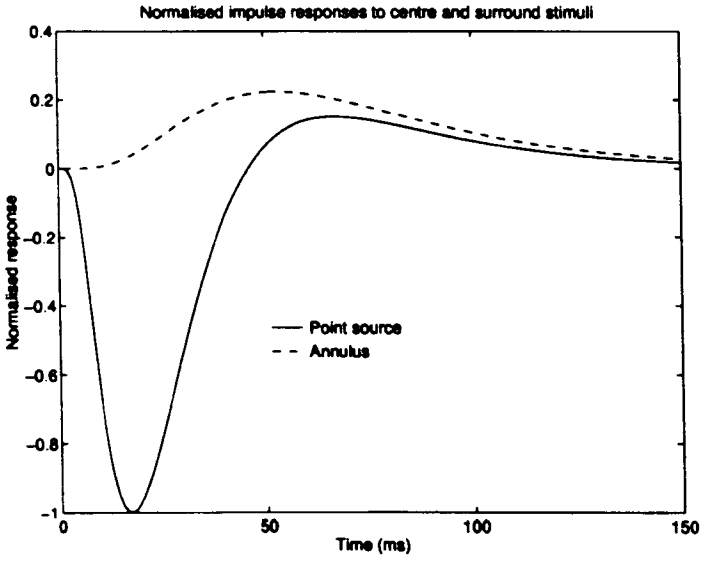

(a)

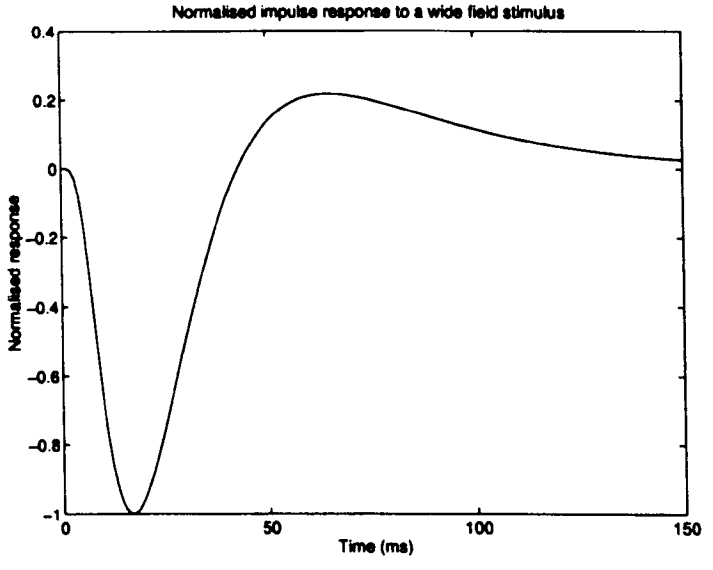

(b)

Figure 6.3: Normalised impulse responses of a model LMC when stimulated with brief flashes from: (a) centre stimulus (solid line) and surround stimulus (dashed line); (b) a wide field stimulus. Wide eye: acceptance angle, 2.0°; angular separation, 3.3°.

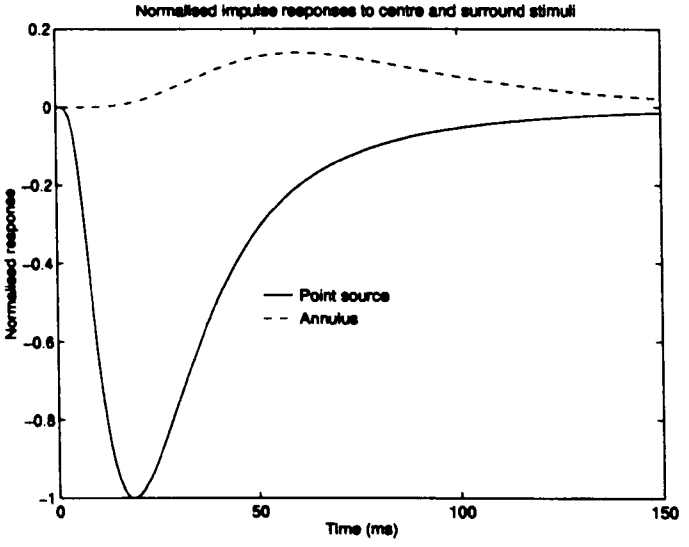

(a)

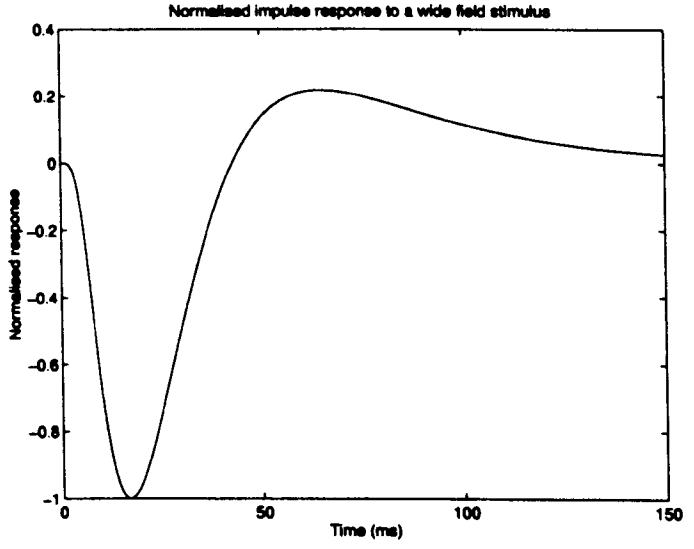

(b)

Figure 6.4: Normalised impulse responses of a model LMC when stimulated with brief flashes from: (a) centre stimulus (solid line) and surround stimulus (dashed line); (b) a wide field stimulus. Narrow eye: acceptance angle, 1.5°; angular separation, 1.25°.

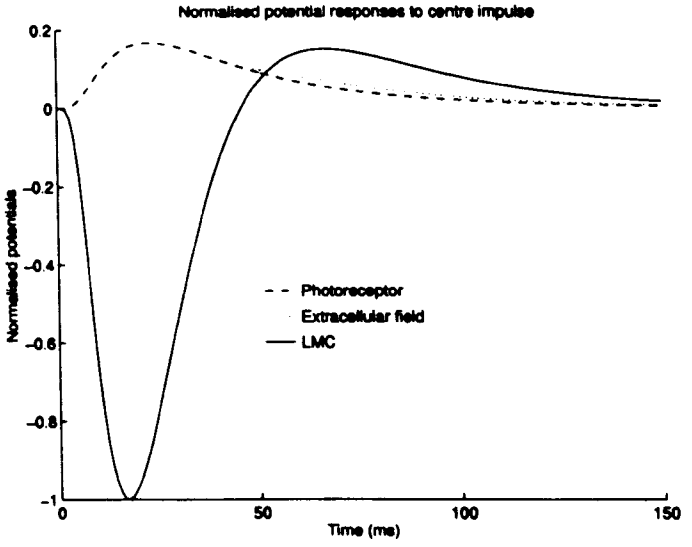

(a)

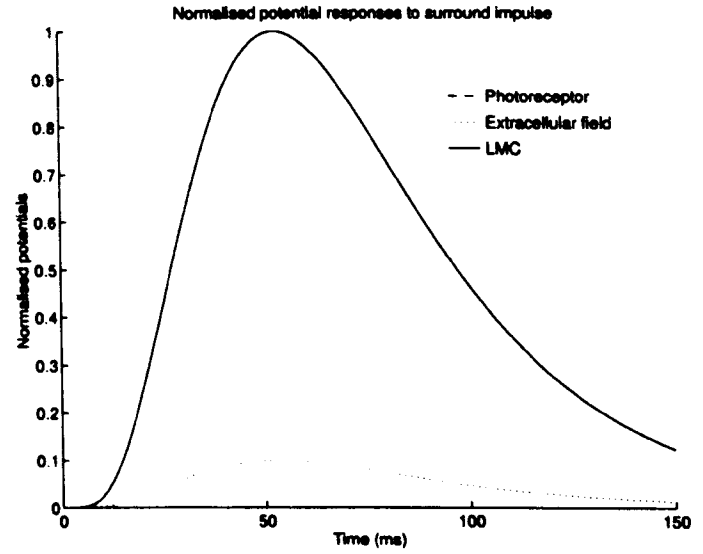

(b)

Figure 6.5: Potential changes underlying model LMC impulse responses for the wide eye. All potentials are adjusted to normalise the LMC response. (a) Centre stimulus. (b) Surround stimulus. Broken line, photoreceptor potential; dotted line, extracellular field potential, solid line, LMC potential.

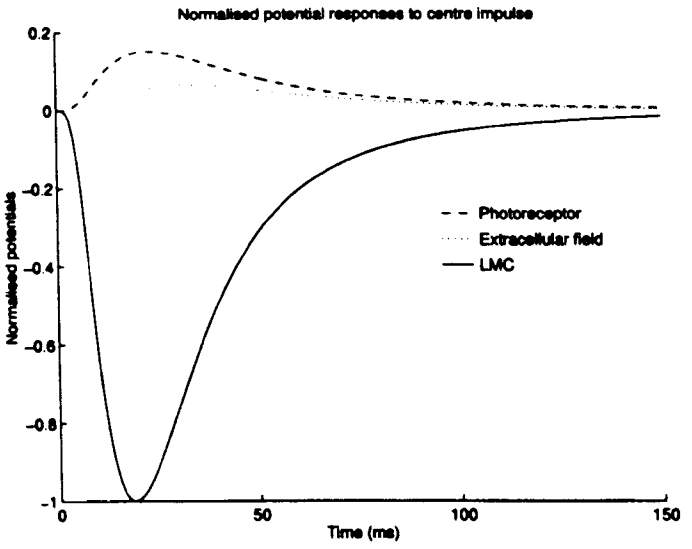

(a)

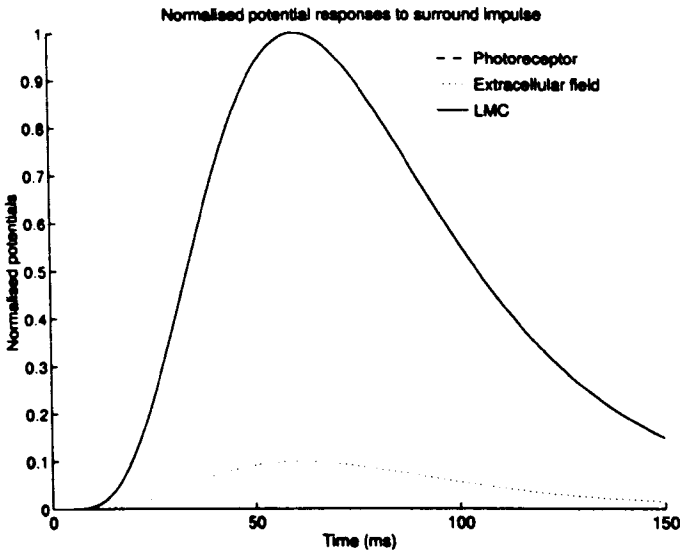

(b)

Figure 6.6: Potential changes underlying model LMC impulse responses for the narrow eye. All potentials are adjusted to normalise the LMC response. (a) Centre stimulus. (b) Surround stimulus. Broken line, photoreceptor potential; dotted line, extracellular field potential, solid line, LMC potential.

Steps

The responses of the model to step changes in intensity illustrate well the effects of the inhibition by the field potential on the outputs of the LMCs.

Figure 6.7 shows the responses to a step increase in the intensity of the centre stimulus. The LMC response hyperpolarises rapidly at the start of the response due to the depolarisation of the photoreceptor. Gradually the extracellular field potential depolarises, reducing the difference between itself and the photoreceptor potential, and the LMC response is reduced. After approximately 50ms, the amplitudes of all three potentials decay slowly due to the adaptation of the photoreceptor: the speed of adaptation of the photoreceptor controls the rate of this decay.

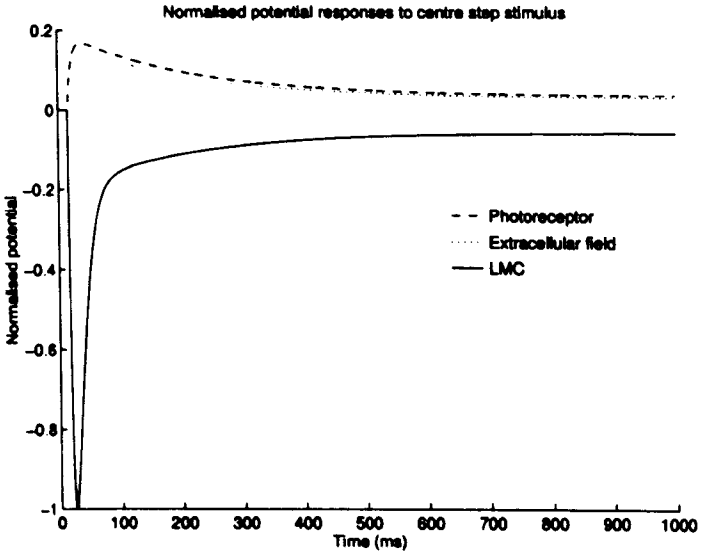

Figure 6.7: Normalised step response of a model LMC in the wide eye when stimulated with the centre stimulus. Broken line, photoreceptor potential; dotted line, extracellular field potential, solid line, LMC potential.

The responses to a step increase in a wide-field stimulus is shown in figure 6.8. This response is very similar to the centre step response, but the early decay of the LMC potential is more severe due to more rapid depolarisation of the field potential. The absence of any lateral current flow (all cartridges have the same field potential due to the uniform stimulus) results in higher field potentials

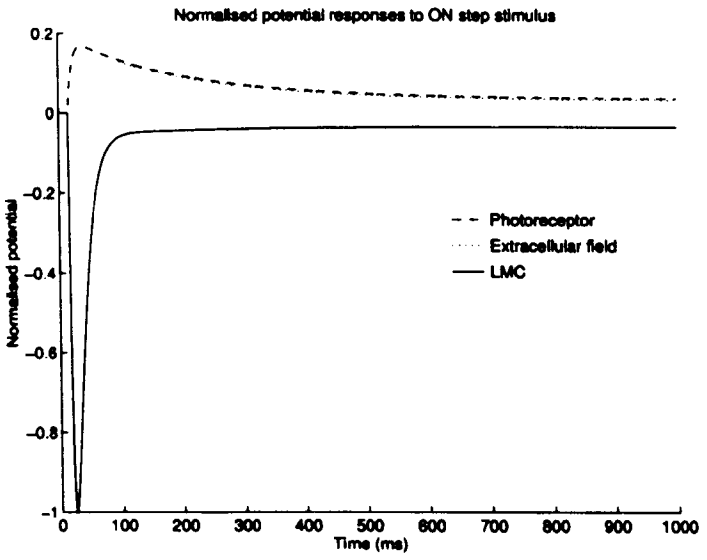

Figure 6.8: Normalised step response of a model LMC in the wide eye when stimulated with the wide-field stimulus. Broken line, photoreceptor potential; dotted line, extracellular field potential, solid line, LMC potential.

Figure 6.9 shows the responses to a step increase in the intensity of the surround stimulus. The LMC response rises as the field potential depolarises due to the lateral flow of current into the cartridge from neighbouring cartridges. The decay in the response is controlled by the adaptation of the stimulated photoreceptors.

6.3.2 Moving stimuli

Much of the data presented below was recorded from the central row of the model (figure 6.10).

Edges

The responses of the model photoreceptors and LMCs to edges moving at a range of angular velocities are shown in figure 6.11. In both the photoreceptors and the LMCs, the responses lag behind the position of the edge and this lag increases with edge velocity.

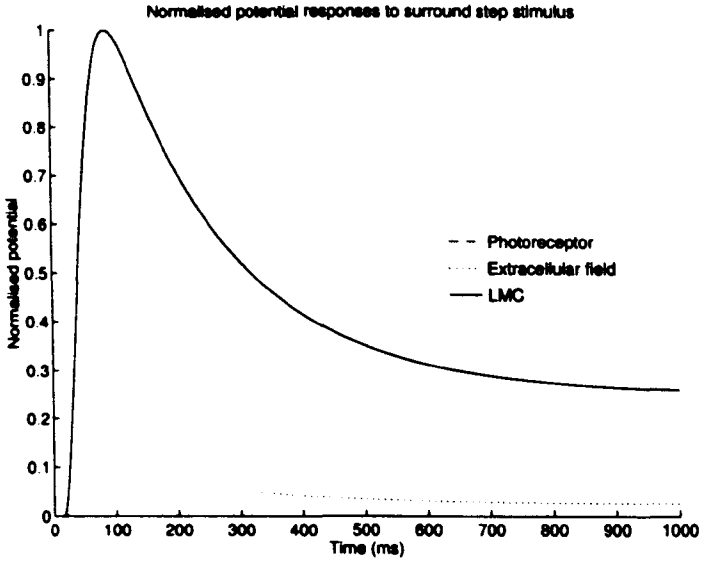

Figure 6.9: Normalised step response of a model LMC in the wide eye when stimulated with the surround stimulus. Broken line, photoreceptor potential; dotted line, extracellular field potential, solid line, LMC potential.

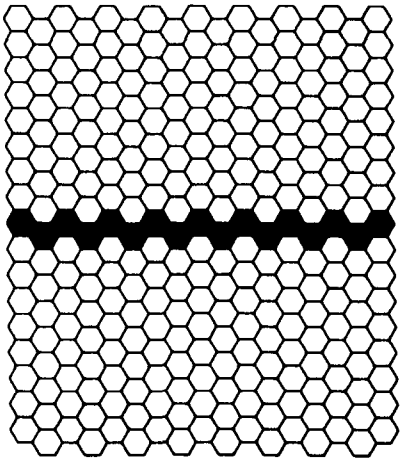

Figure 6.10: Recording site in the model for moving stimuli

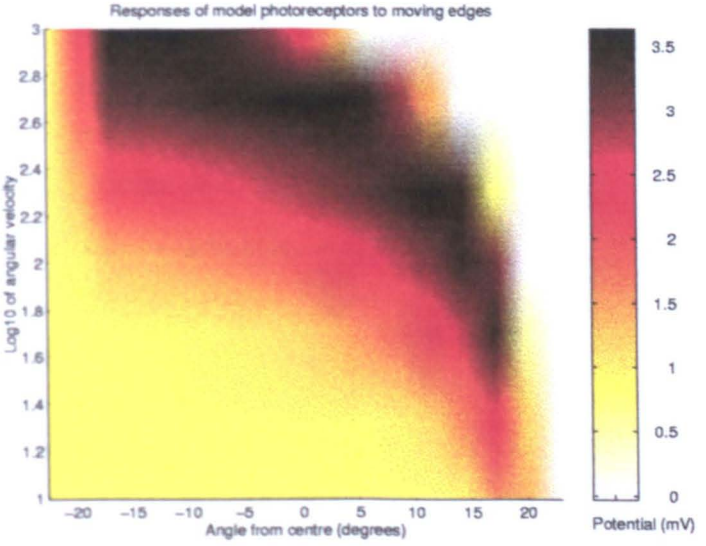

(a)

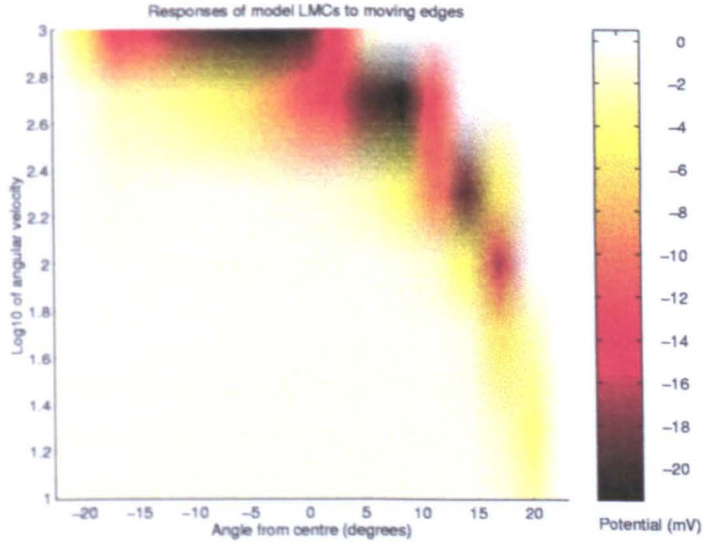

(b)

Figure 6.11: Responses of the model photoreceptors and LMCs to moving edges. The activity in one line of the model along the direction of motion is shown for a range of angular velocities (10°/s, 20°/s, 50°/s, 100°/s, 200°/s, 500°/s, 1000°/s) when the edge is at 20°. The edges moved from $-20°$ to 20°. (a) Photoreceptors. (b) LMCs.

In the photoreceptors the peak amplitude of the response is approximately equal for all edge velocities, but the responses to the lower velocities are weaker than the responses to higher velocities in the LMCs. The rate of change of the LMC responses, shown in figure 6.12, is interesting, with the peak rate of change occuring closer to the edge than the peak LMC response.

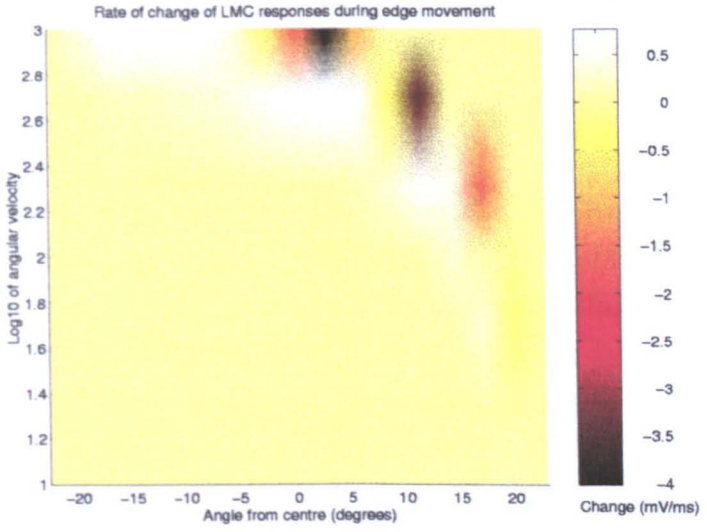

Figure 6.12: Rate of change of LMC potential in response to moving edges. The activity in one line of the model along the direction of motion is shown for a range of angular velocities (10°/s, 20°/s, 50°/s, 100°/s, 200°/s, 500°/s, 1000°/s) when the edge is at 20°. The edges moved from −20° to 20°.

Figures 6.13 and 6.14 reveal the cause of the weaker responses to slow moving edges. A fast moving edge crosses the photoreceptor's receptive field quickly, producing a rapid change in the intensity seen by the photoreceptor. The intensity change resembles the step change described above and the response mirrors the step response closely: the photoreceptor depolarising more rapidly than the extracellular field, producing a large hyperpolarisation in the LMC. However, at lower velocities the edge takes longer to cross the receptive field of the photoreceptor, resulting in a gradual change in the intensity seen. The resulting depolarisation of the photoreceptor is much slower than for the fast edge and the depolarisation of the extracellular field matches the depolarisation of the photoreceptor more closely. This reduces the difference between the two potentials and gives a smaller

response from the LMC.

The discrete steps seen in figure 6.14 are caused by pixel noise in the stimulus resulting from the slow movement of the edge. In the 1ms time period used in these simulations the edge moves less than one pixel across the screen and the stimulus appears to move in a series of jumps. The amplitude of the noise increases as the speed of edge movement decreases, and the LMC response to an edge moving at 10°/s (figure 6.15) shows a large amount of noise.

Objects

The responses to moving edges described above affect the responses of the model LMCs to approaching objects. Figures 6.16, 6.17 and 6.18 show the LMC responses to a square approaching at three different speeds, along with the stimulus.

For all speeds the response is small when the object is distant and the angular velocity of the edges is low. As the angular velocity increases during the approach, so does the LMC response. In the final stages of approach the LMCs respond strongly although the response lags behind the edges of the stimulus, particularly for high approach speeds.

As for edges moving at constant velocity, the rate of change of the LMC responses peaks earlier than the LMC response itself and marks the passage of the object's edges more closely (figure 6.19).

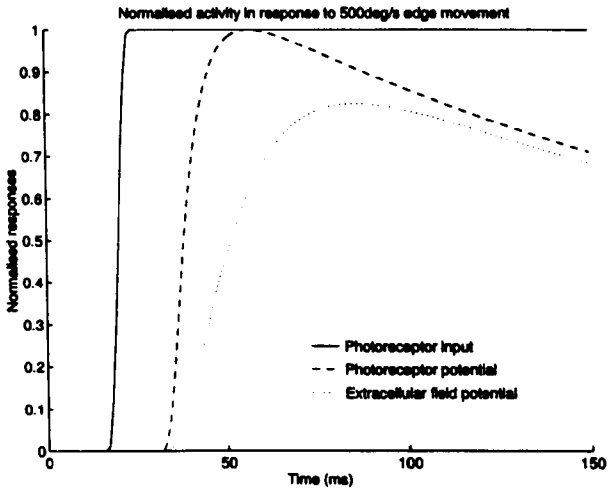

(a)

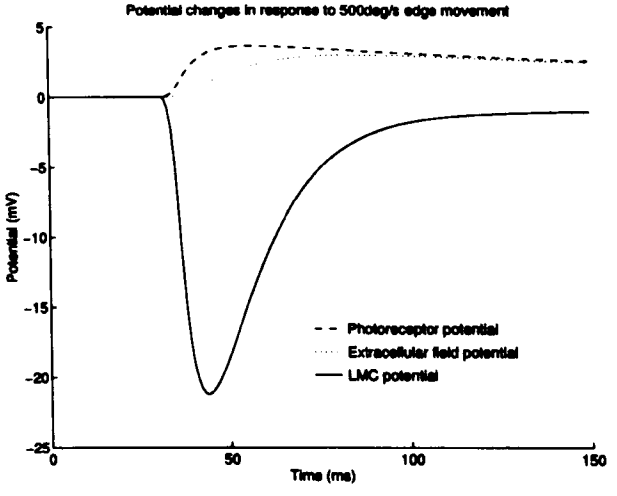

(b)

Figure 6.13: Responses of the model photoreceptors and LMCs to a 500deg/s edge. The activity in one unit of the model is shown. (a) Normalised activity: solid line, intensity; dashed line, photoreceptor potential; dotted line, extracellular field potential. The field potential is normalised using the maximum response of the photoreceptor potential in order to preserve the relative amplitudes. (b) Potential changes: dashed line, photoreceptor potential; dotted line, extracellular field potential; solid line, LMC potential.

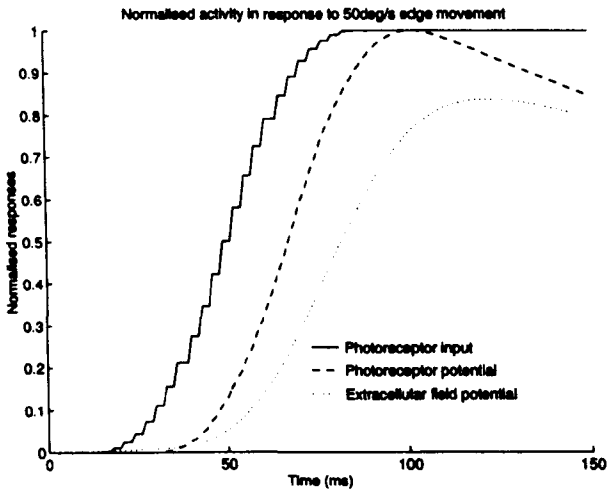

(a)

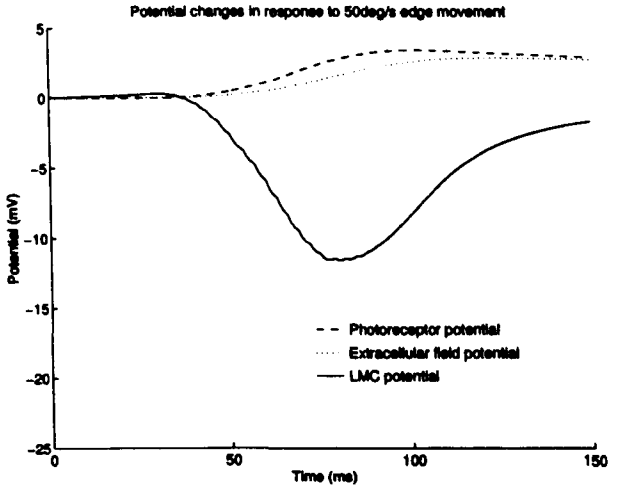

(b)

Figure 6.14: Responses of the model photoreceptors and LMCs to a 50deg/s edge. The activity in one unit of the model is shown. (a) Normalised activity: solid line, intensity; dashed line, photoreceptor potential; dotted line, extracellular field potential. The field potential is normalised using the maximum response of the photoreceptor potential in order to preserve the relative amplitudes. (b) Potential changes: dashed line, photoreceptor potential; dotted line, extracellular field potential; solid line, LMC potential.

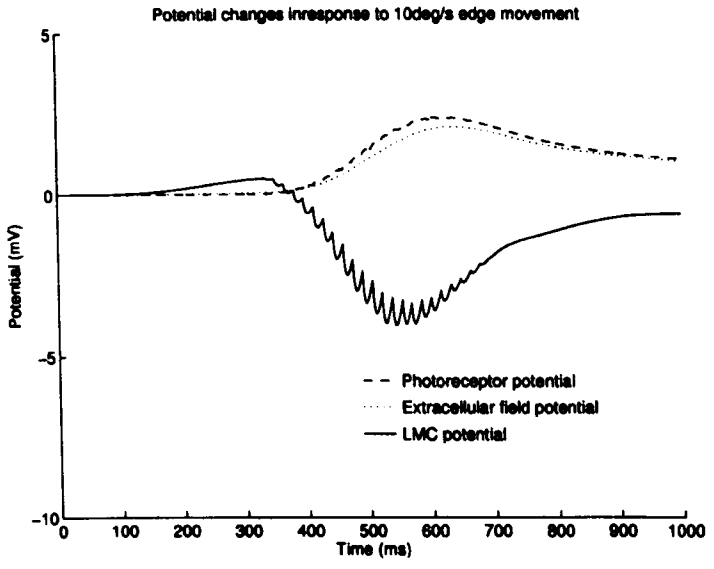

Figure 6.15: Potential changes in the photoreceptors and LMCs in response to a 10deg/s edge. The activity in one unit of the model is shown. The LMC potential shows the effects of the pixel noise in the stimulus. Dashed line, photoreceptor potential; dotted line, extracellular field potential; solid line, LMC potential.

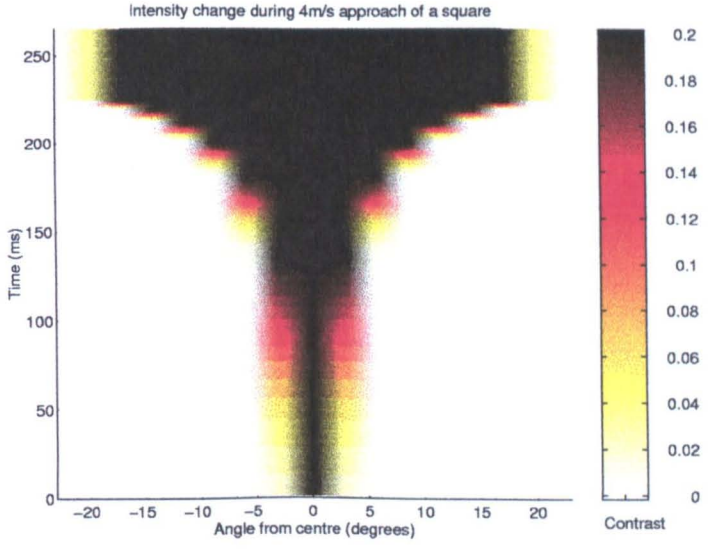

(a)

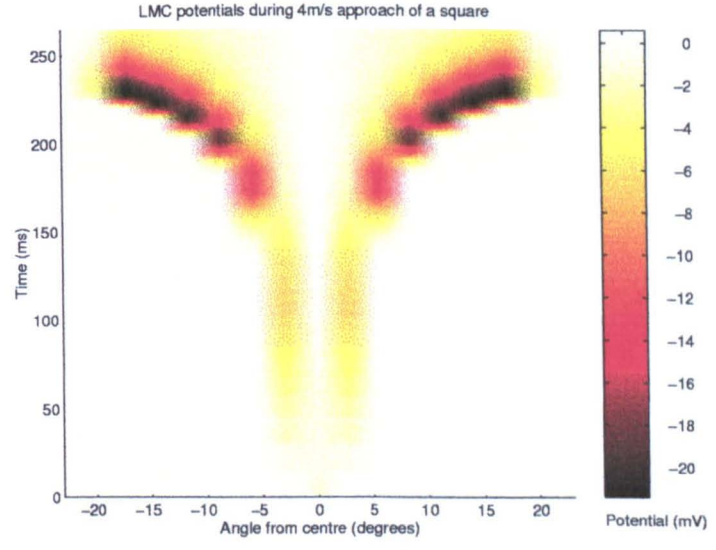

(b)

Figure 6.16: Responses of the model LMCs to a 70mm square approaching at 4m/s. The square moved from 1000mm to 100mm distance from the eye. The activity in one row of units is shown. (a) Stimulus. (b) LMC potential.

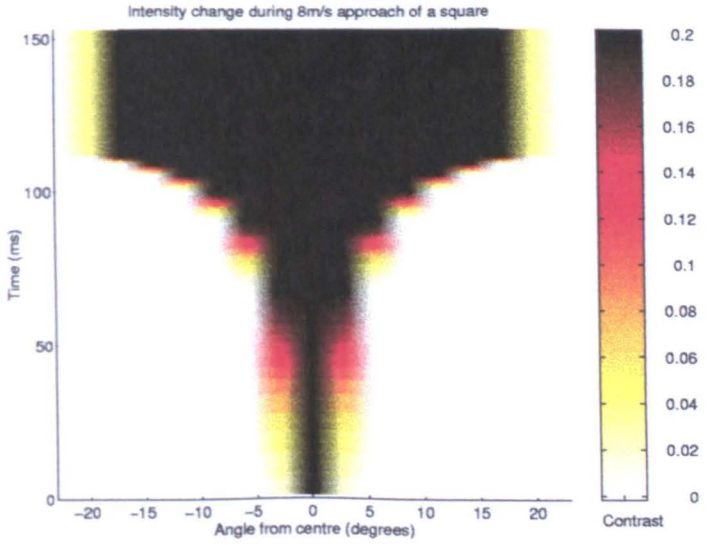

(a)

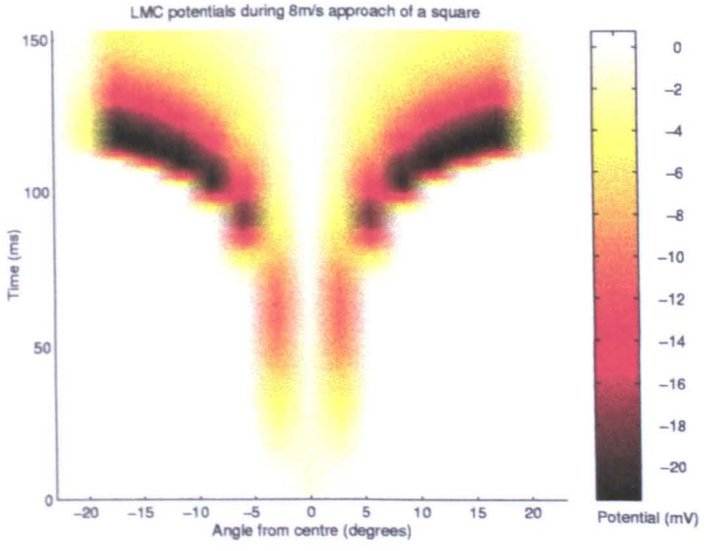

(b)

Figure 6.17: Responses of the model LMCs to a 70mm square approaching at 8m/s. The square moved from 1000mm to 100mm distance from the eye. The activity in one row of units is shown. (a) Stimulus. (b) LMC potential.

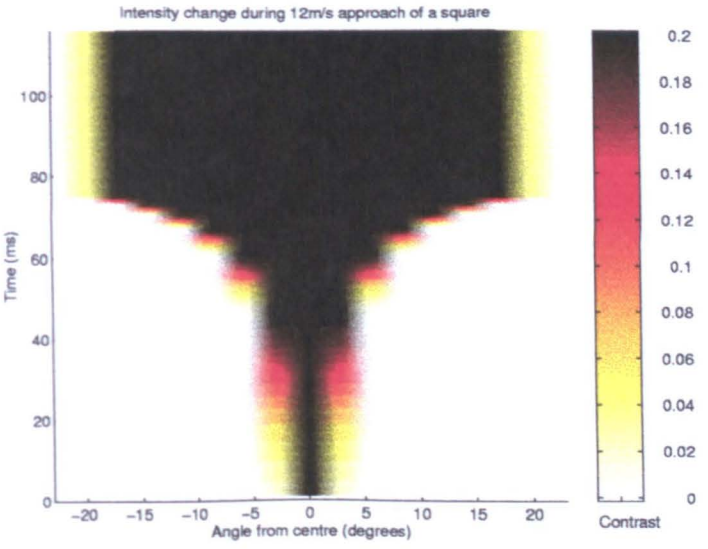

(a)

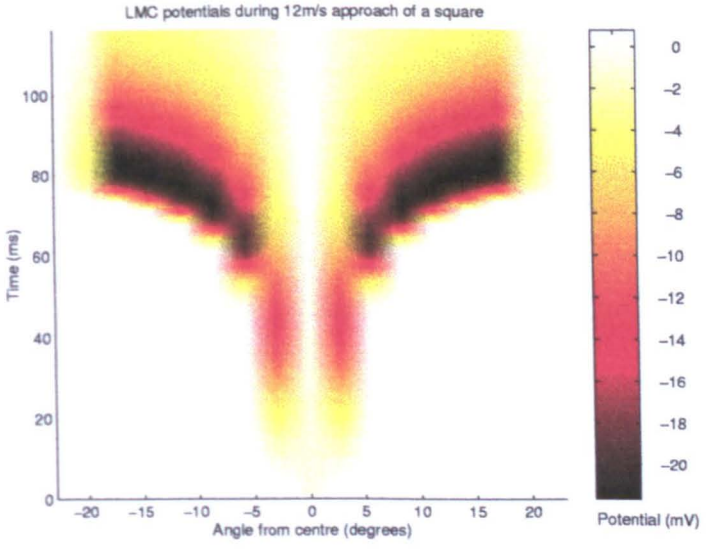

(b)

Figure 6.18: Responses of the model LMCs to a 70mm square approaching at 12m/s. The square moved from 1000mm to 100mm distance from the eye. The activity in one row of units is shown. (a) Stimulus. (b) LMC potential.

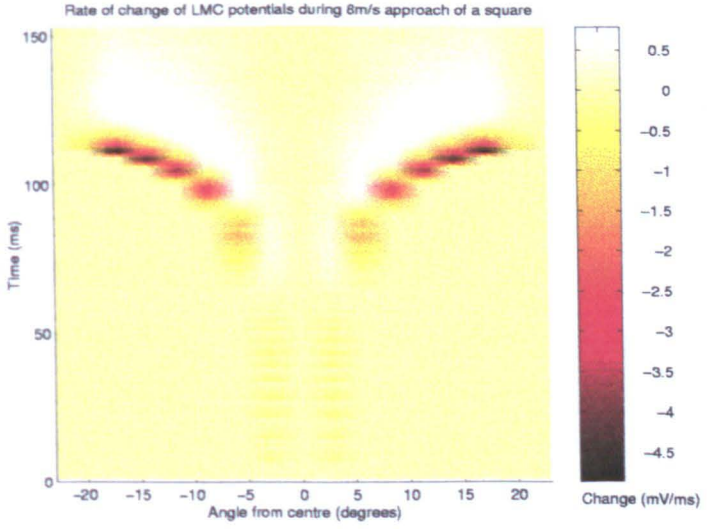

Figure 6.19: Rate of change of LMC responses to a 70mm square approaching at 8m/s. The square moved from 1000mm to 100mm distance from the eye. The activity in one row of units is shown.

6.4 Discussion

The model described in this chapter incorporates two new features not used in previous models, the capacitance C_c which models the extracellular space within a cartridge and the conductance g_s which connects a cartridge to its neighbours. These elements combine to produce the lateral and feedback inhibition seen in LMC responses.

A number of important assumptions have been made:

- Current flowing from the lamina into the photoreceptors does not affect their membrane potential. The photoreceptor soma has a low membrane resistance (in a light-adapted cell) and a large volume (Weckström 1994) while the lamina cartridge has a small volume (Shaw 1977) and the photoreceptor terminal has a high membrane resistance (van Hateren 1986b). As a result the current flowing from the lamina into the photoreceptors will be too small to produce an appreciable effect in the soma.

- The rate limiting steps are the photoreceptor response and the generation of the field potential. The LMC membrane capacitance is assumed to be insignificant, and the speed of synaptic transmission assumed to be instantaneous (Laughlin et al. 1987, Laughlin and Osorio 1989).

- The synaptic gain is constant and linear. The work of Laughlin et al. (1987) shows that the characteristic curve of the photoreceptor-LMC synapses in blowflies shifts with light-adaptation to keep the mid-region, where the curve is approximately linear, centred on the operating point

- Only the current from the photoreceptors contributes to the field potential, with no contribution from the LMC currents. The arrangement implies that, during the response to an intensity change, no transients will be generated in the field potential, and this was seen by (Shaw 1968).

  However, recent work by Kettunen, Weckström and Laughlin (personal communication) on the blowfly questions this assumption. Recordings of the field potential were differentiated to reveal the underlying current, and this resembles quantitatively the light-induced current recorded in the

LMCs. This finding is supported by considering the photoreceptor and LMC input resistances in the lamina. The LMC has a much lower membrane resistance of the LMCs than the photoreceptor terminals, and hence the LMC currents will be larger than the photoreceptor currents.

These assumptions have produced a generic model which may be applied equally well to other insect species. There is insufficient experimental evidence to verify the assumptions made and no published values for the majority of the parameters used. However, the model provides a useful starting point from which to assess the effects of inhibiton in the lamina.

Given the lack of published data, the model was tuned by matching the impulse responses to the first order Wiener kernels calculated from white-noise responses by James and Osorio (1996). With Wiener kernels, the first order kernel equals the impulse response for a linear system. The second order kernels calculated for the LMCs are small when compared with the first order kernels, so the assumption was made that the first order kernels are approximately equal to the impulse response.

The responses to moving edges resemble those predicted by Juusola and French (1997) for the blowfly. The precise tuning of the response is dependent on the spatiotemporal responses of the photoreceptors. For a slow moving edge the time taken to cross the receptive field of a photoreceptor is longer than the time taken for the cell to respond and the response is dictated by the amount of receptive field that the edge covers. As the speed of the edge movement increases the time taken for the edge to cross the receptive field decreases and becomes shorter than the response time of the photoreceptor. The edge is now seen as a step input by each photoreceptor. For larger receptive fields the speed at which the edge becomes a step input is higher.

The lag between the edge and the response is dependent on the speed of the photoreceptor's response, with slower photoreceptors giving a greater lag. Comparison between the responses of the model described in this chapter and the predictions of Juusola and French (1997) reinforces this idea, with the faster blowfly photoreceptors introducing less lag. The relationship between the lag in the LMCs and the photoreceptors is different in the two studies, and this results from the different stimuli used. In the blowfly study a point source was used which resembles

a flash as it passes across the receptive field of a photoreceptor. This produces an impulse response from both the photoreceptor and the LMC, which have similar temporal properties (Laughlin et al. 1987) and hence give a similar lag. For the edges used in this study, the passage of the edge across a photoreceptor's receptive field produces a step response which is a prolonged depolarisation in the photoreceptor but only a transient hyperpolarisation in the LMC, which has a peak earlier than the photoreceptor response (Laughlin et al. 1987) and hence a shorter lag. The rate of change of the LMC response has the shortest lag, and signals the passage of the edge most accurately.

The strong responses to edges produced by this model were predicted by Srinivasan, Pinter and Osorio (1990), who proposed that LMCs are matched filters optimised for the detection of moving edges at high light levels by a combination of strong temporal inhibition and weak lateral inhibition. The response of the model presented here increases with edge velocity, reaching a maximum when the speed of the edge makes its passage across a photoreceptor's receptive field resemble a step input. This corresponds qualitatively with the profile of a cell optimised to detect edge velocities between two finite extremes, which was referred to as system 1 by Srinivasan et al. (1990). However, more analysis of this model, including the calculation of the spatiotemportal impulse responses, is needed before any firm conclusions can be made.

At low light levels, when both types of inhibition are inactive, Srinivasan et al. (1990) claim that the optimisation alters to detect moving 'blobs'. In the model shown here, this change in optimisation could arise by two methods, either by an increase of the lateral conductance between cartridges (g_s), which extends the range of lateral current flow, reducing the accumulation of charge in any one cartridge, or by an increase in the cartridge leakage conductance (g_c), which discharges the current entering the cartridge and prevent any accumulation of charge.

This theory is not supported by either van Hateren (1992) or Laughlin (1994), who argue that the strong responses to moving edges are a byproduct of more general processing, rather than the extraction of specific features from the scene, and that the LMCs maximise the flow of information. However, as noted by van Hateren (1992), the presence of several types of LMCs, each with subtlely different response properties, suggests that these neurons may emphasise different

features in a scene.

Implications of LMC responses for the LGMD

If the LMCs are on the input pathway to the LGMD, the responses described above may have a significant effect on the input the LGMD receives.

Already in the lamina there is a preference for faster moving edges, which produce large responses while slow moving edges produce only weak responses. As a result the edges of approaching objects produce little response when the object is distant and the edges move slowly, but this response increases dramatically as the object nears the eye and the edge velocity increases. This preference could be responsible for the dependence of the LGMD response on increasing edge velocity (Simmons and Rind 1992), which increases rapidly up to edge velocities of 120°/s and increases only slowly thereafter.

LMC responses have a distinct sustained phase, which suggests that the transient responses proposed for the input to the LGMD may be generated from the rate of change of the LMC response rather than the response itself. A similar proposal has been made for the synapses between the large second-order 'L-neurons' of locust ocelli (Simmons 1985). The rate of change also signals the position of the edge more accurately than the LMC response, although if the transient cells recorded by Osorio (1987) are the input to the LGMD this more precise timing is lost.

Chapter 7

Conclusions

The aim of the research described in this thesis was the development of a biologically inspired neural network for detecting approaching objects based on the lobula giant movement detector (LGMD) system of the locust. Particular emphasis was given to aspects of the biological system not considered previously. The results of the simulations presented in this thesis show that:

- the responses of the LGMD neural network model of Rind and Bramwell (1996) are dependent on the shape of the stimulus used when the edges of the stimulus are aligned with the receptive fields of the P cells. Expanding the receptive fields of the input P cells of the model removes this dependency, but the presence of the resulting responses in the biological system is uncertain.

- the average conductance change produced by a single photon can be calculated from a photoreceptor's impulse response by using an electrical model of the cell's membrane. A parameter search suggests that the peak of this conductance change is likely to coincide with the peak of the impulse response in photoreceptors which have voltage-dependent conductances. The method used here could be used in a quantitative study of the effects of light adaptation.

- a leaky integrator photoreceptor model is a useful component for use in large simulations. The model presented here displays the latency and low-

pass filtering characteristics of photoreceptor transient responses, and the gain control of light adaptation, and this basic model can be expanded as new experimental data becomes available.

- early visual processing by LMCs may play a significant role in the preference of the LGMD for fast moving edges and approaching objects. The responses of the LMCs are stronger for fast moving edges than for slow moving edges, and approaching objects produce little response until they are close to the eye.

Future research

In light of the findings of Kettunen, Laughlin and Weckström (personal communication), the model of electrical inhibition in the lamina must be extended to include the LMC currents. This would require more detailed data about the membrane properties of the LMCs than is available for the locust at present, but there is sufficient data available from the blowfly to allow this study to continue. One important aspect of this extended model will be the need to balance the time constants of the various components in order to prevent unstable oscillations in the response. By enhancing the photoreceptor model used in the simulations, the responses of the LMCs to natural images could also be studied and compared with the study of van Hateren (1997).

The modelling approach used during this work attempts to simulate the processing performed by the neurons which form the LGMD input circuit. The "black box" approach taken by Hatsopoulos, Gabbiani and Laurent (1995) is substantially different, but the two approaches are complementary. Models of the LGMD input circuitry allow the mechanisms used to extract the stimulus paramaters required by the "black box" model to be studied, and testing different circuit configurations may suggest ways to reformulate the "black box" input-output relationship. The techniques for encoding of the stimulus parameters by the arrays of neurons can be explored.

The offline stimulus generation method used in this study is restricted to use with only short stimuli. For longer stimuli the time taken to produce a stimulus and the memory required to store it become excessively large. This problem can

be overcome if a more efficient stimulus system is adopted. One possible method is to use a camera mounted on a mobile robot to sense the environment as the robot moves, although the number of stimulus frames seen per second is lower than is offered by the offline method. This approach is simplified by the use of the Xmorph software package (Verschure 1997), which provides interfaces to the robot and camera and a graphical user interface to aid the design of simulations. In its simplest form, this approach would use the robot moving in a straight line towards a stimulus and use the responses of the LGMD model to stop the robot before collision. A more sophisticated design would use the responses of the LGMD to control a collision avoidance behaviour: this situation would test the ability of the feed-forward inhibition connection within the LGMD model to suppress the responses during motion in the whole visual field.

A second method is to design a neuromorphic model of the LGMD using analogue components. The model could be based on the modified neural network model described in chapter 4 or an extension of the model of the fly retina designed by Liu (in press). The continuous time operation of the analogue components in these models removes the problems of low frame rate that may result from the camera-based method, but the internal workings of the model are more difficult to examine and the cost and time for development are much larger.

Bibliography

Anderson, J. and Hardie, R. C. (1996). Different photoreceptors within the same retina express unique combinations of potassium channels, *Journal of Comparative Physiology A* **178**: 513–522.

Becker, K. and Backhaus, W. (1998). A physiological model of dark and light adapted photoreceptors in the honeybee worker, *in* N. Elsner and R. Wehner (eds), *Proceedings of the 26th Göttingen Neurobiology Conference*, Vol. I, Georg Thieme Verlag, p. 7.

Bennett, R. R., Tunstall, J. and Horridge, G. A. (1967). Spectral sensitivity of single retinula cells of the locust, *Zeitschrift für vergleichende Physiologie* **55**: 195–206.

Blanchard, M. and Rind, F. C. (1997). Collision avoidance: a neural network model of the locust LGMD capable of resolving natural images, *Brain Research Association Abstracts*, Vol. 14, p. 54.

Blanchard, M. and Rind, F. C. (1998). Light-activated conductance changes in a locust photoreceptor may sum linearly, *in* N. Elsner and R. Wehner (eds), *Proceedings of the 26th Göttingen Neurobiology Conference*, Vol. II, Georg Thieme Verlag, p. 395.

Bower, J. M. and Beeman, D. (1995). *The book of GENESIS*, TELOS.

Burrows, M. and Rowell, C. H. F. (1973). Connections between descending visual interneurones and metathoracic motoneurones in the locust, *Journal of Comparative Physiology* **85**: 221–234.

Burtt, E. T. and Catton, W. T. (1952). Nerve impulses originating from the compound eye of the locust, *Nature* **170**: 285.

Burtt, E. T. and Catton, W. T. (1964). The potential profile of the insect compound eye and optic lobe, *Journal of Insect Physiology* **10**: 689–710.

Cheney, W. and Kincaid, D. (1994). *Numerical mathematics and computing*, 3rd edn, Brooks/Cole Publishing Company.

Coles, J. A. and Schneider-Picard, G. (1989). Amplification of small signals by voltage-gated sodium channels in drone photoreceptors, *Journal of Comparative Physiology A* **165**: 109–118.

Cone, R. A. (1973). The internal transmitter model for visual excitation: some quantitative implications, *in* H. Langer (ed.), *Biochemistry and physiology of visual pigments*, Springer-Verlag, pp. 275–282.

Contzen, K. and Nagy, K. (1996). A mathematical model for the components of the receptor current in *Limulus* ventral nerve photoreceptors, *Journal of Photochemistry and Photobiology B: Biology* **35**: 123–132.

Cuttle, M. F., Hevers, W., Laughlin, S. B. and Hardie, R. C. (1995). Diurnal modulation of photoreceptor potassium conductance in the locust, *Journal of Comparative Physiology A* **176**: 307–316.

de Schutter, E. (1994). Modelling the cerebellar purkinje cell: experiments in computo, *Progress in Brain Research* **102**: 427–441.

Delbrück, T. and Mead, C. A. (1994). Analog VLSI adaptive, logarithmic, wide-dynamic-range photoreceptor, *Proceedings of the International Circuits and Systems Meeting*.

Douglas, R., Mahowald, M. and Mead, C. (1995). Neuromorphic analogue VLSI, *Annual Review of Neuroscience* **18**: 255–281.

Douglass, J. K. and Strausfeld, N. J. (1996). Visual motion-detection circuits in flies: parallel direction- and non-direction-sensitive pathways between the medulla and lobula plate, *Journal of Neuroscience* **16**: 4551–4562.

Egelhaaf, M. and Borst, A. (1993a). A look into the cockpit of the fly: visual orientation, algorithms, and identified neurons, *Journal of Neuroscience* **13**: 4563–4574.

Egelhaaf, M. and Borst, A. (1993b). Motion computation and visual orientation in flies, *Comparative Biochemistry and Physiology: Comparative Physiology* **104**: 659–673.

Eggers, A. and Gewecke, M. (1993). The dorsal rim area of the compound eye and polarization vision in the desert locust (*Schistecerca gregaria*), *in* K. Wiese, F. G. Gribakin, A. V. Popov and G. Renninger (eds), *Sensory systems of arthropods*, Birkhäuser Verlag, pp. 101–109.

French, A. S. and Kuster, J. E. (1985). Nonlinearities in locust photoreceptors during transduction of small numbers of photons, *Journal of Comparative Physiology A* **156**: 645–652.

Fulpius, B. and Baumann, F. (1969). Effects of sodium, potassium, and calcium ions on slow and spike potentials in single photoreceptor cells, *Journal of General Physiology* **53**: 541–561.

Gewecke, M. and Hou, T. (1993). Visual brain neurons in (*Locusta migratoria*), *in* K. Wiese, F. G. Gribakin, A. V. Popov and G. Renninger (eds), *Sensory systems of arthropods*, Birkhäuser Verlag, pp. 119–144.

Hardie, R. C. (1989). A histamine-activated chloride channel involved in neurotransmission at a photoreceptor synapse, *Nature* **339**: 704–706.

Hardie, R. C. (1991a). Voltage-sensitive potassium channels in *Drosophila* photoreceptors, *Journal of Neuroscience* **11**: 3079–3095.

Hardie, R. C. (1991b). Whole-cell recordings of the light-induced current in dissociated *Drosophila* photoreceptors - evidence for feedback by calcium permeating the light-sensitive channels, *Proceedings of the Royal Society of London B* **245**: 203–210.

Hardie, R. C. and Minke, B. (1992). The trp gene is essential for a light-activated Ca^{2+} channel in *Drosophila* photoreceptors, *Neuron* **8**: 643–651.

Hardie, R. C. and Minke, B. (1994). Calcium-dependent inactivation of light-sensitive channels in *Drosophila* photoreceptors, *Journal of General Physiology* **103**: 409–427.

Hardie, R. C. and Minke, B. (1995). Phosphoinositide-mediated phototransduction in *Drosophila* photoreceptors: the role of Ca^{2+} and trp, *Cell Calcium* **18**: 256–274.

Hardie, R. C. and Weckström, M. (1990). Three classes of potassium channels in large monopolar cells of the blowfly *Calliphora vicina*, *Journal of Comparative Physiology A* **167**: 723–736.

Harrison, R. R. and Koch, C. (in press). An analog VLSI model of the fly elementary motion detector, *Advances in Neural Information Processing Systems*, Vol. 10.

Hatsopoulos, N., Gabbiani, F. and Laurent, G. (1995). Elementary computation of object approach by a wide-field visual neuron, *Science* **270**: 1000–1003.

Hevers, W. and Hardie, R. C. (1995). Serotonin modulates the voltage dependence of delayed rectifier and Shaker potassium channels in *Drosophila* photoreceptors, *Neuron* **14**: 845–856.

Hochstrate, P. (1991). Electrogenic Na^{+}-Ca^{2+} exchange contributes to the light response of fly photoreceptors, *Zeitschrift für Naturforschung C* **46**: 451–460.

Hodgkin, A. L. and Huxley, A. F. (1952). A quantitative description of membrane current and its application to conduction and excitation in nerve, *Journal of Physiology* **117**: 500–544.

Horridge, G. A. (1975). *The compound eye and vision of insects*, Clarendon Press.

Horridge, G. A. (1978). The separation of visual axes in apposition compound eyes, *Philosophical Transactions of the Royal Society of London B* **285**: 1–59.

Horridge, G. A. and Tsukahara, Y. (1978). The distribution of bumps in the tail of the locust photoreceptor afterpotential, *Journal of Experimental Biology* **73**: 1–14.

Horridge, G. A., Duniec, J. and Marčelja, L. (1981). A 24-hour cycle in single locust and mantis photoreceptors, *Journal of Experimental Biology* **91**: 307–322.

Howard, J. (1981). Temporal resolving power of the photoreceptors of *Locusta migratoria*, *Journal of Comparative Physiology* **144**: 61–66.

Howard, J. (1983). Variations in the voltage response to single quanta of light in the photoreceptors of *Locusta migratoria*, *Biophysics of Structure and Mechanism* **9**: 341–348.

Howard, J., Dubs, A. and Payne, R. (1984). The dynamics of phototransduction in insects: a comparative study, *Journal of Comparative Physiology* **154**: 707–718.

Indiveri, G. (in press). Analog VLSI model of locust DCMD neuron for computation of object approach, *Proceedings of the 1st European workshop on neuromorphic systems*.

Jack, J. (1979). An introduction to linear cable theory, *in* F. O. Schmitt and F. G. Worden (eds), *The Neurosciences: Fourth Study Program*, The MIT Press, pp. 423–437.

James, A. C. (1992). Nonlinear operator network models of processing in the fly lamina, *in* R. B. Pinter and B. Nabet (eds), *Nonlinear vision: determination of neural receptive fields, function, and networks*, CRC Press, pp. 39–73.

James, A. C. and Osorio, D. (1996). Characterisation of columnar neurons and visual signal processing in the medulla of the locust optic lobe by system identification techniques, *Journal of Comparative Physiology A* **178**: 183–199.

Jansonius, N. M. (1990). Properties of the sodium-pump in the blowfly photoreceptor cell, *Journal of Comparative Physiology A* **167**: 461–467.

Jeffrey, A. (1989). *Mathematics for engineers and scientists*, 4th edn, Van Nostrand Reinhold International.

Judge, S. J. and Rind, F. C. (1997). The locust DCMD, a movement-detecting neurone tightly tuned to collision trajectories, *Journal of Experimental Biology* **200**: 2209–2216.

Juusola, M. and French, A. S. (1997). Visual acuity for moving objects in first- and second-order neurons of the fly compound eye, *Journal of Neurophysiology* **77**: 1487–1495.

Juusola, M. and Weckström, M. (1993). Band-pass filtering by voltage-dependent membrane in an insect photoreceptor, *Neuroscience Letters* **154**: 84–88.

Juusola, M., Uusitalo, R. O. and Weckström, M. (1995). Transfer of graded potentials at the photoreceptor-interneuron synapse, *Journal of General Physiology* **105**: 117–148.

Krapp, H. G. and Hengstenberg, R. (1996). Estimation of self-motion by optic flow processing in single visual interneurons, *Nature* **384**: 463–466.

Krapp, H. G., Gabbiani, F., Koch, C. and Laurent, G. (1998). Neuronal multiplication in the locust visual system, *in* N. Elsner and R. Wehner (eds), *Proceedings of the 26th Göttingen Neurobiology Conference*, Vol. II, Georg Thieme Verlag, p. 410.

Laughlin, S. B. (1973). Neural integration in the first optic neuropile of dragonflies. I. Signal amplification in dark-adapted second-order neurons, *Journal of Comparative Physiology* **84**: 335–355.

Laughlin, S. B. (1974). Neural integration in the first optic neuropile of dragonflies. II. Receptor signal interactions in the lamina, *Journal of Comparative Physiology* **92**: 357–375.

Laughlin, S. B. (1981). A simple coding procedure enhances a neuron's information capacity, *Zeitschrift für Naturforsch C* **36**: 910–912.

Laughlin, S. B. (1989). Coding efficiency and design in visual processing, *in* D. G. Stavenga and R. C. Hardie (eds), *Facets of vision*, Springer-Verlag, pp. 213–234.

Laughlin, S. B. (1994). Matching coding, circuits, cells, and molecules to signals - general principles of retinal design in the fly's eye, *Progress in Retinal and Eye Research* **13**: 165–196.

Laughlin, S. B. (1996). Matched filtering by a photoreceptor membrane, *Vision Research* **36**: 1529–1541.

Laughlin, S. B. and Hardie, R. C. (1978). Common strategies for light adaptation in the peripheral visual systems of fly and dragonfly, *Journal of Comparative Physiology* **128**: 319–340.

Laughlin, S. B. and Osorio, D. (1989). Mechanisms for neural signal enhancement in the blowfly compound eye, *Journal of Experimental Biology* **144**: 113–146.

Laughlin, S. B. and Weckström, M. (1993). Fast and slow photoreceptors - a comparative study of the functional diversity of coding and conductances in the diptera, *Journal of Comparative Physiology A* **172**: 593–609.

Laughlin, S. B., Howard, J. and Blakeslee, B. (1987). Synaptic limitations to contrast coding in the retina of the blowfly *Calliphora*, *Proceedings of the Royal Society of London B* **231**: 437–467.

Lillywhite, P. G. (1977). Single photon signals and transduction in an insect eye, *Journal of Comparative Physiology* **122**: 189–200.

Lillywhite, P. G. and Laughlin, S. B. (1979). Transducer noise in a photoreceptor, *Nature* **277**: 569–572.

Liu, S. (in press). Silicon retina with adaptive filter properties, *Advances in Neural Information Processing Systems*.

Mahowald, M. A. and Mead, C. (1991). The silicon retina, *Scientific American* **264**: 76–82.

Mahowald, M. and Douglas, R. (1991). A silicon neuron, *Nature* **354**: 515–518.

Matić, T. and Laughlin, S. B. (1981). Changes in the intensity-response function of an insect's photoreceptors due to light adaptation, *Journal of Comparative Physiology* **145**: 169–177.

Mead, C. (1989). *Analog VLSI and neural systems*, Addison-Wesley.

Meinertzhagen, I. A. (1976). The organization of perpendicular fibre pathways in the insect optic lobe, *Philosophical Transactions of the Royal Society of London B* **274**: 555–594.

Murre, J. M. J. (1995). Neurosimulators, *in* M. A. Arbib (ed.), *The handbook of brain theory and neural networks*, The MIT Press, pp. 634–639.

Nässel, D. R., Hagberg, M. and Seyan, H. S. (1983). A new, possibly serotonergic, neuron in the lamina of the blowfly optic lobe: an immunocytochemical and golgi-em study, *Brain Research* **280**: 361–367.

Nicol, D. and Meinertzhagen, I. A. (1982). An analysis of the number and composition of the synaptic populations formed by photoreceptors of the fly, *Journal of Comparative Neurology* **207**: 29–44.

Nilsson, D. (1989). Optics and evolution of the compound eye, *in* D. G. Stavenga and R. C. Hardie (eds), *Facets of vision*, Springer-Verlag, pp. 30–73.

Nowel, M. S. and Shelton, P. M. (1981). A Golgi-electron-microscopical study of the structure and development of the lamina ganglionaris of the locust optic lobe, *Cell and Tissue Research* **216**: 377–401.

Oberwinkler, J. and Stavenga, D. G. (1998). Ca^{2+} dynamics in the rhabdomeres of intact fly eyes, *in* N. Elsner and R. Wehner (eds), *Proceedings of the 26th Göttingen Neurobiology Conference*, Vol. II, Georg Thieme Verlag, p. 402.

O'Carroll, D. C., Osorio, D., James, A. C. and Bush, T. (1992). Local feedback mediated via amacrine cells in the insect optic lobe, *Journal of Comparative Physiology A* **171**: 447–455.

O'Shea, M. and Rowell, C. H. F. (1975a). Protection from habituation by lateral inhibition, *Nature* **254**: 53–55.

O'Shea, M. and Rowell, C. H. F. (1975b). A spike-transmitting electrical synapse between visual interneurones in the locust movement detector system, *Journal of Comparative Physiology* **97**: 143–158.

O'Shea, M. and Williams, J. L. D. (1974). The anatomy and output connection of a locust visual interneurone; the lobular giant movement detector (LGMD) neurone, *Journal of Comparative Physiology* **91**: 257–266.

O'Shea, M., Rowell, C. H. F. and Williams, J. L. D. (1974). The anatomy of a locust visual interneurone: the descending contralateral movement detector, *Journal of Experimental Biology* **60**: 1–12.

Osorio, D. (1987). The temporal properties of non-linear, transient cells in the locust medulla, *Journal of Comparative Physiology A* **161**: 431–440.

Osorio, D. (1991). Mechanisms of early visual processing in the medulla of the locust optic lobe: how self-inhibition, spatial-pooling, and signal rectification contribute to the properties of transient cells, *Visual Neuroscience* **7**: 345–355.

Osorio, D. (1992). Retinotopic vision in the locust, *in* R. B. Pinter and B. Nabet (eds), *Nonlinear vision: determination of neural receptive fields, function, and networks*, CRC Press, pp. 377–390.

Payne, R. (1982). Fluoride blocks an inactivation step of transduction in a locust photoreceptor, *Journal of Physiology* **325**: 261–279.

Payne, R. and Howard, J. (1981). Response of an insect photoreceptor: a simple log-normal model, *Nature* **290**: 415–416.

Pece, A. E. C. and French, A. S. (1992). Sublinear summation of responses in locust photoreceptors, *Journal of Comparative Physiology A* **170**: 729–738.

Pinter, R. B. (1972). Frequency and time domain properties of retinular cells of the desert locust (*Schistocerca gregaria*) and the house cricket (*Acheta domesticus*), *Journal of Comparative Physiology* **77**: 383–397.

Pinter, R. B. (1979). Inhibition and excitation in the locust DCMD receptive field: spatial frequency, temporal and spatial characteristics, *Journal of Experimental Biology* **80**: 191–216.

Pinter, R. B., Olberg, R. M. and Abrams, T. W. (1982). Is the locust DCMD a looming detector?, *Journal of Experimental Biology* **101**: 327–331.

Rall, W. (1989). Cable theory for dendritic neurons, *in* C. Koch and I. Segev (eds), *Methods in neuronal modeling: from synapses to networks*, The MIT Press, pp. 9–62.

Rall, W. (1995). Perspective on neuron model complexity, *in* M. A. Arbib (ed.), *The handbook of brain theory and neural networks*, The MIT Press, pp. 728–732.

Rind, F. C. (1984). A chemical synapse between two motion detecting neurones in the locust brain, *Journal of Experimental Biology* **110**: 143–167.

Rind, F. C. (1987). Non-directional, movement sensitive neurons of the locust optic lobe, *Journal of Comparative Physiology A* **161**: 477–494.

Rind, F. C. (1990). Identification of directionally selective motion-detecting neurons in the locust lobula and their synaptic connections with an identified descending neuron, *Journal of Experimental Biology* **149**: 21–43.

Rind, F. C. (1996). Intracellular characterization of neurons in the locust brain signaling impending collision, *Journal of Neurophysiology* **75**: 986–995.

Rind, F. C. and Bramwell, D. I. (1996). Neural network based on the input organization of an identified neuron signaling impending collision, *Journal of Neurophysiology* **75**: 967–985.

Rind, F. C. and Simmons, P. J. (1992). Orthopteran DCMD neuron: a reevaluation of responses to moving objects. I. Selective responses to approaching objects, *Journal of Neurophysiology* **68**: 1654–1666.

Rind, F. C. and Simmons, P. J. (1997). Signaling of object approach by the DCMD neuron of the locust, *Journal of Neurophysiology* **77**: 1029–1033.

Rind, F. C. and Simmons, P. J. (1998). Local circuit for the computation of object approach by an identified visual neuron in the locust, *Journal of Comparative Neurology* **395**: 405–415.

Rowell, C. H. F. (1971). The opthopteran descending movement detector (DMD) neurones: a characterisation and review, *Zeitschrift für vergleichende Physiologie* **73**: 167–194.

Rowell, C. H. F. and O'Shea, M. (1976a). Neuronal basis of a sensory analyser, the acridid movement detector system. III. Control of response amplitude by tonic lateral inhibition, *Journal of Experimental Biology* **65**: 617–625.

Rowell, C. H. F. and O'Shea, M. (1976b). The neuronal basis of a sensory analyser, the acridid movement detector system. I. Effects of simple incremental and decremental stimuli in light and dark adapted animals, *Journal of Experimental Biology* **65**: 273–288.

Rowell, C. H. F., O'Shea, M. and Williams, J. L. (1977). The neuronal basis of a sensory analyser, the acridid movement detector system. IV. The preference for small field stimuli, *Journal of Experimental Biology* **68**: 157–185.

Schlotterer, G. R. (1977). Response of the locust descending contralateral movement detector neuron to rapidly approaching and withdrawing visual stimuli, *Canadian Journal of Zoology* **55**: 1372–1376.

Scholes, J. (1965). Discontinuity of the excitation process in locust visual cells, *Cold Spring Harbor Symposia on Quantitative Biology* **30**: 517–527.

Segev, I., Fleshman, J. W. and Burke, R. E. (1989). Compartmental models of complex neurons, *in* C. Koch and I. Segev (eds), *Methods in neuronal modeling: from synapses to networks*, The MIT Press, pp. 63–96.

Shaw, S. R. (1968). Organization of the locust retina, *Symposia of the Zoological Society of London* **23**: 135–163.

Shaw, S. R. (1975). Retinal resistance barriers and electrical lateral inhibition, *Nature* **255**: 480–482.

Shaw, S. R. (1977). Restricted diffusion and extracellular space in the insect retina, *Journal of Comparative Physiology* **113**: 257–282.

Shaw, S. R. (1978). The extracellular space and blood-eye barrier in an insect retina: an ultrastructural study, *Cell and Tissue Research* **188**: 35–61.

Shaw, S. R. (1984). Early visual processing in insects, *Journal of Experimental Biology* **112**: 225–251.

Simmons, P. (1980). Connexions between a movement-detecting visual interneurone and flight motoneurones of a locust, *Journal of Experimental Biology* **86**: 87–97.

Simmons, P. J. (1985). Postsynaptic potentials of limited duration in visual neurones of a locust, *Journal of Experimental Biology* **117**: 193–213.

Simmons, P. J. and Rind, F. C. (1992). Orthopteran DCMD neuron: a reevaluation of responses to moving objects. II. Critical cues for detecting approaching objects, *Journal of Neurophysiology* **68**: 1667–1682.

Single, S., Haag, J. and Borst, A. (1997). Dendritic computation of direction selectivity and gain control in visual interneurons, *Journal of Neuroscience* **17**: 6023–6030.

Srinivasan, M. V., Laughlin, S. B. and Dubs, A. (1982). Predictive coding: a fresh view of inhibition in the retina, *Proceedings of the Royal Society of London B* **216**: 427–459.

Srinivasan, M. V., Lehrer, M., Kirchner, W. H. and Zhang, S. W. (1991). Range perception through apparent image speed in freely flying honeybees, *Visual Neuroscience* **6**: 519–535.

Srinivasan, M. V., Pinter, R. B. and Osorio, D. (1990). Matched filtering in the visual system of the fly: large monopolar cells of the lamina are optimized to detect moving edges and blobs, *Proceedings of the Royal Society of London B* **240**: 279–293.

Srinivasan, M. V., Zhang, S. W. and Chandrashekara, K. (1993). Evidence for two distinct movement-detecting mechanisms in insect vision, *Naturwissenschaften* **80**: 38–41.

Stern, M., Thompson, K. S. J., Zhou, P., Watson, D. G., Midgley, J. M., Gewecke, M. and Bacon, J. P. (1995). Octopaminergic neurons in the locust brain: morphological, biochemical and electrophysiological characterization of potential modulators of the visual system, *Journal of Comparative Physiology A* **177**: 611–625.

Strausfeld, N. J. (1976). *Atlas of an insect brain*, Springer-Verlag.

Strausfeld, N. J. (1989). Beneath the compound eye: neuroanatomical analysis and physiological correlates in the study of insect vision, *in* D. G. Stavenga and R. C. Hardie (eds), *Facets of vision*, Springer-Verlag, pp. 317–359.

Strausfeld, N. J. and Campos-Ortega, J. A. (1977). Vision in insects: pathways possibly underlying neural adaptation and lateral inhibition, *Science* **195**: 894–897.

Tsukahara, Y. and Horridge, G. A. (1977). Miniature potentials, light adaptation and afterpotentials in locust retinula cells, *Journal of Experimental Biology* **68**: 137–149.

Tunstall, J. and Horridge, G. A. (1967). Electrophysiological investigation of the optics of the locust retina, *Zeitschrift für vergleichende Physiologie* **55**: 167–182.

Vallet, A. M. and Coles, J. A. (1993). Is the membrane voltage-amplifier of drone photoreceptors useful at physiological light intensities?, *Journal of Comparative Physiology A* **173**: 163–168.

van Hateren, J. H. (1986a). An efficient algorithm for cable theory, applied to blowfly photoreceptor cells and LMCs, *Biological Cybernetics* **54**: 301–311.

van Hateren, J. H. (1986b). Electrical coupling of neuro-ommatidial photoreceptor cells in the blowfly, *Journal of Comparative Physiology A* **158**: 795–811.

van Hateren, J. H. (1992). Theoretical predictions of spatiotemporal receptive fields of fly LMCs, and experimental validation, *Journal of Comparative Physiology A* **171**: 157–170.

van Hateren, J. H. (1997). Processing of natural time series of intensities by the visual system of the blowfly, *Vision Research* **37**: 3407–3416.

van Hateren, J. H. and Laughlin, S. B. (1990). Membrane parameters, signal transmission, and the design of a graded potential neuron, *Journal of Comparative Physiology A* **166**: 437–448.

Verschure, P. F. M. J. (1997). Xmorph: a software tool for the synthesis and analysis of neural systems, *Technical report*, Institute of Neuroinformatics.

Vishnevskaya, T. M., Byzov, A. L. and Cherkasov, A. D. (1993). Adaptational shifts in the dynamic range of photoreceptors and monopolar neurons in insect eyes, *in* K. Wiese, F. G. Gribakin, A. V. Popov and G. Renninger (eds), *Sensory systems of arthropods*, Birkhäuser Verlag, pp. 196–203.

Walz, B., Zimmermann, B. and Seidl, S. (1994). Intracellular Ca^{2+} concentration and latency of light-induced Ca^{2+} changes in photoreceptors of the honeybee drone, *Journal of Comparative Physiology A* **174**: 421–431.

Weckström, M. (1994). Voltage-activated outward currents in adult and nymphal locust photoreceptors, *Journal of Comparative Physiology A* **174**: 795–801.

Weckström, M. and Laughlin, S. B. (1995). Visual ecology and voltage-gated ion channels in insect photoreceptors, *Trends in Neurosciences* **18**: 17–21.

Weckström, M., Hardie, R. C. and Laughlin, S. B. (1991). Voltage-activated potassium channels in blowfly photoreceptors and their role in light adaptation, *Journal of Physiology* **440**: 635–657.

Weckström, M., Juusola, M. and Laughlin, S. B. (1992). Presynaptic enhancement of signal transients in photoreceptor terminals in the compound eye, *Proceedings of the Royal Society of London B* **250**: 83–89.

Williams, D. S. (1983). Changes of photoreceptor performance associated with the daily turnover of photoreceptor membrane in locusts, *Journal of Comparative Physiology* **150**: 509–519.

Wilson, M. (1975). Angular sensitivity of light and dark adapted locust retinula cells, *Journal of Comparative Physiology* **97**: 323–328.

Wilson, M. A. and Bower, J. M. (1989). The simulation of large-scale neural networks, *in* C. Koch and I. Segev (eds), *Methods in neuronal modeling: from synapses to networks*, The MIT Press, pp. 291–333.

Wilson, M., Garrard, P. and McGinness, S. (1978). The unit structure of the locust compound eye, *Cell and Tissue Research* **195**: 205–226.

Zaretsky, M. and Rowell, C. H. F. (1979). Saccadic suppression by corollary discharge in the locust, *Nature* **280**: 583–585.

Zettler, F. and Järvilehto, M. (1972). Lateral inhibition in an insect eye, *Zeitschrift für vergleichende Physiologie* **76**: 233–244.

Zettler, F. and Straka, H. (1987). Synaptic chloride channels generating hyperpolarizing on-responses in monopolar neurons of the blowfly visual system, *Journal of Experimental Biology* **131**: 435–438.

Zimmerman, R. P. (1978). Field potential analysis and the physiology of second-order neurons in the visual system of the fly, *Journal of Comparative Physiology* **126**: 297–316.